Electrical Imaging of Aberrant Activity in Neural Tissues Using High Density Microelectrode Arrays

**Inaugural-Dissertation
zur Erlangung des Doktorgrades
der Humanwissenschaften**

**der Medizinischen Fakultät
der Eberhard Karls Universität
zu Tübingen**

**vorgelegt
von**

Channappa, Lakshmi

2016

Dekan: Professor Dr. I. B. Autenrieth

1. Berichterstatter: Professor. Dr. T. Euler

2. Berichterstatter: Professor. Dr. A. Nieder

This thesis is dedicated to my beloved parents

ABSTRACT

In the central nervous system, different brain regions communicate through neural signals. A normal neurophysiological activity is based upon the balance between the excitatory and the inhibitory neuronal networks. However, in certain neurological disorders, an imbalanced activity results due to a decreased inhibitory or exacerbated excitatory drive in neural tissues. So far, the study of such network activity has been achieved with single electrodes/patch clamp technique or low-density microelectrode arrays (MEAs). Towards a better understanding of the underlying features during imbalanced network activity, high-density CMOS MEAs were here used to study the aberrant electrical activity in hippocampal slices and in blind *ex vivo* retinas.

In this thesis, aberrant electrical activity was investigated in organotypic and in acute hippocampal slices. The pharmacologically induced epileptiform-like activity (ELA) in organotypic hippocampal slices revealed propagating local field potentials (LFPs) from dentate gyrus (DG) towards the hippocampal CA3 region. Unexpected and not reported previously p-spikes of the LFPs propagated backwards from CA3 to DG along the same pathway. Also forward and backward propagating LFPs were identified in acute slices.

Epileptiform hippocampal activity was compared to the imbalanced activity recorded in photoreceptor degenerated *ex vivo* mouse retina (*rd10* mouse model). High-density recordings revealed local field potentials as well. The quantitative differences in LFP frequency and propagation pattern between hippocampus and retina were investigated and related to morphological differences. Finally, pharmacological experiments revealed that gap junctions and excitatory synaptic transmission are required for the generation of aberrant LFPs in both systems, the hippocampus and the blind retina.

ZUSAMMENFASSUNG

Im zentralen Nervensystem kommunizierenverschiedene Hirnregionen mittels neuronaler Signale. Das neurophysiologische Aktivitätsmuster wird durch die Balance zwischen exzitatorischen und inhibitorischen Netzwerken bestimmt. In neurologischen Erkrankungen führt ein verringerter inhibitorischer Einfluss oder eine Erhöhung der exzitatorischen Anregung zu einem Ungleichgewicht, welches sich in aberranter elektrischer Aktivität äußert. Solche pathologischen Aktivitätsmuster wurden bisher hauptsächlich mit Hilfe von Einzelzellableitungen (z.B. „Patch-Clamp") oder mittels „Micro Electrode Arrays" (MEAs) gemessen. Letztere sind jedoch durch die Anzahl und die Dichte der Messpunkte limitiert. Um die zu Grunde liegenden Eigenschaften aberranter elektrischer Aktivität zu studieren, wird hier ein CMOS MEA mit hoher räumlicher und zeitlicher Auflösung verwendet.

In dieser Arbeit wird die aberrante elektrische Aktivität in organotypischen und akuten hippocampalen Gewebeschnitten untersucht. Die pharmakologisch induzierte, epileptiforme Aktivität in organotypischen Hirnschnitten ist durch nichtstationäre Feldpotentiale gekennzeichnet, die vom Gyrus Dentatus zur CA3 Region wandern. Zudem wurde während der epileptiformen Aktivität eine Propagation der frühen LFP-Phase „p-spikes" beobachtet, die entgegengesetzt der normalen Propagation verläuft und bisher noch nicht beschrieben wurde. Die Propagation von Feldpotentialen in beiden Richtungen wurde auch in akuten Schnitten bestätigt.

Die epileptiforme hippocampale Aktivität wurde dann mit der Aktivität in Retina-Explantaten (*ex vivo*) von Mäusen verglichen, in denen die Photorezeptoren aufgrund einer Mutation degenerieren (*rd10* Maus). Die Messungen zeigten, dass auch hier Feldpotenziale auftreten. Quantitative Unterschiede hinsichtlich Frequenz und Ausbreitungsrichtung der Feldpotenziale in den beiden Systemen konnten auf morphologische Unterschiede zurückgeführt werden. Pharmakologische Experimente legen nahe, dass elektrische Synapsen und exzitatorische synaptische Übertragung für das Entstehen aberranter Feldpotenziale im Hippocampus und der blinden Retina notwendig sind.

Acknowledgment

Table of Contents

List of Figures

List of Tables

List of Abbreviations

ACSF	Artificial cerebrospinal fluid
AMPA	α-Amino-3-hydroxy-5-methyl-4-isoxazolepropionic acid
AP	Action potential
4-AP	4-Aminopyridine
BMI	Bicuculline methiodide
CMOS	Complementary metal oxide semiconductor
CA	Cornu ammonis
CBP	Cone bipolar cell
CNS	Central nervous system
DIV	Day *in vitro*
DG	Dentate gyrus
DNQX	6,7-dinitroquinoxaline-2,3-dione
EEG	Electroencephalography
EC	Entorhinal cortex
ELA	Epileptiform-like activity
EPSC	Excitatory post synaptic current
FWHM	Full-width at half-amplitude minimum
GABA	γ-Aminobutyric acid
GBSS	Gey's balanced salt solution
GluR	Glutamate receptor
HBSS	Hank's balanced salt solution
iGluR	Ionotropic glutamate receptor
INL	Inner nuclear layer
ID	Interictal epileptiform discharges
ILAE	International league against epilepsy
$[K^+]$	Potassium concentration

KA	Kainate
LFP	Local field potential
LTLE	Lateral temporal lobe epilepsy
Mg^{2+}	Magnesium ion
MFA	Meclofenamic acid
MEA	Microelectrode array
MEM	Minimal essential medium
µECoG	Micro-electrocorticography
mGluR	Metabotropic glutamate receptor
MRI	Magnetic resonance imaging
MTLE	Medial temporal lobe epilepsy
NMDA	N-methy-D-aspartate
NR	N-methyl-D-aspartate receptor
PSD	Post synaptic density
SUA	Single unit activity
STA	Spike triggered average
SEM	Standard error of mean
SO	Stratum oriens
SP	Stratum pyramidale
SR	Stratum radiatum
SLM	Stratum lacunosum moleculare
TLE	Temporal lobe epilepsy
OHC	Organotypic hippocampal slice culture
ONL	Outer nuclear layer
RP	Retinitis Pigmentosa
RBC	Rod bipolar cell
RGC	Retinal ganglion cell
V_{ext}	Extracellular voltage

1 Introduction

1.1 Hippocampus

The hippocampus, one of the major parts of the brain, is located in the temporal lobe, and has been the topic of intensive studies. The hippocampus plays an important role in various functional processes in the brain, such as learning (Jarrard, 1993), memory (Murray & Mishkin, 1984), and spatial navigation (O'Keefe & Recce, 1993). Apart from its role in normal functioning of the brain, it is a region of high susceptibility to neurological disorders such as Alzheimer's (Gosche *et al.*, 2002) and epilepsy (Schwartzkroin, 1994). It has a highly laminated structure where the cell bodies, and the cell processes are segregated into different layers. It is one of the most highly excitable parts of the brain (Jung, 1949; Andersen *et al.*, 2006) and, therefore, susceptible to seizure-like activity. In this thesis, characterization of aberrant network activity, i.e. spatiotemporal dynamics within the hippocampal formation during epileptiform-like discharges, was investigated.

1.1.1 Trisynaptic circuitry of the hippocampus

The trisynaptic circuitry (or trisynaptic pathway) is a set of excitatory synaptic connections which link different subregions of the hippocampus (Figure 1.1). The major subfields that make up the hippocampus are dentate gyrus (DG), Cornu Ammonis 3 (CA3) and Cornu Ammonis 1 (CA1). Recently, a smaller subfield Cornu Ammonis 2 (CA2), has received increased attention (Kohara *et al.*, 2014). Of the three synapses, the first synapse is formed between the projection neurons of the entorhinal cortex (EC) and the granule cells of the DG. The input projections termed perforant path fibres reach the DG from layer II of EC (Steward & Scoville, 1976). These perforant path fibres (marked green in Figure.1.1) terminate in the molecular layer of the DG which comprises the dendrites of granule cells. Granule cells are the principal cells of the DG. The DG furthermore comprises of many types of inhibitory neurons. The

1

unmyelinated axons of granule cells, known as mossy fibres, are the only projections that reach the dendrites of pyramidal cells of the CA3 region (Hamlyn, 1962; Blackstad *et al.*, 1970; Claiborne *et al.*, 1986) and they make up the second synapse of the trisynaptic loop. The third synaptic connection is through Schaffer collaterals (Schaffer, 1892), in which the axons of pyramidal cells of the CA3, synapse onto the dendrites of the pyramidal cells in the CA1 region (Ishizuka *et al.*, 1990). Additionally, neurons in the layer II of the EC also project to the CA3 via perforant pathway (Andersen *et al.*, 2006) and neurons from the layer III of the EC project to the CA1 region, and provide additional input to the hippocampus.
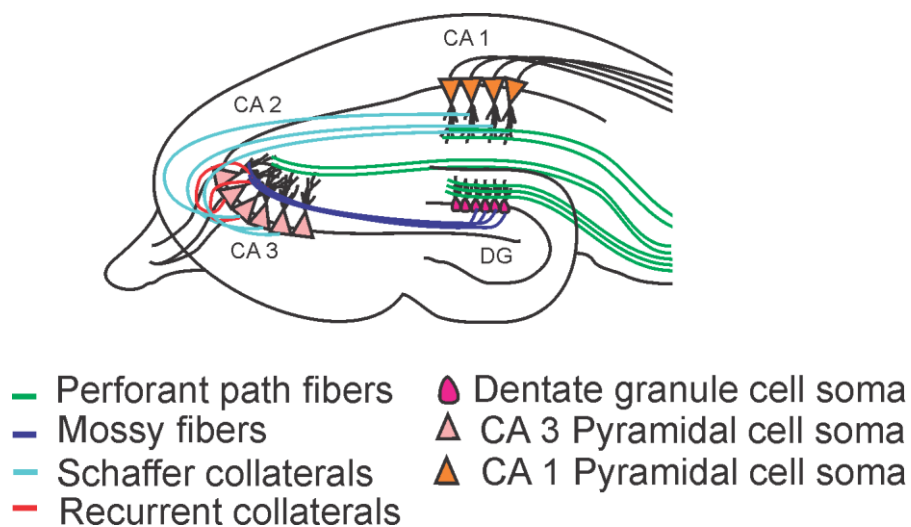
Figure 1.1: Schematic drawing of transverse section of a hippocampus. Trisynaptic connections from EC (not shown) - DG-CA3-CA1. Figure modified from Deng *et al.*, 2010 (Deng *et al.*, 2010).

1.1.2 Subfields of the hippocampus

Dentate gyrus

The DG, which receives the major part of its input from the EC via perforant path fibres, is divided into a **molecular layer,** which mainly consists of the terminal ends of the perforant path fibres; the **granule cell layer** which is populated by granule cells, and the **polymorphic layer** consisting of a variety of neuronal types. The molecular layer contains the apical dendrites of granule cells and is basically a cell-free layer with an average thickness of about 250

μm. The granule cell layer, which lies below the molecular layer, is about four to eight granule cells thick (Andersen *et al.*, 2006). The most prominent cell type of the polymorphic layer is the mossy cell, another excitatory cell of the DG (Amaral, 1978).

Cornu Ammonis fields: CA1, CA2, CA3 of hippocampus proper

The term "cornu ammonis" was coined by De Garengeot (1742) after the name of an Egyptian God Amun Kneph, whose symbol was a Ram (Andersen *et al.*, 2006). However, the terms CA1, CA2 and CA3 coined by Lorente de Nó (Lorente de Nó, 1934) is used more commonly (Andersen *et al.*, 2006). These subregions that are connected along the trisynaptic circuitry exhibit unique features with regard to cell size, axonal and dendritic arborisation and synaptic connectivity. The pyramidal cells (glutamatergic) are responsible for signal propagation along the hippocampal subfields. The interneurons (GABAergic) are a smaller neuronal subgroup which form the local circuits (Freund & Buzsaki, 1996). Based on the cell size of the pyramidal cells and their synaptic connections, the CA region is subdivided into CA1, CA2 and CA3 (Lorente de Nó, 1934), as will be described below. The CA region is also structured into defined layers based on neurons cell body position and arborisation of the nerve fibres (Figure 1.2): **Stratum oriens (SO)** – contains basket cells, **Stratum pyramidale (SP)** – consists of cell bodies of the neurons, **Stratum radiatum (SR)** – consists of the dendrites of the pyramidal cells and **Stratum lacunosum-moleculare (SLM)** – here the apical dendrites of the pyramidal cells branch and form an apical tuft.

Cornu ammonis 1 (CA1)

The somata of the pyramidal cells in the CA1 region are smaller than those in the CA3 region. The CA1 region receives input from the CA3 pyramidal cells via Schaffer collaterals and from layer III of the EC via the perforant path. The CA1 region is mainly responsible for outflow of information from the hippocampus to higher areas of the cortex via subiculum.
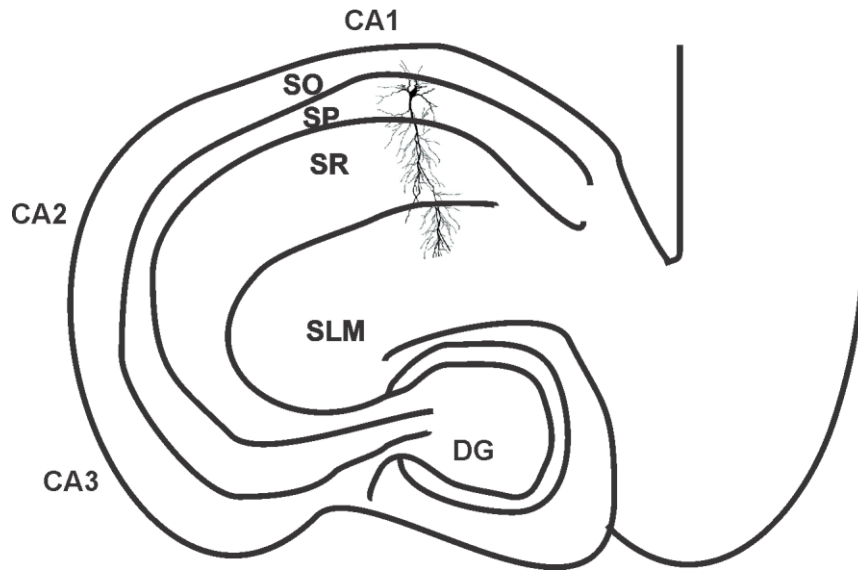
Figure 1.2: Schematic drawing of the hippocampus showing different strata of each subfield. SO – Stratum oriens, SP – Stratum pyramidale, SR – Stratum radiatum, SLM – Stratum lacunosum-moleculare. Figure modified from Capogna M, 2011 (Capogna, 2011).

Cornu ammonis 2 (CA2)

The CA2 region is a small narrow region between the CA1 and the CA3 region. The pyramidal cells of the CA2 have larger somata as compared to CA3 cells. The CA2 cells do not receive any projections from the DG but are innervated by collaterals of their own axons: associational and commissural connections (Andersen *et al.*, 2006).

Cornu ammonis 3 (CA3)

The CA3 region is the subfield of hippocampus proper adjacent to the DG. It receives input from granule cells of the DG along the mossy fibres and from the projection cells of the EC via perforant path fibres. The pyramidal cells of the CA3 are similar in structure to those of the CA1. The largest pyramidal cells of the CA3 are located in the distal portion of the CA3 (closer to CA1) and the smallest ones are located in the limbs of the DG (Amaral *et al.*, 1990). Based on the appearance of the dendritic and axonal patterns of neurons in Golgi preparations, Lorente de Nó (1934) divided the CA3 region into - **CA3a**: region adjacent to the CA2; **CA3b**: the middle portion of CA3, and **CA3c**: the most proximal part closest to the DG (Ishizuka *et al.*, 1990). As a whole, the CA3

region serves as a "pacemaker" of the hippocampus (Wittner & Miles, 2007; Engel *et al.*, 2008; Engel *et al.*, 2009). The pyramidal cells of the CA3 region send a large number of axons to the CA2 and the CA1 (Schaffer collaterals), as well as some axons to the hilus (Li *et al.*, 1994). In addition, some of the axons terminate within the CA3 region forming an excitatory recurrent collateral network. This is one of the hallmarks of the CA3 region. Due to these recurrent collaterals, under conditions of increased excitation and/or decreased inhibition, the CA3 region was proposed to have the lowest seizure threshold compared to other regions in the hippocampus, and hence a high seizure susceptibility (Green, 1964). As a result, such an imbalance between excitation and inhibition can lead to epileptiform activity, which is characterized by synchronous, spontaneous rhythmic network activity.

The major excitatory neurotransmitter responsible for relaying of neural signals along this trisynaptic pathway is L-glutamate (Storm-Mathisen, 1977). The α-amino-3-hydroxyl-5-methyl-4-isoxazolepropionate (AMPA) type glutamate receptors mediate fast excitatory postsynaptic currents (EPSCs). The AMPA receptors are composed of four subunits (GluR1-4) and are found at all excitatory synapses in the post synaptic density (PSD). Most AMPA receptors found in pyramidal neurons of rodent hippocampus are tetramers of GluR1-2 or GluR2-3. N-methyl-D-aspartate (NMDA) ionotropic glutamate receptors and certain metabotropic glutamate receptors (mGluRs) mediate slow EPSCs (Andersen *et al.*, 2006). The NMDA receptors are heteromultimers of the NR1 and the NR2A-D subunits. The NMDA receptors are both ligand-gated and voltage-dependent. Mg^{2+} ions play a crucial role in influencing the ion flux through the NMDA receptor by blocking the channel's pore in a voltage-dependent manner. The NMDA receptors require co-activation by two ligands: glutamate and either D-serine or glycine. Additionally, Kainate receptors, which are tetrameric assemblies, composed of GluR5, -6, -7, KA1 and KA2 subunits are also found in the hippocampus.

1.1.3 Epilepsy

Epilepsy is a brain disorder characterized predominantly by recurrent and unpredictable interruptions of normal brain function, called epileptic seizures. According to the International League against Epilepsy (ILAE) and the International Bureau for Epilepsy, an Epileptic seizure is defined as a "transient occurrence of signs and symptoms due to abnormal excessive or synchronous neuronal activity in the brain" (Lopes da Silva *et al.*, 2003; Milton & Jung, 2003; Fisher *et al.*, 2005; Voss *et al.*, 2009; Filatov *et al.*, 2011). Epilepsy is the most common neurological problem (Ngugi *et al.*, 2010). The incidence of the disorder is about 50 in 100,000 people a year in developed countries and the prevalence is about 700 in 100,000 (Hirtz *et al.*, 2007). For developing countries, the incidences are even higher (Hauser, 1995; Kotsopoulos *et al.*, 2002; Sander, 2003; Burneo *et al.*, 2005; Preux & Druet-Cabanac, 2005; Ngugi *et al.*, 2010). Therefore, epilepsy imposes a substantial public health burden throughout the world.

1.1.4 Types of epilepsy

Epileptic seizures are categorized into generalized seizures and partial seizures (Angeles, 1981). Generalized seizures occur if the abnormal activity affects all or most of the brain. Here, the symptoms involve most of the body. Generalized seizures are further classified into (i) tonic-clonic seizures, where the patient loses consciousness, the whole body stiffens and experiences convulses due to uncontrollable muscle contractions; (ii) absence seizures, where the patient loses consciousness and awareness briefly, but without signs of any convulsions; (iii) myoclonic seizures, which are mainly characterized by sudden contraction of muscles leading to jerks; (iv) tonic seizures, which are characterized by muscle stiffness that may lead to collapsing to the ground; (v) atonic seizures, during which the patient becomes limp and experiences a brief loss of consciousness. In partial (or focal) seizures, on the other hand, electrical activity starts and stays in one part of the brain. Such seizures are further classified into (i) simple partial seizures, which arise in only a small part of the

brain and are characterized by muscular jerks without any loss of consciousness or awareness, and (ii) complex partial seizures, which initially arise from any lobe of the brain and affect larger part of the brain leading to loss of consciousness. In this thesis, a model of partial seizure will be studied as described below (1.1.6).

1.1.5 Causes of epilepsy

Underlying causes of epilepsy may be genetic (Kullmann, 2002), in which case the altered genes affect the functioning of the ion channels, enzymes, receptors etc., or may be due to structural changes because of neuronal loss, enhanced neuronal connectivity or metabolic deficits such as vitamin B_6 deficiency in neonates. In the case of young people, genetic, congenital and developmental conditions are the factors that lead to epilepsy. In the case of older people, epilepsy may arise due to a consequence of other health problems such as brain tumours and strokes.

1.1.6 Temporal lobe epilepsy

Temporal lobe epilepsy (TLE) represents approximately 60% of all partial epilepsies (Engel, 2001). It is broadly classified into (i) medial temporal lobe epilepsy (MTLE), which arises mainly in the hippocampus and the amygdala and (ii) lateral temporal lobe epilepsy (LTLE), which arise in the neocortex (Engel, 2001). In the MTLE, there is loss of neurons in regions of the hippocampus (CA1, CA3) accompanied by damage to mossy cells and inhibitory interneurons in the hilar region (De Lanerolle *et al.*, 2003). As a result of the neuronal loss, an imbalance between excitatory and inhibitory drive occurs, leading to abnormal synchronous brain activity, which can be detected in the form of abnormal electrical activity using electroencephalography (EEG) or extracellular recordings with microelectrode arrays.

1.1.7 Ictal, postictal and interictal phase of an epileptiform activity

An epileptic discharge pattern comprises an ictal phase (the seizure), a preictal phase (the stage before the seizure), a postictal phase (the stage after the seizure), and an interictal phase (the period between seizures). Spatial characterization of these electrical discharges during epileptiform activity provides valuable information regarding what changes influence the transitions between interictal and ictal phases.

The propensity of a seizure depends not only on the site of seizure initiation but also on the speed and pattern of seizure spread. The normal physiological activity transforms into synchronous behaviour of epileptiform activity depending on the spread and recruitment of neuronal cell populations because of the enhanced connectivity, increased excitation or decreased inhibition. Therefore, it is of paramount importance to understand how a network that usually maintains normal physiological activity becomes "epileptic" and to investigate the physiological changes that accompany the process of epileptogenesis in the hippocampus.

Previous studies have shown that during potassium channel blocker 4-aminopyridine (4-AP) induced epileptiform-like activity, interictal-like epileptiform activity originated in CA3 region and spread to EC and basolateral nuclei of the amygdala (Benini *et al.*, 2003). It has also been demonstrated in brain slices that, during epileptiform discharges, the CA3 hippocampal network controls and inhibits the more distant entorhinal network, and upon lesioning the CA3 region, the two networks become independent (Avoli & Barbarosie, 1999). This suggests that the CA3 region of the hippocampus plays a crucial role in recruiting different regions of the brain for an abnormal synchronization during temporal lobe epilepsy. Therefore, as the CA3 region of the hippocampus appears to be responsible for the generation of epileptic seizures, investigation of electrical discharges in the hippocampal subfields during epileptic events

may provide an insight into how the seizures originate, amplify, spread and most importantly prevented.

1.1.8 Extracellular high K$^+$ and zero Mg^{2+} as a model for epileptic activity induction

It is known that epileptiform discharges recorded in certain brain structures such as the hippocampus are accompanied by an increased extracellular potassium concentration [K$^+$] (Somjen & Giacchino, 1985). Although, it remains uncertain if the elevated extracellular [K$^+$] leads to epileptiform discharges or if it results from the epileptic activity, it is conceivable that changes in [K$^+$] influence neuronal excitability and thereby also features propagation of these discharges to distant areas. In addition to elevated potassium, magnesium deficient extracellular medium elicits epileptiform discharges by removing the Mg^{2+} block of the NMDA receptor (Anderson *et al.*, 1986).

1.1.9 Hippocampal brain slices for *in vitro* experimental epilepsy studies

Studies using hippocampal brain slices have elucidated some of the neuronal and synaptic properties that appear to be involved in the generation of typical epileptiform electrical features (Schwartzkroin, 1994). Hippocampal slices serve as an experimental model to study initiation and propagation of epileptiform activity. Particularly, transverse sections (schematically shown in Figures 1.1 & 1.2) of the hippocampus are an ideal preparation for analyzing the electrical activity. This mode of preparation preserves the trisynaptic connections (Andersen *et al.*, 1971; Skrede & Westgaard, 1971; Gähwiler, 1981; Stoppini *et al.*, 1991), morphological and electrophysiological properties (Gähwiler, 1984; Zimmer & Gähwiler, 1984). For experimental epilepsy studies, either organotypic hippocampal slice preparations or acute slice preparations can be used. Both methods of preparations have their advantages and limitations, as described below.

1.1.10 Organotypic hippocampal slice cultures

Organotypic hippocampal slice cultures (OHCs) are prepared from animals between postnatal day 3 and 9. Neural tissues from young animals are more resistant to mechanical stress caused by the slicing procedure. Therefore, the age of the animal influences viability of slices (Connelly *et al.*, 2000) and also the incidence of seizure-like events (Albus *et al.*, 2013). Organotypic slice cultures have to be used within 2 weeks in culture, as they undergo synaptic reorganization over long term culturing (over 3 weeks) and develop spontaneous epileptiform activity (Albus *et al.*, 2013), which may be due to the formation of aberrant mossy fibre pathway *in vitro*. For organotypic slice cultures, one relies on the membrane interface method. The principle of the membrane interface culture method is to maintain the brain slices on a porous membrane filter at the interface between culture medium and a humidified atmosphere (Stoppini *et al.*, 1991). The medium provides adequate nutrition to the tissue through the membrane via capillary action. Investigation of induced epileptiform-like activity in hippocampal slices is a feasible approach for studying the propagation mechanisms, as it preserves the synaptic circuits as well as the cytoarchitecture, and also minimizes the number of animals for experimental usage.

1.1.11 Acute hippocampal slices

Acute hippocampal slices are prepared from older animals (> P12) and are used immediately on the day of preparation for recordings. The preparation of acute hippocampal slices is easier than organotypic slice culture preparation. Synaptic connectivity is altered to a lesser extent compared to the connectivity present under *in vivo* conditions at the time of preparation. Despite the limitation to record single unit activity, due to the presence of dead cells on the acute slice surface resulting from the slicing procedure, experimental recordings from acute preparations provide a stronger base to the recordings obtained from slice culture preparations (Cho *et al.*, 2007; Lein *et al.*, 2011). Therefore, acute slices

are considered the most appropriate *in vitro* model for investigation of brain structures.

1.1.12 Local field potentials and single unit activity

Recording of extracellular signals like local field potentials (LFPs) and single-unit activity (SUA) provide valuable information about how groups of neurons function collectively and how an individual neuron functions independently. LFP in the brain is an electrophysiological unit comprising the sum of dendritic synaptic activity occurring within a localized network of cells (Berens *et al.*, 2010). They are produced by synchronous activation of the dendrite of a neuron through synaptic input. The dendrite becomes a virtual sink and the soma, a source. The resulting dipole contributes to the measured LFP. In the case of pyramidal cells in the hippocampus, all dendritic arbours face in one direction opposing their soma. In this open field arrangement (Johnston *et al.*, 1995), their dendrites and somas are neatly aligned with each other. As a consequence of such a laminar structure of the hippocampus, currents evoked by synchronous activity in many synapses can be detected as a large summed up negative voltage deflection in the dendritic region (current sink – ionic current moves from extracellular space into neurons). A corresponding positive voltage (current source – ionic current flowing out of the principal neurons) in the cell body layer can be recorded by the extracellular electrodes (Andersen *et al.*, 2006).

In addition to characterization of LFP, investigation of SUA may provide a better understanding of network activity by correlating the spiking activity to the local network activity i.e., the LFPs. For example, one can search for cells taking the lead in huge synchronized network activities. Prediction of the time course of LFP with respect to spikes has been reported in certain areas of the brain (Rasch *et al.*, 2009). A change in firing rate of a certain subset of cells during interictal epileptiform discharges (IDs) is observed in human hippocampal formations (Alvarado-Rojas *et al.*, 2013). Heterogeneous spiking of neuronal populations during initiation, spread and course of a seizure and their

suppression during seizure termination has been reported in studies on human focal epilepsy (Truccolo *et al.*, 2011).

Therefore, investigation and characterization of network activity reflected in LFPs may provide valuable information regarding their origin and spread in epileptic conditions and aid in developing better treatment strategies.

1.2 Retina

The retina, which opens the door of perception to the visual world, functions as a miniature brain itself, where the neural signals are processed through distinct cell layers. The retina consists of three major cell layers (Figure. 1.3): **the outer nuclear layer** (ONL) comprising rods and cone cell bodies, **the inner nuclear layer** (INL) consisting of the somata of bipolar cells, amacrine cells and horizontal cells, and **the ganglion cell layer** comprising retinal ganglion cells (RGC) and displaced amacrine cell somata. RGCs constitute the retinal output through which information is passed on to higher areas of the central nervous system.

1.2.1 Cells of the outer retina (photoreceptors)

The first crucial step of converting the light signal to a neural signal occurs in the photoreceptors. Photoreceptors are of two types – rods and cones. According to the current state of knowledge, rods are capable of functioning at dim light (10^{-6} – 10^{2} cd/m^2) and cones function in bright light (10^{-2} – 10^{6} cd/m^2). However, rodent rods may function in bright light as well, as shown by a recent study (Tikidji-Hamburyan *et al.*, 2015). Cone photoreceptors are sensitive to different wavelengths and, are responsible for colour vision. These two types of photoreceptors have a pronounced outer segment that contacts the pigment epithelial cells of the retina. The outer segment of a rod has long, cylindrical structure comprising many discs and the outer segment of a cone is tapering with fewer discs. These outer segments play an important role in converting the light signal to electrical signal. The electrical signals are then passed on to the

pre-synaptic terminals of the photoreceptors that synapse with the bipolar and horizontal cells. In scotopic conditions (darkness), sodium channels in the photoreceptor membrane are open and allow an inward current (so-called "dark current"). This depolarizing current finally leads to a continuous release of glutamate.
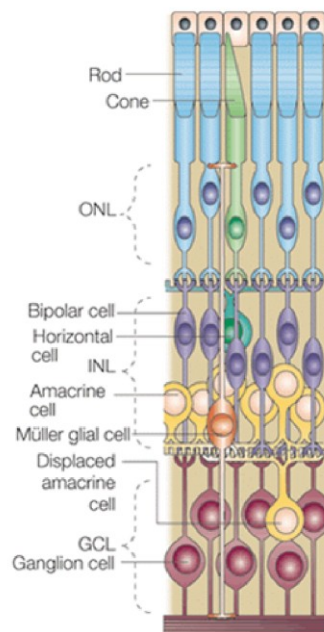
Figure 1.3: Schematic drawing of the retina. A detailed description is given in the text. Figure adopted from Dyer & Cepko, 2001 (Dyer & Cepko, 2001)

1.2.2 Cells of the inner retina (horizontal cells, bipolar cells, amacrine cells, ganglion cells)

The inner nuclear layer of the retina comprises horizontal cells, bipolar cells, and amacrine cells. Horizontal cells make lateral connections in the outer plexiform layer between photoreceptors and bipolar cells providing local and distant inhibition. Horizontal cells are coupled to each other by gap junctions. During scotopic condition, upon depolarization by the released glutamate from photoreceptors, they release the inhibitory neurotransmitter GABA onto nearby photoreceptors. Though the role of horizontal cells is controversial, they are

assumed to play an important role in providing lateral inhibition and regulate the amount of GABA released back onto the photoreceptors.

Bipolar cells connect the outer retina with the inner retina and transmit signals from photoreceptors to the ganglion cells. There are more than ten types of bipolar cells (Ghosh *et al.*, 2004; Wassle *et al.*, 2009), and are divided into ON and OFF cells (Kolb & Nelson, 1995; Euler *et al.*, 1996; Hartveit, 1997). ON bipolar cells are depolarized by light increments and OFF bipolar cells are depolarized by light decrements. Bipolar cells receiving information from rods are termed rod bipolar cell (RBC) and those that receive information from cones are referred to as cone bipolar cells (CBC). RBCs are of ON type only, whereas CBCs are of both ON and OFF types. Classification of cone bipolar cells is based on their response to the glutamate release at the presynaptic site which results in different polarizing mechanisms (Brandstätter *et al.*, 1994; Nomura *et al.*, 1994; Haverkamp *et al.*, 2001). ON cone bipolar cells depolarize at light increment which is caused by the sign-inverting synapse mediated by metabotropic (mGluR6) glutamate receptors. OFF cone bipolar cells preserve the polarity of the photoreceptor signal which is mediated by ionotropic (iGluRs) glutamate receptors (Ayoub & Copenhagen, 1991). Importantly, the synaptic connection between CBCs and ganglion cells occurs via iGluRs.

In the primary rod pathway, rod bipolar cells piggy-back on the cone bipolar cells via AII amacrine cells. The circuitry involves glutamatergic synapses from rod bipolar cells to AII amacrine cells. Gap junctional coupling connects AII amacrine cells with ON CBCs. AII amacrine cells make glycinergic synapses onto OFF cone bipolar cells. In a secondary pathway, rods directly interact with the cones via gap junctions (Raviola & Gilula, 1973; Famiglietti Jr & Kolb, 1975; Kolb & Nelson, 1993; Feigenspan *et al.*, 2001).

Amacrine cells are inhibitory neurons with cell bodies present in the inner plexiform layer and in the ganglion cell layer of the vertebrate retina. The term 'amacrine' means "axon – less" in Greek and was coined by Ramon y Cajal. However, poly-axonal amacrine cells have been reported (Vaney *et al.*, 1988; Greschner *et al.*, 2014). Their cell bodies are located in the inner nuclear layer

(INL) or in the ganglion cell layer. Notably ~50% of amacrine cells are "displaced" in the mouse retina (Wong & Hughes, 1987). Amacrine cells receive input from bipolar cells and other amacrine cells and also provide input to other amacrine cells, bipolar cells, and ganglion cells. More than twenty types of amacrine cells have been morphologically identified (Masland, 2001).

Retinal ganglion cells (RGCs) receive excitatory input from bipolar cells and inhibitory input from amacrine cells. Some RGCs are connected by gap junctions (Bloomfield & Volgyi, 2004). RGCs differ in their response to light, (Wassle & Boycott, 1991; Rodieck & Rodieck, 1998). Based on their response to light, they are broadly classified into ON RGC, OFF RGC, and ON-OFF RGC. ON ganglion cells are activated by light increment and OFF ganglion cells by a light decrement. ON-OFF ganglion cells are activated to both light increment and light decrement (Nelson *et al.*, 1993). Ganglion cells are the retinal output neurons and transmit the visual information to higher centres of the brain by generating action potentials.

1.2.3 Retinitis Pigmentosa

Retinitis Pigmentosa (RP) is a degenerative eye disorder caused by the progressive loss of photoreceptors in the retina (Jones & Marc, 2005). Several mouse lines mimicking the human disease of RP are currently investigated. These mouse lines differ in the onset time of photoreceptor degeneration – in the *rd1* mouse, photoreceptor degeneration starts early in the development whereas, in the *rd10* mouse, which is investigated in this thesis, photoreceptor degeneration starts later (around postnatal day 18). Loss of these photoreceptors results in the deprivation of the excitatory driving force i.e., a continuous source of glutamate release. This in turn results in alterations of the electrical activity of the inner and outer retinal neurons. Sodium channels and gap junctions shape the active oscillations in the *rd1* retina (Borowska *et al.*, 2011). Gap-junctionally coupled cones that are modulated by GABAergic inhibition from horizontal cells are involved in the generation of spontaneous synchronous activity in outer retinal neurons in *rd1* mice retina (Haq *et al.*,

2014). Aberrant spontaneous hyperactivity has also been detected in the inner retinal neurons – retinal ganglion cells in *rd1* mice (Stasheff, 2008; Stasheff *et al.*, 2011; Margolis *et al.*, 2014). Electrical coupling of AII amacrine cells and ON-cone bipolar cells as a source for such spontaneous activity has been reported in the same retinal degenerative model (Menzler & Zeck, 2011; Trenholm *et al.*, 2012). Similar spontaneous oscillatory activity has also been observed in *rd10* mice, a likely more realistic animal model for human RP in which photoreceptors degenerate at a slower rate than that of *rd1* (Goo *et al.*, 2011; Menzler *et al.*, 2014). Understanding the factors that influence such spontaneous electrical activity in a degenerated retina would help significantly in developing an efficient approach towards retinal prosthesis.

1.3 High density microelectrode arrays, a tool to study and characterize network activity under *in vitro* conditions

To understand the processing of neural activity within complex brain circuits, recording of electrical activity over a larger area of the neuronal tissue with high spatiotemporal resolution is required. So far, characterization of epileptiform-like discharges was achieved using metallic microelectrode arrays with limited spatial resolution (Pisciotta *et al.*, 2010; Gonzalez-Sulser *et al.*, 2012). High-density microelectrode arrays (Ferrea *et al.*, 2012) and high-density complementary metal oxide semiconductor (CMOS) based multitransistor arrays (Hutzler *et al.*, 2006) consist of thousands of recording sensors packed with a small inter-electrode distance. They provide an unprecedented spatial and temporal resolution for characterizing electrophysiological activity. Such arrays allow for spatiotemporal characterization of epileptiform discharges and may improve our understanding of neural dynamics in disorders of the central nervous system (CNS). Although SUA recording using low-density MEAs (Gonzalez-Sulser *et al.*, 2012) has been achieved, investigation of SUA with high-density MEAs provides single unit characteristics at higher spatial and temporal resolution. Recently, LFP patterns have been recorded *in vivo* using flexible, foldable low-density electrode arrays (Viventi *et al.*, 2011).

1.4 Aim of the study

Many studies have been carried out to investigate aberrant activity in neural tissues such as the cortex, the hippocampus or the retina independently. Only a few studies compare aberrant activity between different tissues and different models. Therefore, the aim of the current study was to characterize aberrant network activity in two neural tissues namely the hippocampus and the retina at different developmental stages, using a CMOS-based high-density microelectrode array at high spatial and temporal resolution. The comparison of aberrant electrical activity in different neuronal tissues may provide a better understanding about the mechanisms of neural degeneration that progress under neuropathological conditions. Additionally, it may also provide a better understanding of the organization of the cellular architecture and how it differs between different regions of the brain.

2 Materials and Methods

2.1 Animal Preparation

All animal preparations were performed in accordance with the animal use committee of the Natural and Medical Sciences Institute at the University of Tübingen.

Sprague Dawley (SD) rats (Janvier labs, France) were used for both organotypic and acute hippocampal slice preparations. The SD rats were used mainly for two reasons – their calm behaviour and ease of handling. For organotypic hippocampal slice preparations, young animals between postnatal day (P) 5 to 8 were used as they provide good viable slices for a longer duration. To avoid the challenges with dissection, younger animals (< P5) were ruled out and, as the preparations from older animals (> P8) yield slices which survive only a few days *in vitro,* animals older than P8 were not used for preparations (Thompson & Mason, 2005). In the case of acute slice preparations, rats aged between P13 to P30 were used.

Adult B6.CXB1-Pde6brd10/J (*rd10)* mice (mouse colony of Helmholtz Centre, Munich) aged between postnatal day P90-P100 were used for the retinal preparations.

2.2 Preparation of organotypic hippocampal slice cultures

For slice preparations, the brain was removed after quick decapitation and placed in ice cold Gey's balanced salt solution (GBSS, 100 ml GBSS + 1.5 ml 50% glucose, Sigma-Aldrich Chemie GmbH, Germany). It was trimmed by cutting off the rostral and caudal part. Transverse slice sections (400 µm thickness) of the cortico-hippocampal region were obtained using a Leica Vibratome (VT 1200S, Leica). The slices were gently slid onto the membrane insert (Merck Millipore, Merck Chemicals GmbH) and supplemented with pre-incubated culture medium (50% Minimum essential medium (MEM), 25%

Hank's balanced salt solution (HBSS), 25% heat inactivated horse serum, 1 mM Glutamine, 25 mM D-Glucose), and placed in an incubator with 5% CO_2, 95% O_2 at 37°C. Thereafter, the medium in the culture dish was replaced with pre-incubated fresh medium every other day. The preparation followed the protocol of Stoppini *et al* (Stoppini *et al.*, 1991) with a few modifications (SD rats instead of Wistar rats and animal aged between P5 to P8 instead of P2 to P23). Slices with good gross morphological structure were selected. Cultures between DIV (Day *in vitro*) 6 and DIV14 were used for experimental recordings to avoid spontaneous epileptiform-like activity (ELA) which develops upon longer cultivation under *in vitro* conditions (Albus *et al.*, 2013).

2.3 Preparation of acute hippocampal slices

All the chemicals used hereafter were purchased from Carl Roth GmBH+Co.KG, Karlsruhe, Germany unless otherwise stated.

Prior to brain isolation, the animal was initially anaesthetized using CO_2 followed by quick decapitation with large sharp scissors or a guillotine. The brain was isolated and placed in ice-cold sucrose buffer (250 mM Sucrose, 2 mM KCl, 1.2 mM $NaH_2PO_4^.H_2O$, 0.5 mM $CaCl_2^.2H_2O$, 7 mM $MgCl_2·6H_2O$, 11 mM Glucose, 26 mM $NaHCO_3$) supplemented with carbogen gas (95% O_2 and 5% CO_2) for 10 minutes to recover from the dissection stress. Small parts from the rostral and caudal side were trimmed. All the following steps were carried out under ice cold conditioned sucrose buffer supplemented with carbogen, until the incubation of slices. The two hemispheres were separated with a cut in the sagittal plane. Each hemisphere was cut in the horizontal plane from the dorsal side to obtain the ventral part of the brain. The trimmed hemispheres were glued and placed in the slicing chamber with the dorsal side towards the microtome stage. Afterwards, transverse slices of cortico-hippocampal sections of 400 μm thickness were obtained. The prepared slices were trimmed off the cortical region to obtain the hippocampal slices and incubated at 37°C for an hour and later stored at room temperature for rest of the recordings in low Ca^{2+} high Mg^{2+} ACSF solution (125 mM NaCl, 2.5 mM KCl, 1.25 mM $NaH_2PO_4^.H_2O$,

2 mM $CaCl_2·2H_2O$, 1.3 mM $MgCl_2·6H_2O$, 25 mM Glucose, 26 mM $NaHCO_3$) supplemented with carbogen gas. Acute slices with good gross anatomical structure were selected for recording.

2.4 Retina preparation

All the retina preparations were carried out under dim red light. Prior to eye removal, the *rd10* mouse was anesthetized with CO_2 and killed by cervical dislocation. The eyeballs were removed with the help of tweezers and placed in AMES (A1420, Sigma-Aldrich Chemie GmbH, Germany) solution saturated with carbogen. The eye was initially hemisected and the lens and vitreous body were removed. The retina was gently peeled off the sclera and stored in AMES solution until used for recording. The entire preparation was performed at room temperature.

2.5 Neurochip and technical specifications

Extracellular recordings were made using the so-called "Neurochip" (version G1183), a high-density multitransistor array comprising 16,384 sensors in an area of about 1 mm^2 (Figure 2.1A and B). Details of this chip have already been presented (Lambacher *et al.*, 2011; Zeck *et al.*, 2011). The sensors are arranged in a 128 x 128 layout. The entire sensor array can be sampled at 6 kHz. The equally spaced sensors have a distance of 7.4 µm and a sensor diameter of 6.3 µm. The chip surface has a homogenous coating of ~30 nm TiO_2/ZrO_2 which separates the recording solution from the sensor transistors. As a default configuration, 8192 sensors i.e. alternative columns (128 x 64) at a sampling frequency of 12,207 Hz was used for recording of extracellular voltages. Prior to every measurement, the sensor's transistors were calibrated by applying an AC voltage of 3 mV peak-to-peak amplitude at a frequency of 70 Hz (Eversmann *et al.*, 2003; Lambacher *et al.*, 2004) to the recording solution. This voltage couples through the insulating oxide to the gate of the sensor transistor and thereby modulates the source-drain current. During experiments,

the ionic currents produced at the surface of the slice facing the recording array changes the local voltage with respect to the bath electrode. The response of each sensor transistor is solely determined by the potential above the insulating TiO_2/ZrO_2 layer, averaged over the diameter (6.3 µm) of the top contact. The continuous recording was restricted initially to only one second. Technical changes performed on the recording setup allowed continuous recording time up to 5 seconds. In recordings longer than 5 seconds, for technical reasons, a reset frame of ~100 ms was introduced every 5 seconds to avoid drift. These short reset frames are removed in the concatenated recordings shown later in the results section.
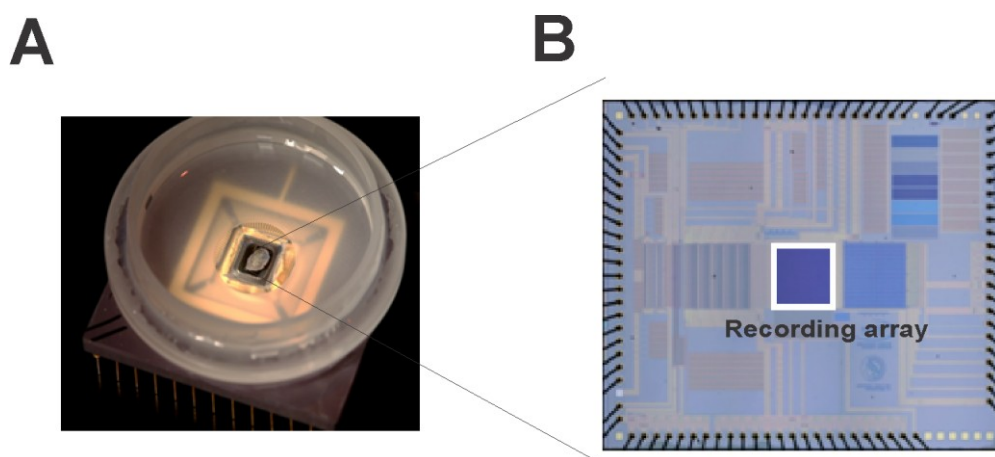
Figure 2.1: Neurochip and its features. A: Prototype of a "Neurochip" with the recording chamber. A piece of retina (white) is interfaced onto the planar chip surface. This neurochip is surrounded by a large culture chamber (grey) to provide the tissue with medium. B: Top view of the chip surface showing the recording array of 1 mm^2 with 16,384 sensors.

2.6 Microelectrode array and technical specifications

Additionally extracellular recordings were made using microelectrode arrays (256MEA200/30-ITO) supplied by Multichannel Systems MCS GmbH, Reutlingen, Germany. The recording array had 252 recording electrodes and 4 ground electrodes arranged in a 16 X 16 layout grid which was embedded in a transparent glass substrate. The recording electrodes were 30 µm in diameter each and had an inter-electrode spacing of 200 µm. The electrodes were made of titanium nitride (TiN). Contact pads and tracks were made of transparent indium tin oxide (ITO), whereas the lines were isolated with silicon nitride.

These 30 µm diameter electrodes had an impedance of approximately 30-50 kΩ. All the recordings were made at a sampling rate of 25 kHz.

2.7 Placement of organotypic hippocampal slice cultures from membrane inserts on Neurochip and microelectrode array

The hippocampal slice along with the membrane insert was cut using a sharp scalpel blade without damaging the slice of interest under a sterile bench. The remaining slices on the insert were returned to the incubator. A small volume of recording buffer was placed on the recording array pre-coated (1hr) with poly-L-lysine (1 mg/ml, P2636, Sigma-Aldrich Chemie GmbH, Germany). The insert with the attached slice was placed over the recording array such that the slice was in direct contact with the recording array. Care was taken for a precise placing of the hippocampal region of interest and, good attachment was achieved by gently removing the excess buffer with a small piece of filter paper. For recordings on low-density MEA, a small platinum grid with nylon threads glued to one side of the platinum grid (weighing 492 mg) was placed over the slice to prevent it from detachment. Control ACSF solution was added and the electrode array was mounted onto the recording socket.

2.8 Placement of acute hippocampal slices on Neurochip and microelectrode array

The pre-incubated cortico-hippocampal slice was trimmed to obtain only the hippocampal slice. A small volume (~50 µl) of recording buffer was placed on the recording array pre-coated (1 hr) with poly-L-lysine and the slice was placed into this volume. A good attachment of the slice was achieved by gently removing the excess buffer with a small piece of filter paper. For experiments performed on low-density MEAs, a small platinum grid with nylon treads glued to one side of the platinum grid (weighing 492 mg) was placed over the slice to prevent detachment. The recording chamber was filled with control ACSF solution and mounted on to the recording socket.

2.9 Recording of organotypic and acute hippocampal slices on Neurochips

The Neurochip with the hippocampal slice culture mounted on the recording array was placed into the recording socket and the inlet and outlet tubing's for perfusion were fixed. The slice was perfused with oxygenated (95% O_2 and 5% CO_2) control ACSF solution (126 mM NaCl, 2 mM KCl, 1.2 mM $NaH_2PO4^{.}H_2O$, 2 mM $CaCl_2^{.}2H_2O$, 2 mM $MgCl_2^{.}6H_2O$, 11 mM Glucose, 26 mM $NaHCO_3$; pH 7.4) to maintain physiological conditions. The temperature of the inlet flow was set between 36°C and 37°C using a temperature control system. A flow rate of 5 ml/min was maintained throughout the recording protocol. The recording setup, comprising a battery-powered amplifier, a custom-built computer with 16 data-acquisition cards (GaGe, Canada) and a function generator is shown in Figure 2.2A. The Neurochip recording chamber and the perfusion system is shown in Figure 2.2B.
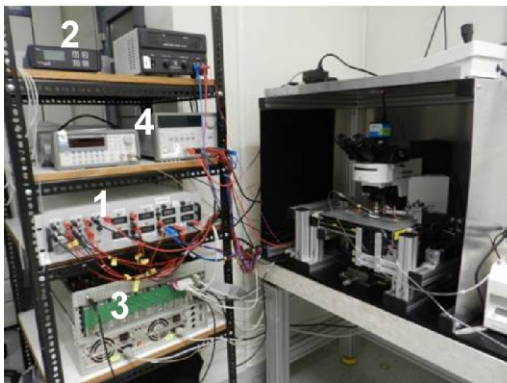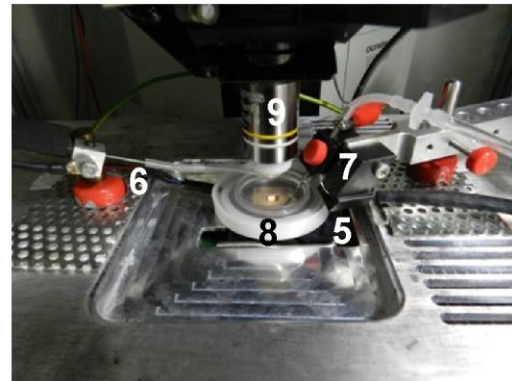
Figure 2.2: Neurochip recording setup. A: Picture of the Neurochip recording set up with power supply (1), temperature controller (2), data acquisition cards (3), function generator (4).B: Recording stage with Neurochip placed in the recording socket (5), inlet (6) and outlet (7) of the perfusion attached with the overflow detector (8), objective (9) for visual control of slice orientation.

2.10 Recording of organotypic and acute hippocampal slices on microelectrode arrays

Microelectrode arrays with the hippocampal slice culture were placed on the recording socket and the inlet, outlet tubings for perfusion were fixed. The inlet flow temperature was maintained between 36°C and 37°C using a temperature control system. The slice was perfused with oxygenated ACSF solution (95% O_2 and 5% CO_2) with a pH of 7.4 to maintain the physiological environment and the flow rate was maintained at 1.5 ml/min.

2.11 Induction of epileptiform–like activity (ELA) in organotypic and acute hippocampal slices

For inducing ELA in both organotypic and acute hippocampal slices, high K^+ zero Mg^{2+} ACSF solution (126 mM NaCl, 5 mM KCl, 1.2 mM $NaH_2PO_4^.H_2O$, 2 mM $CaCl_2^.2H_2O$, 11 mM Glucose, 26 mM $NaHCO_3$) was used. In a second protocol, control ACSF solution with $GABA_A$ receptor blocker bicuculline methiodide (BMI, 10 µM /30 µM, 2503, R & D systems, Germany) was used to induce epileptiform-like activity. For changing the recording solution during different treatments, the source of perfusion inlets was changed accordingly.

2.12 Retina placement and recording

The isolated retina was trimmed to discard tissue that was damaged during surgical handling. The retinal portion was then sucked gently and pipetted onto the Neurochip recording chamber (pre-coated with poly-L-lysine), containing the recording solution. Care was taken to place the retinal ganglion cell surface onto the recording electrodes. Excess buffer was then gently removed with a filter paper, to bring the retina in close contact with the recording array. No additional grid was necessary to hold the retina in place. The retina was then

perfused with carbogenated AMES medium maintained between 33°C and 36°C at a flow rate of 7 ml/min.

2.13 Pharmacological agents

All pharmacological drugs were prepared as stock solutions in distilled water. For drug application during experiments, the stock solutions were first dissolved in the recording solution, and later bath-applied through continuous perfusion. Drugs included strychnine (S0532, Sigma-Aldrich Chemie GmbH, Germany), gabazine (SR106, Sigma-Aldrich Chemie GmbH, Germany), 6,7-dinitroquinoxaline-2,3-dione disodium salt (DNQX, 2312, Tocris Biosciences), meclofenamic acid, (M4531, Sigma-Aldrich Chemie GmbH, Germany), carbenoxolone (C4790, Sigma-Aldrich Chemie GmbH, Germany), and bicuculline methiodide (2503, R & D systems, Germany).

2.14 Data analysis

2.14A Detection of extracellular action potentials and local field potentials in Neurochip data.

The bandwidth of the acquisition hardware of the Neurochip was set between 0.1 Hz - 12 kHz. This was chosen in order to cover the relevant frequency components of both single action potentials (APs) and LFPs during a single measurement. This thereby allowed for coincidence analysis between these two phenomena. Although the bandwidth could be increased to 20 kHz by skipping sensors which did not record any region of the slice, it was only done occasionally. The resulting dataset is essentially a superposition of all detected frequency components within the hardware's bandwidth. Digital signal processing was applied to separate frequency bands after recording to create virtual channels for APs and LFPs. These channels were derived using selected high- and low-pass filters. For the LFP channel, quasi-stationary charge distributions were eliminated and signal quality improved with a temporal high-

pass of 6 Hz and a temporal low-pass of 40 Hz. For the AP channel, residual LFP-Signal components were eliminated using a 350 Hz high-pass filter.

Automated thresholding at 5-Sigma (in normal distribution equivalent units) of median absolute deviation was used to extract timings of AP and LFP occurrences. The successful separation and detection of these events were confirmed by parallel visual inspection of both channels; taking into account the spatial extent of the detected signals. Temporal traces from somatic cell layer were used for characterization of field potentials and SUA.

2.14B Estimation of propagation velocity of a local field potential

Custom-written software in Python (Python 2.7) was used to estimate the propagation velocity based on centre of mass tracking. This software was developed by F. Helmhold, a scientist in the Neurochip Research Group, Natural and Medical Sciences Institute at the University of Tuebingen.

Centre of Activation

Calculation

To derive a measure for the mean propagation velocity of an LFP, a measure for its position was established first. For this purpose, a centre of activation (COA) was defined, analogous to the concept of centre of mass. Each sensor-position ($\vec{r_i}$) of the array contributes to the centre of activation ($\vec{R}$) with a weight (P_i) that was derived from the signal strength at that particular point (Figure.2.3).

$$\vec{R} = \frac{1}{P_{tot}} \sum_{i=1}^{N} \vec{r_i} P_i$$

The total weight (P_{tot}) which normalizes the expression was defined as:

$$P_{tot} = \sum_{i=1}^{N} P_i$$
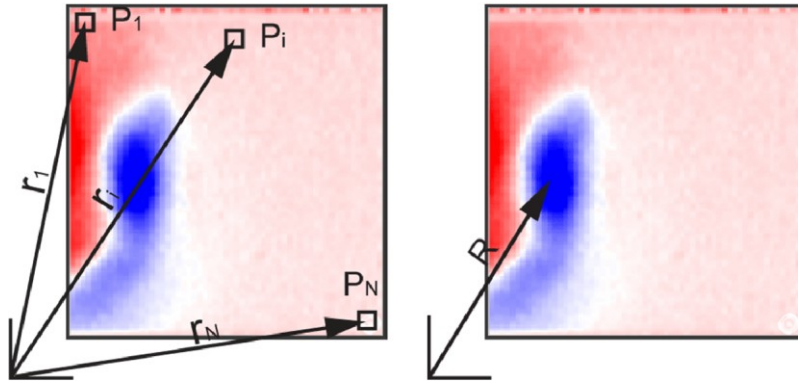
Figure 2.3: Illustration of positions, weights and resulting centre of activation. Two copies of the same electrical image taken during an LFP event are superimposed with vectors to illustrate the association of pixel positions ($\vec{r_i}$) and weights (P_i) (left) and the centre of activation ($\vec{R}$) yielded by weighted summation of all pixel positions (right).

As signals can be positive and negative, while weights have to be positive, only one polarity can be considered at a time. In all of our recordings, a negative polarity was selected to track the localised p-spike.

Using the power of the signal (P) as the weight instead of the raw voltage value (U) proved to be more robust and resulted in tighter tracking adhesion. The relationship between voltage and power/weighting was, therefore:

$$P = U^2$$

In Figure 2.3, the blue colour represents negative values of the extracellular voltage, whereas the red colour represents positive values of the extracellular voltage.

Differentiation

The previous process applied to a sequence of frames yields, successive centres of activation ($\vec{R_i}$) . Numerical differentiation of subsequent COA transforms this into a set of finite differences ($\overrightarrow{\Delta R_i}$), each representing the distance which the centre of activation travelled between two sampled time points.

$$\overrightarrow{\Delta R_i} = \vec{R}_{i+1} - \vec{R}_i$$

$$\vec{R}_1, \vec{R}_2, \ldots, \vec{R}_M \xrightarrow{\Delta} \overrightarrow{\Delta R_1}, \overrightarrow{\Delta R_2}, \ldots, \overrightarrow{\Delta R_{M-1}}$$
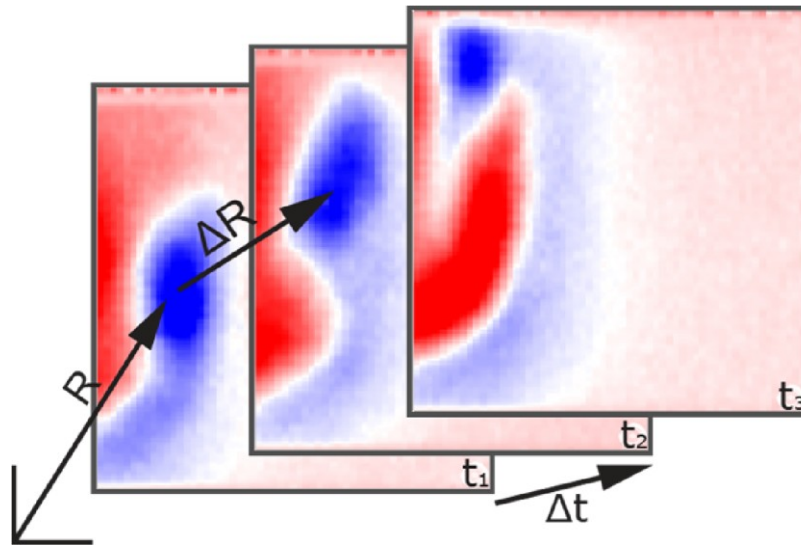
Figure 2.4: Concept of differentiation in space and time. Stacked electrical images of an LFP at successive time points from bottom to top. $\vec{R}$ points to the location of the COA at timepoint t_0. $\overrightarrow{\Delta R}$ and Δt indicate the change in location and the time passed between t_0 and t_1 respectively.

Velocities

The velocity of propagation of the centre of activation was then calculated by dividing the length of each spatial step $(\overrightarrow{\Delta R})$ by the corresponding time step (Δt).

$$V = \frac{\|\overrightarrow{\Delta R}\|}{\Delta t}$$

2.14C Microelectrode array data recording and analysis

MC rack (Software from Multichannel system, MCS GmbH) was used for recording and displaying low-density MEA data. A custom-written software using MATLAB (Release 2011b, Mathworks, Nattick, USA) was used for frequency analysis of LFPs. The software was developed by T. Herrmann, a scientist in the Neurochip Research Group, Natural and Medical Sciences Institute at the University of Tuebingen. Each data file comprised a recording of 4 minutes. Recordings were done during control conditions, induced ELA and pharmacological treatments.

2.14D Detection of local field potentials and estimation of its count

The raw data from each electrode signal was smoothed with a Savitzky-Golay algorithm, 101 supporting data points, a polynomial model with a degree of 3, to reduce the portion of high frequencies. For the following step of threshold detection, the absolute values of the smoothed signal were taken to obtain negative as well as positive field potentials. The detection threshold was set manually to 13.5 times the standard deviation of the signal. The threshold is set in such a way, as to retain the spikes by preventing the loss due to high threshold values, and to avoid false signals due to noise crossing in a low threshold. When the processed signal crosses the threshold, an occurrence of an LFP was assumed and counted. To obtain the accurate timing of an LFP, peak detection of the LFP was done and half the maximum value was obtained by extrapolation. The crossing between the linear extrapolation and the baseline gives the accurate time stamp of the LFP and the number of timestamps gives the LFP count.

2.15 Statistical analysis

To test for statistical significance, mean propagation velocities of forward and backward propagations were compared with two sample t-tests.

3 Results

3.1 Characterization of electrical activity in organotypic hippocampal slices

3.1.1 Electrical imaging of spontaneous local field potentials and single unit activity

To electrophysiologically characterize spontaneous field potentials in organotypic hippocampal slices, hippocampal slice cultures were prepared by membrane interface method (Stoppini *et al.*, 1991). Slice cultures between DIV 6 and DIV 14 were used for electrophysiological recordings. The slice cultures were tightly interfaced to the recording array of the Neurochip (Figure 3.1A-D) and spontaneous activity was investigated from slice preparations perfused continuously with ACSF solution (flow rate of 5 ml/minute). The bath temperature was maintained between 36°C and 37°C throughout the measurements.

A total of 26 membrane interfaced organotypic slices were measured and evaluated. In 50% of them (n=13), spontaneous LFPs were detected. To investigate the spontaneous LFPs in hippocampal subregions, different slices were positioned with different subregions onto the 1 mm^2 recording area of the Neurochip: DG (Figure 3.1A), CA3 (Figure 3.1B) and CA1 (Figure 3.1C). Spontaneous LFPs and SUA were recorded simultaneously in short epochs of 4 to 5 seconds. For these and other examples (Figure.3.1D) the electrical activities were recorded and assigned to the directions DG-CA3 or CA3-CA1. Different temporal filter settings as mentioned in the methods section 2.13A were used for the identification of LFPs and SUA. Spontaneous SUA was detected without averaging across multiple regions. An example of a temporal trace recorded on one sensor (marked in Figure 3.1D) is shown (Figure 3.2A). The highest number of single units identified per slice was 5. These units were detected in the recording of short epochs of 4 seconds and the spiking occurred too infrequently, to determine their firing rate. A zoomed trace of a single spike

with spike amplitude between –0.2 and –0.4 mV (Figure 3.2C), and the corresponding spatial electrical image of the spike at sensor position is marked with a square (Figure 3.2E).

Spontaneous LFPs (Figure 3.2B) were detected simultaneously with SUA. LFP amplitude ranged between ±0.2 and ±0.4 mV (Figure 3.2D). These spontaneous LFPs were further characterized for their pattern of occurrence. LFPs were observed along the pyramidal cell layer. Spontaneous stationary field potentials (n=10 slices) and field potentials which emerge and disappear across the array (n=3 slices) were observed. An electrical image of a stationary LFP in the CA3 region is shown (Figure 3.2F). A concatenated trace from twelve consecutive recordings shows the occurrence of few spontaneous LFPs in another slice (Figure 3.3C). The trace of a single field potential in Figure 3.3D shows the waveform of a spontaneous LFP. Spontaneous field potentials lacked the typical p-spike seen in field potentials during epileptiform-like activity. These spontaneous field potentials appeared and disappeared across the pyramidal cell layer and were active for 10 to 15 ms. Colour coded spatial electrical image of extracellular voltage recording of this LFP is shown in Figure 3.3E with an inter-frame interval of 2 ms.

Summary

During the spontaneous activity in cultured slices, both spontaneous SUA and LFPs were observed. In the majority of slices (76%), the spontaneous LFPs were stationary.
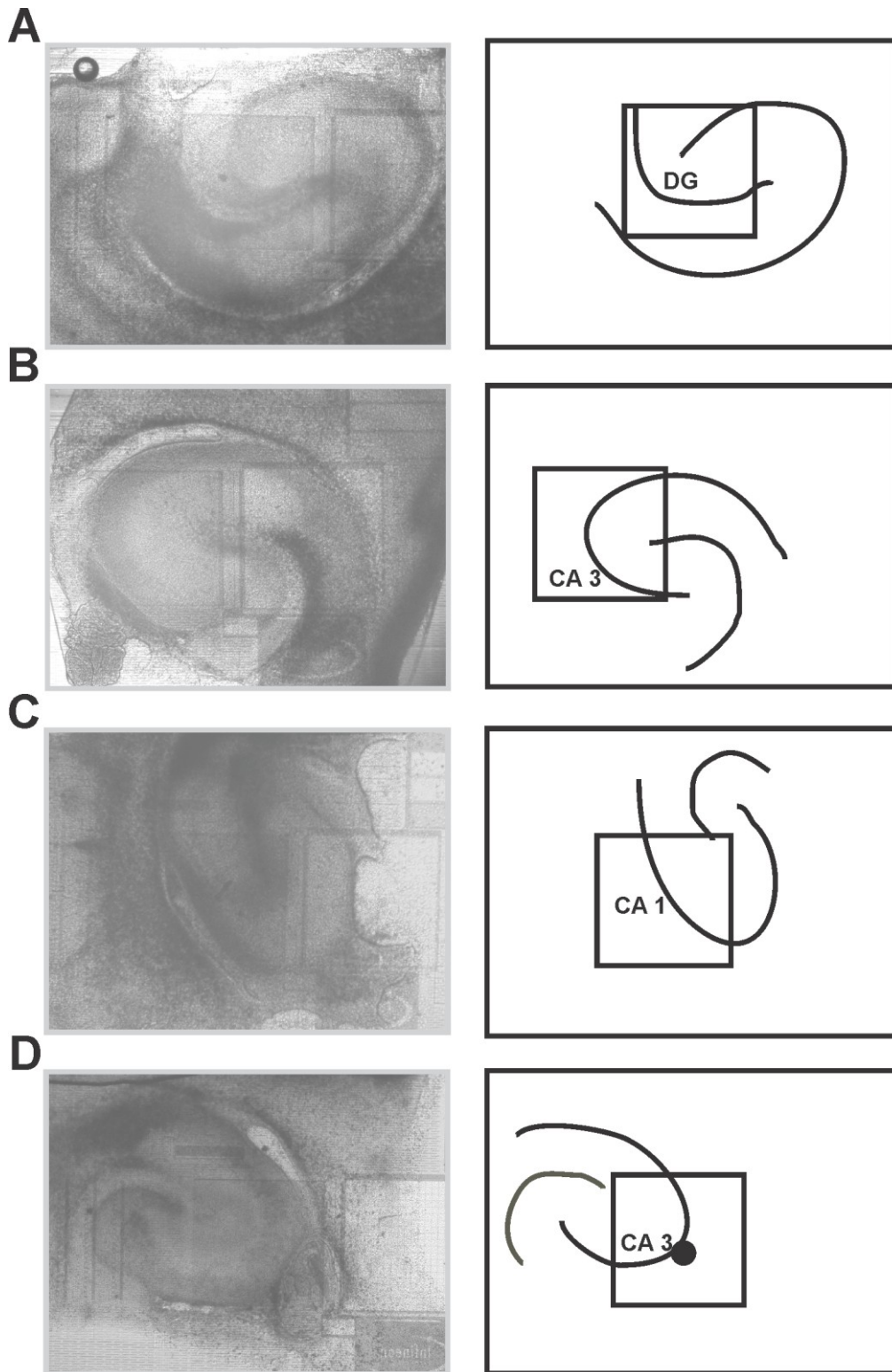
Figure 3.1: Different regions of organotypic hippocampal slice cultures interfaced to the recording array of the Neurochip. The left panel represent images of the interfaced slices, the right panel represents the schematics of the interfaced hippocampal subregions with the square-shaped recording array. A: OHC at DIV 6 with the DG region on the recording array. B: OHC at day 9 with the CA3 region on the recording array. C: OHC at DIV 7 with the CA1 region on the recording array. D: OHC at DIV 10 with the CA3 region on the recording array.
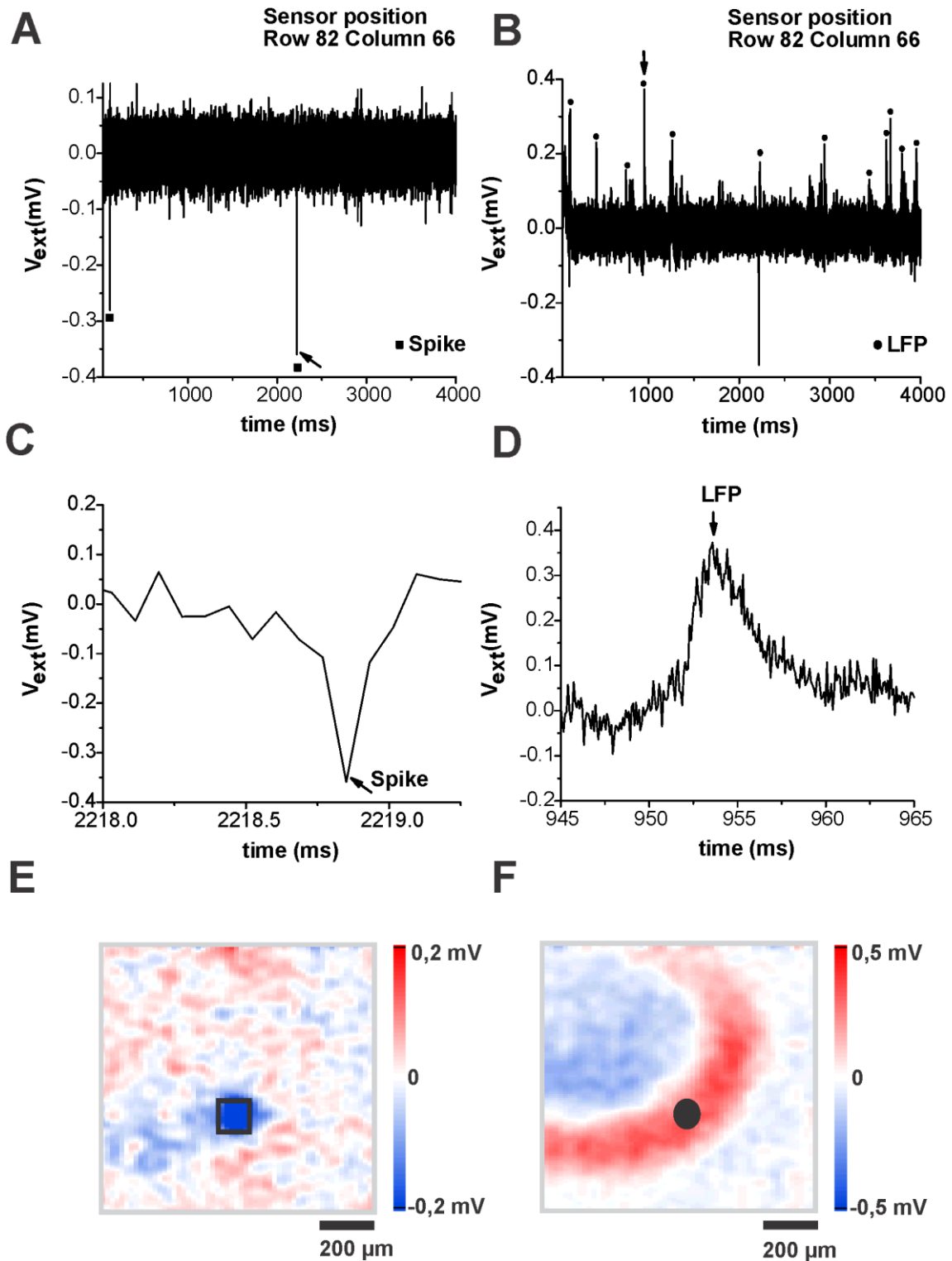
Figure 3.2: Spontaneous stationary local field potentials and single unit activity in the CA3 region of organotypic hippocampal slice cultures. A: Temporal trace of spontaneous SUA. B: Temporal trace of a spontaneous LFP. C: Zoomed temporal trace of a spike marked in Figure 3.2A. D: Zoomed temporal trace of an LFP marked in Figure 3.2B. E: Spatial electrical image of a spike at a sensor position marked with a square. F: Spatial electrical image of an LFP from the same sensor location marked with a dark circle. All the traces were taken from the marked sensor position (row 82, column 66). Row numbers start from 1-128 (top to bottom), column numbers from 1-128 (left to right).
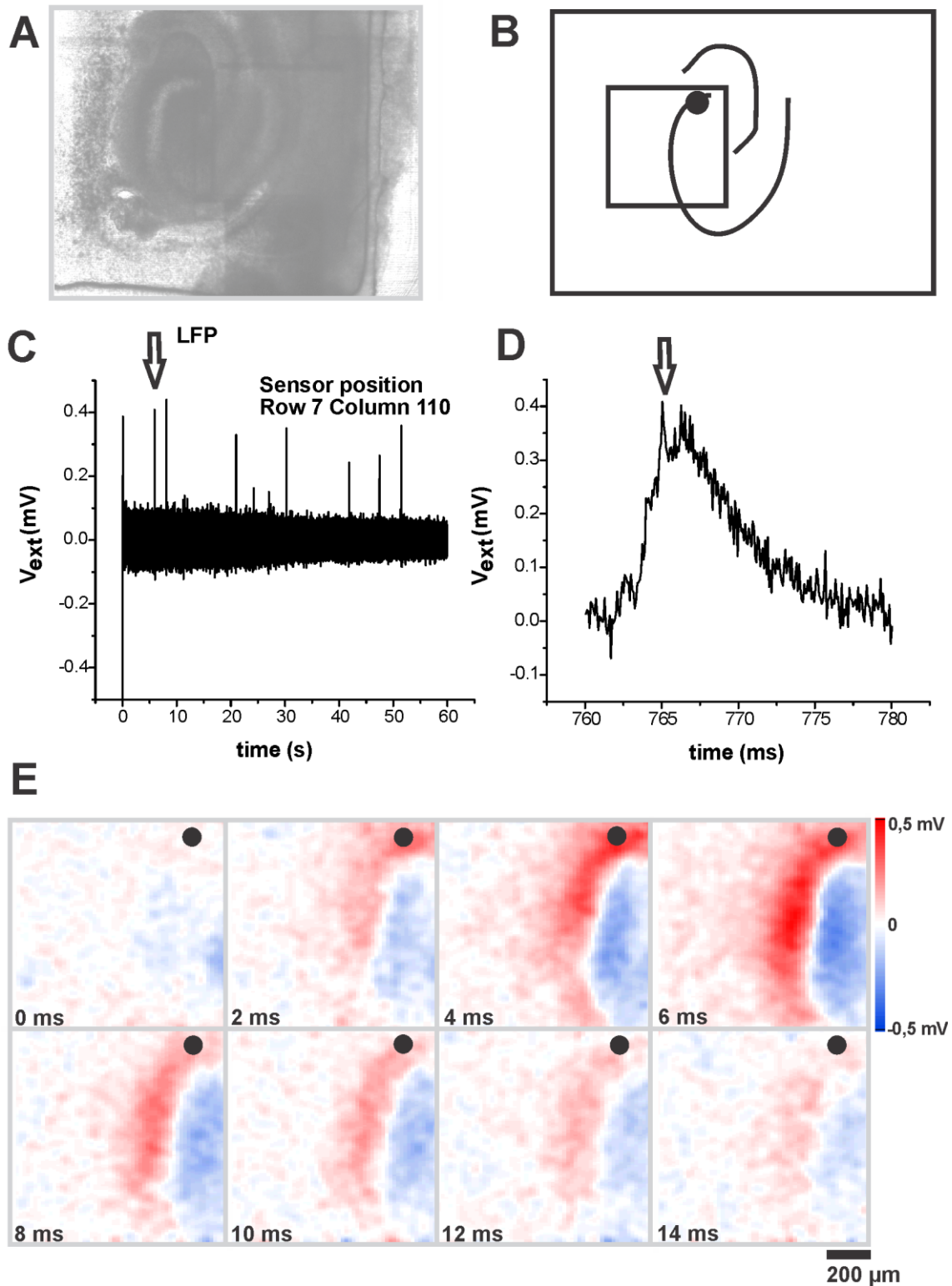
Figure 3.3: Spontaneously emerging and disappearing local field potentials in organotypic hippocampal slice cultures. A: OHC at DIV 7 interfaced to the recording array of the Neurochip. B: Schematic drawing of the region of the hippocampal slice imaged on the Neurochip. C: Concatenated temporal trace of spontaneous activity recorded in the CA3 region at the sensor position marked with a dark circle in panel B. D: Zoomed temporal trace of a spontaneous LFP marked with an arrow in Figure 3.3C. E: Spatial electrical images of spontaneously emerging and disappearing LFP. All the traces were taken from the marked sensor position (row 7, column 110).

3.1.2 Electrical imaging of local field potentials during high K$^+$ zero Mg^{2+} induced epileptiform-like activity

It is well known that elevated potassium (Jiruska *et al.*, 2010) and reduced magnesium concentration (Mody *et al.*, 1987) in the extracellular medium, induces a hyper-excitable condition that leads to ELA in hippocampal slices. In the current study, to investigate and characterize aberrant activity (i.e., ELA), Mg^{2+} free ACSF with elevated K$^+$ (5 mM) concentration in the extracellular medium was used to induce hyper-excitable conditions. This buffer combination is referred to as 'treatment buffer' in this thesis hereafter. For extracellular recordings, the membrane interfaced slices were perfused initially for 15 to 20 minutes with a control solution of normal ACSF, oxygenated with 95% O$_2$ and 5% CO$_2$, with the bath temperature maintained between 36°C and 37°C throughout the measurements.

Thereafter, ELA was induced by perfusing the interfaced slices (n=9) with treatment buffer. ELA was recorded in the CA3 region of the hippocampal slices within 10 minutes of perfusion with the treatment buffer. As a typical ELA lasts for longer than 5 seconds, extracellular recordings were made in epochs of 5 seconds for 1 to 3 minutes (see section 2.5 for details). The short recordings were concatenated to obtain a quasi-continuous trace. A typical temporal trace of an ELA recorded at the position marked in the schematic drawing (Figure 3.4B) is shown in Figure 3.4C. In the following, we consider the first part of the LFP which is determined by the population spike (p-spike). This part is easily identified in the LFP and spatially confined on the recording array. The spatiotemporal dynamics of the p-spike (shown in Figure 3.4E as a zoomed trace of marked LFP from Figure 3.4D) was then further investigated. Colour coded spatial electrical images of the propagation are shown, with an inter-frame interval of 2 ms, with the sensor position marked with a dark circle (Figure 3.4F). The propagation pattern and the propagation velocity were analysed across p-spike. The analysis of SUA will be given in section 3.3.
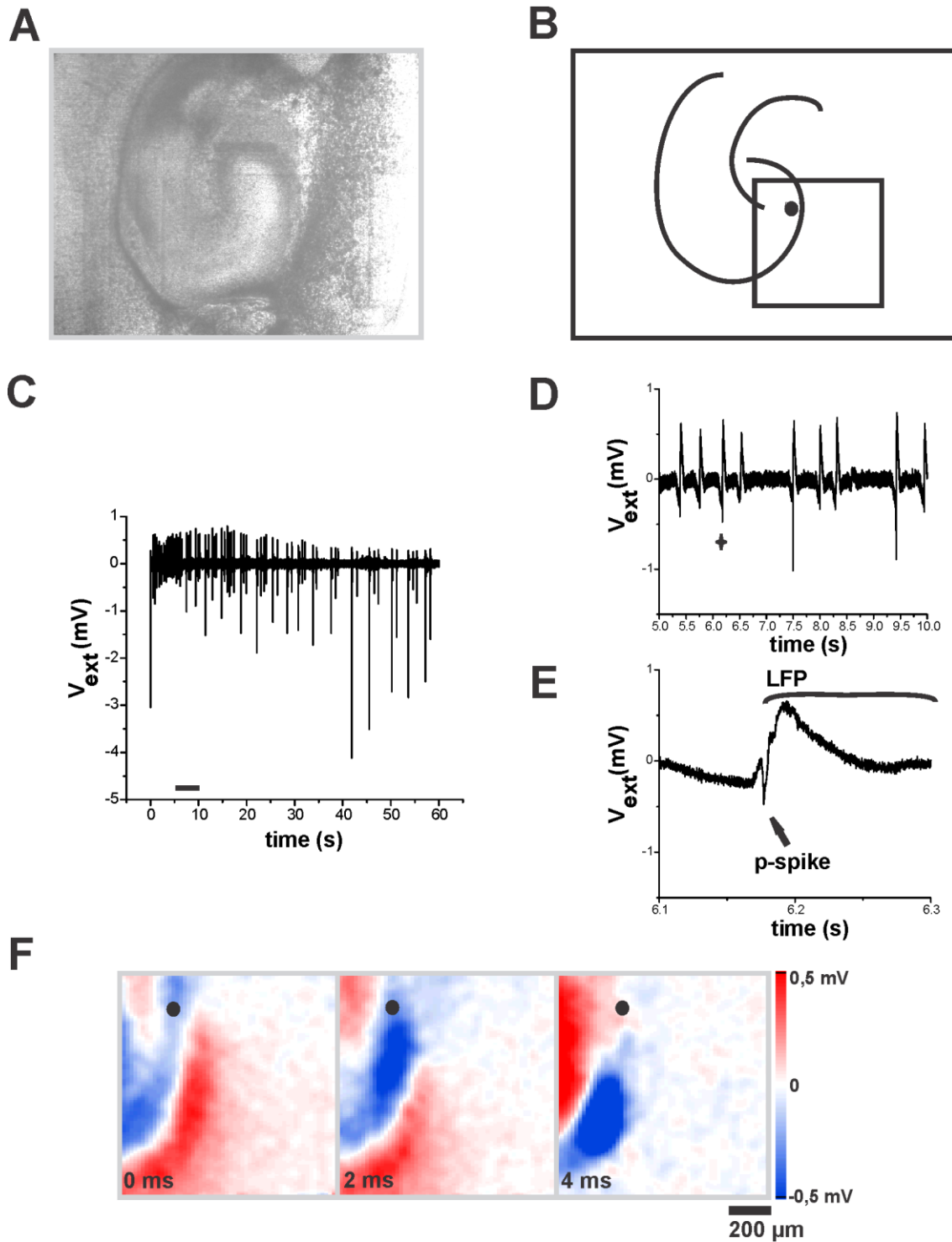
Figure 3.4: Electrical imaging of propagating local field potential during high K$^+$ zero Mg^{2+} induced epileptiform-like activity. A: OHC at DIV 7 interfaced to the recording array of the Neurochip. B: Schematic drawing of the region of the hippocampal slice imaged on the Neurochip. C: Temporal trace of an ELA recorded in the CA3 region (sensor position marked with a dark circle in Figure 3.4B). D: Zoomed temporal trace of a part of C (marked with a bar in Figure 3.4C). E: Zoomed temporal trace of an LFP and its p-spike (marked with a plus in Figure 3.4D). F: Spatial electrical images of a propagating p-spike of an LFP. The dark circle represents the sensor position. All the traces were taken from the marked sensor position (row 25, column 34).

3.1.2a Propagation pattern of the p-spike of a local field potential during high K⁺ zero Mg²⁺ induced epileptiform-like activity

A typical ELA comprises an ictal, a preictal and a postictal phase. The ictal phase mainly consists of high frequency oscillations with high amplitudes, which persists for a long duration of several seconds. This was observed for 10 to 30 seconds in picrotoxin model (Hablitz & Heinemann, 1987) or 5 to 48 seconds in 4-AP model (Avoli *et al.*, 1996). Similar activity of ictal-like activity was observed in our recordings on high-density MEAs (Figure 3.4C). The preictal phase is the initial phase of an ictal activity where the oscillations have just begun. The postictal phase refers to the time following an ictal activity, where the oscillations frequency and amplitude declines and thereby terminates an ictal activity. Interictal phase refers to the time between two ictal activities.

In the following, p-spikes during different phases of induced ELA were evaluated. In Figure 3.5C interictal activity is shown. LFPs recorded from the CA3 region of the hippocampal slice were used to characterize propagation pattern and evaluation of propagation velocities. It was observed that the LFPs propagated from DG towards the CA3 region, in accordance to the classical trisynaptic pathway (forward propagation). The electrical activity propagates via mossy fibres through excitatory connections to the pyramidal cells in the CA3 region. The p-spike of a forward propagating LFP lasted for 1.35±0.1 ms, measured as full-width at half-amplitude minimum.

In total, 601 LFPs in 9 slices exhibiting ELA were analysed for propagation patterns and propagation velocity. Of the evaluated p-spikes, 65% (n=386) showed propagation along the classical trisynaptic pathway. Colour coded spatial electrical images of forward propagating LFP in successive frames with an inter-frame interval of 2 ms are shown in Figure 3.5F, top row.

However, a considerable percentage of p-spikes also propagated from the CA3 region towards the DG. Colour coded spatial electrical images of "backward" propagating LFP in successive frames with an inter-frame interval of 2 ms are

shown in Figure 3.5F, bottom row. The first p-spike in the bursts presented in Figure 3.5C propagated backwards. A zoomed trace of a backward propagating p-spike is shown in Figure 3.5E. The mean duration of the backward propagating p-spike is 1.06±0.08 ms (full-width at half-amplitude minimum was evaluated from a subset of n=13 p-spikes) and has an amplitude of ~3 mV. Backward propagation was exhibited in 35% of the evaluated p-spikes (n=215).

Summary

Forward and backward propagating p-spikes were detected in OHCs under high K^+ zero Mg^{2+} induced epileptiform-like activity.
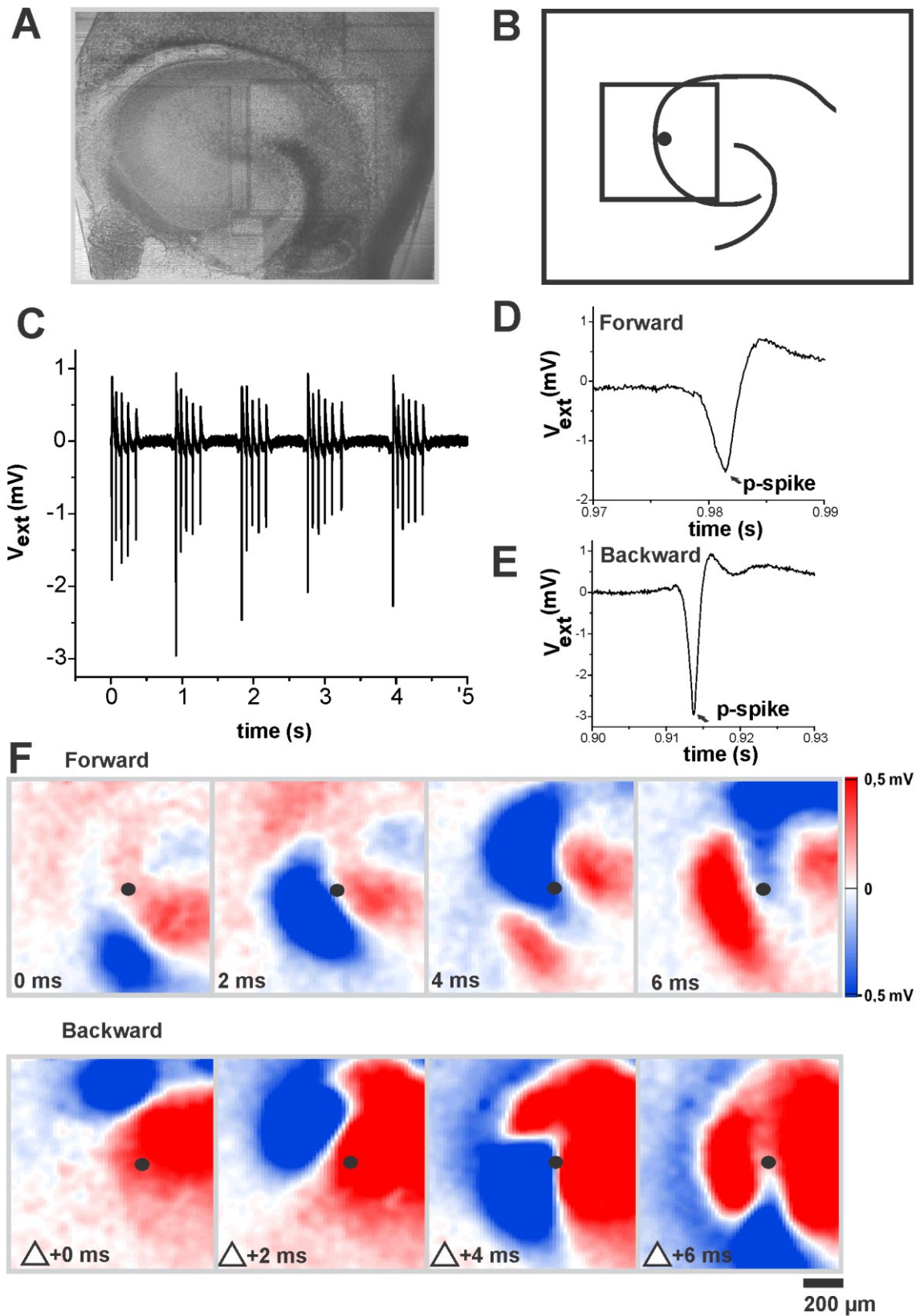
Figure 3.5: Propagation patterns of a p-spike of a local field potential during high K⁺ zero Mg²⁺ induced epileptiform-like activity. A: OHC at DIV 9 interfaced to the recording array of the Neurochip. B: Schematic drawing of the region of the hippocampal slice imaged on the Neurochip. C: Temporal trace of an interictal-like activity recorded in the CA3 region at the sensor position marked with a dark circle in

Figure 3.5B. D and E: Zoomed temporal trace of a forward and backward propagating LFP respectively. F: Spatial electrical images of forward propagating (upper row) and backward propagating p-spikes (bottom row). All the traces were taken from the marked sensor position (row 86, column 60).

3.1.3 Electrical imaging of local field potentials during bicuculline methiodide (BMI) induced epileptiform-like activity

ELA was characterized by reducing the inhibitory inputs to exclude that, the unexpected backward propagation patterns are not only due to increased excitation but are also due to decreased inhibition. Inhibitory GABAergic synapses were blocked by perfusing with ACSF solution containing BMI. Membrane interfaced cultured hippocampal slice (n=7) were placed on the recording array of the Neurochip (Figure 3.6A) and perfused continuously with control ACSF solution for 15 to 20 minutes with the bath temperature maintained between 36°C and 37°C. This was followed by perfusion of ACSF solution containing BMI (10 µM, n=2 slices; or 30 µM, n=5 slices). ELA developed within 5 to 10 minutes of perfusion with BMI containing ACSF solution.

LFPs which occurred during ELA were analysed for the propagation pattern and propagation velocity of the population spike (p-spike) as described in materials and methods section. Ictal-like activity was induced with 30 µM BMI. A concatenated quasi-continuous temporal trace showing different phases of an ELA is shown in Figure.3.6. The three different phases of ELA (Figure.3.6C) were clearly separable: preictal phase (LFP frequency: 0.5 Hz), Ictal phase (3.7Hz), and postictal phase (1.14Hz). The backward propagating p-spikes was predominant during the ictal phase.

A lower concentration of BMI (10 µM) produced interictal-like discharges with very few LFPs. At this concentration, both forward and backward propagating field potentials were observed. The temporal trace during ELA in another slice (Figure 3.7C) from a sensor position marked with a dark circle (Figure 3.7B) shows a series of forward propagating field potentials. Forward propagating p-spike (Figure 3.7E) lasted for 1.35±0.11 ms (measured at full-width at half-amplitude minimum, n=8).

Backward propagating p-spikes (Figure 3.7D) were also observed under these conditions. They lasted for 1.22±0.75 ms (measured at full-width at half-amplitude minimum; Figure 3.7F). In total 74 p-spikes were analysed for propagation patterns, of which 48% showed forward propagation and 52% showed backward propagation. Colour coded spatial electrical images of forward propagating p-spike are shown in Figure 3.7G (upper row) and for backward propagating p-spike in Figure 3.7G (bottom row) with successive frames with an inter-frame interval of 2 ms.

Summary

Both forward and backward propagating LFPs were observed in bicuculline methiodide induced ELA and the waveforms of these p-spikes were similar to those detected in high K^+ zero Mg^{2+} induced ELA.
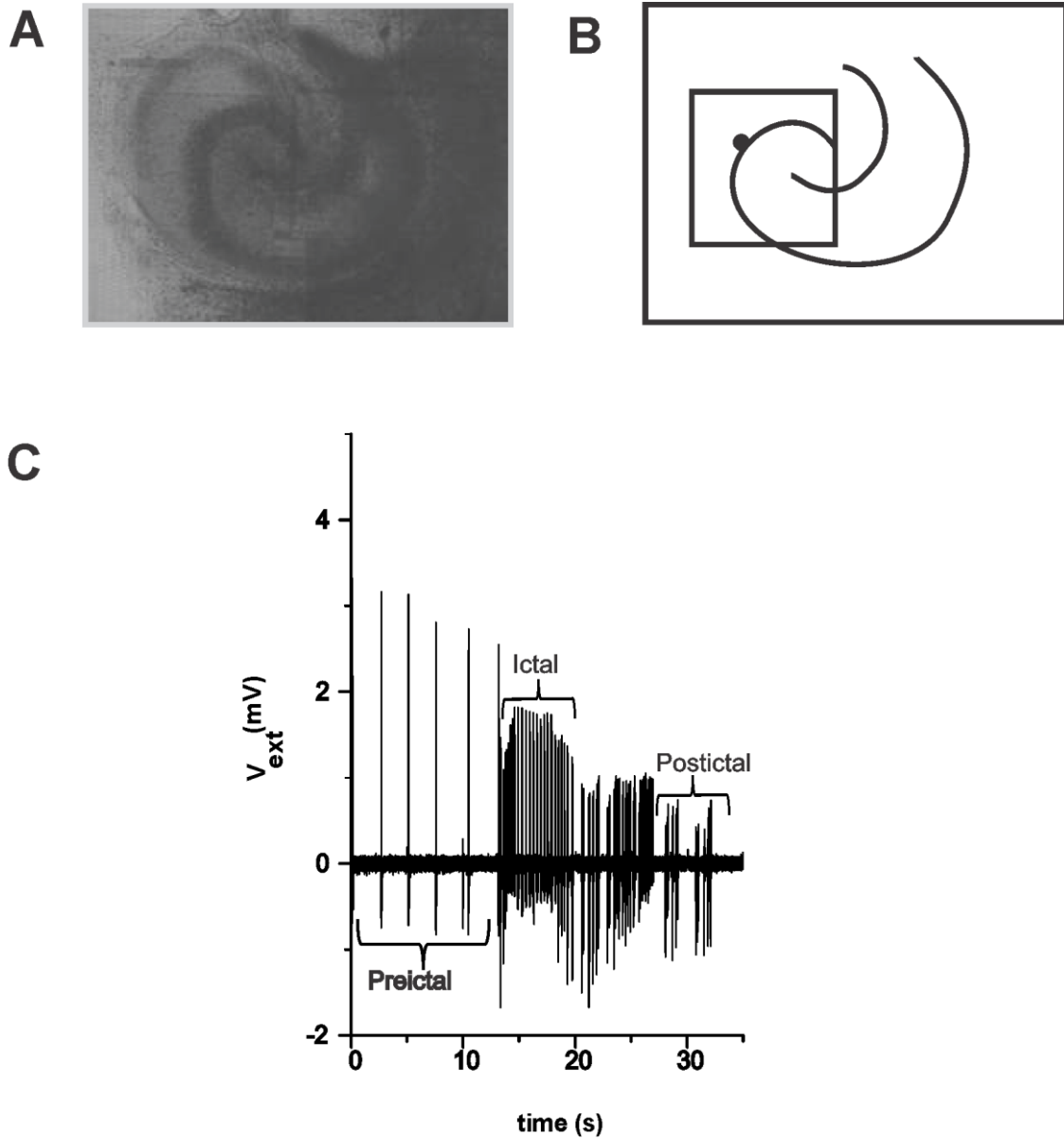
Figure 3.6: Bicuculline methiodide induced epileptiform-like activity. A: OHC at DIV 8 interfaced to the recording array of the Neurochip. B: Schematic drawing of the region of the hippocampal slice imaged on the Neurochip. C: A quasi-continuous temporal trace of an ELA from the sensor position (row 44, column 45) marked with a dark circle in the CA3 region in Figure 3.6B. After each 5 second recording time, a break of ~100 ms occurs (not shown in the Figure).
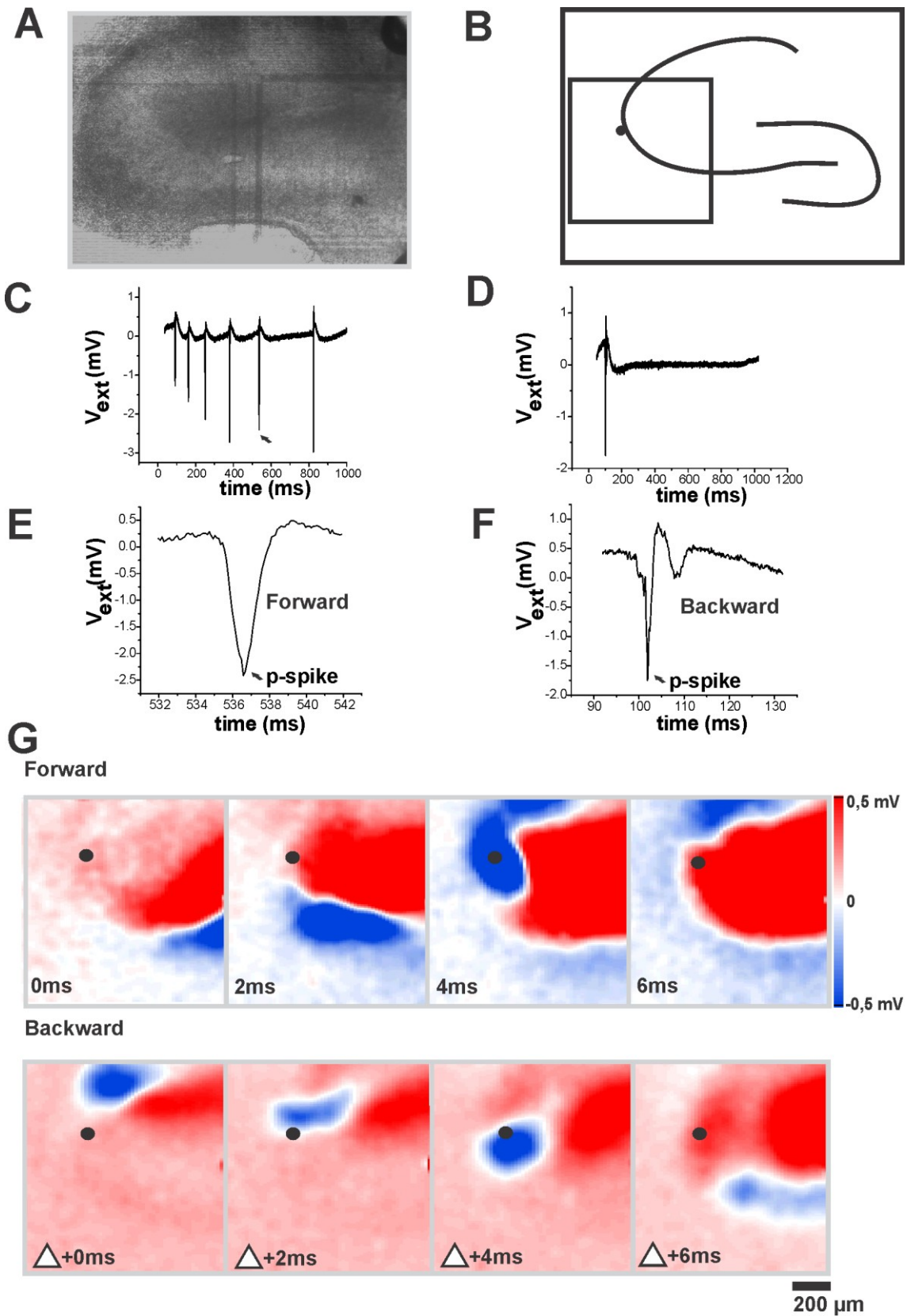
Figure 3.7: Propagation patterns of a p-spike of a local field potential during bicuculline methiodide induced epileptiform-like activity. A: OHC at DIV 14 interfaced to the recording array of the Neurochip. B: Schematic drawing of the region of the hippocampal slice imaged on the Neurochip. C and D: Temporal

trace of forward and backward propagating LFPs recorded during ELA in the CA3 region at the sensor position marked with a dark circle in Figure 3.7B shown respectively. E and F: Zoomed temporal trace of a forward and backward propagating p-spike respectively. G: Colour coded spatial electrical images of forward propagating (upper row) and backward propagating (bottom row) p-spikes corresponding to traces in E and F respectively. All the traces were taken from the marked sensor position (row 45, column 45).

3.1.4 Propagation patterns of p-spikes during different phases of high K$^+$ zero Mg^{2+} induced epileptiform-like activity

ELA can be basically categorized into different phases – preictal, ictal and postictal. The activity between two ictal phases is referred to as the interictal activity. Preictal activity is considered as part of an interictal event. In 4 slices, the propagation patterns of p-spikes during ictal and interictal-like activity were analysed. Analysis of these LFPs showed that all the field potentials exhibited p-spikes, which differed in their pattern of propagation along the trisynaptic pathway.

A Propagation pattern during ictal-like activity

The ictal phase is the phase of an epileptic event when the electrical discharges reflected as high-amplitude LFPs exhibiting a relatively high frequency (3.7±0.1 Hz). In our recordings, ictal-like activity lasted for ~40 – 50 seconds. This value is in agreement with other reports (Avoli, 1990). LFP propagation pattern within an ictal-like activity (n=2) was analysed in the DG-CA3 region of the hippocampus. The p-spikes in ictal-like activity propagated almost exclusively in the backward direction (Figure 3.8A, recorded from the slice shown in Figure 3.4A). In 95% of the investigated LFPs (n = 17), backward propagation from CA3 to DG was detected. Very few forward propagating p-spikes (from DG to CA3) were observed. These showed similar temporal characteristics as the backward propagating p-spikes.

B Propagation pattern during interictal-like activity

During interictal-like activity (Figure 3.8B), bursts of LFPs were observed in the extracellular recordings, obtained from the CA3 region. It was observed that every first p-spike, of the LFP burst, was backward propagating. In contrast, rest of the p-spikes in the burst propagated in the forward direction. Spatial electrical

images of the first four LFPs are shown in Figure 3.8D with an inter-frame interval of 1 ms. In another slice, forward and backward propagating LFPs were randomly occurring. However, backward propagating LFPs occurred in bursts (with an LFP frequency of 5 Hz within the burst).

C Propagation pattern during postictal-like activity

During the postictal-like activity in the two analysed slices, only forward propagating p-spikes were observed (Figure 3.8C).

3.1.5 Propagation velocity of p-spikes during high K$^+$ zero Mg^{2+} or bicuculline methiodide induced epileptiform-like activity

Propagation velocity was calculated based on the centre of activation of the extracellular field potential (section 2.14B). At each time point of the LFP, the centre of activation was calculated and plotted (blue circle in Figure 3.9C). The distance between adjacent centres of activation divided by the time interval gave the local propagation velocity of the LFP. Propagation velocities for forward (red bar) and backward propagating (blue bar) LFPs were calculated from 9 slices under high K$^+$ zero Mg^{2+} induced ELA (Figure 3.9A) and from 7 slices under BMI-induced ELA (Figure 3.9B).

The individual LFP velocities are represented in a histogram (Figure 3.9A). As the velocity distribution was asymmetric, the median value as the representative measure of velocity propagation was considered and the mean of the median velocities was calculated for all the LFPs within one slice.

The mean LFP propagation velocity between ~200–300 mm/s that was obtained is comparable to the velocity value of 0.31±0.08 mm/s. This value corresponded to axonal propagation along the CA3 region of the hippocampus (Kibler & Durand, 2011).

In excitation induced ELA, at the p=0.05 level, the mean forward and backward propagation velocities (Figure 3.9A) of the p-spikes were not significantly different (two sample t-test, p-value: 0.37). These backward and forward

propagating p-spikes followed largely similar spatial pathways (Figure 3.9C). Also for disinhibition induced ELA, the mean forward and backward propagation velocities of the p-spikes (Figure 3.9B) were not significantly different (two sample t-test, p-value: 0.28) either.

To investigate the accelerating circuitries during the LFP propagation, the local velocities for forward and backward propagating field potentials were evaluated in more detail. Calculated velocities for each LFP were plotted over time for all the LFPs. Plots displaying the local velocity changes over time for 6 different LFPs (three forward propagating and three backward propagating) are shown in Figure 3.9D. The central plot (boxed) corresponds to the forward and backward propagating LFP shown in Figure 3.9C. The velocities observed during forward and backward propagation did not show any significant variation over time.

Summary

Unique patterns of propagating LFPs were observed during three different phases of ELA. There was no significant difference in the velocities of forward and backward propagating field potentials in both high K^+ zero Mg^{2+}/BMI induced ELA. Both forward and backward propagating field potentials followed a similar path of propagation.
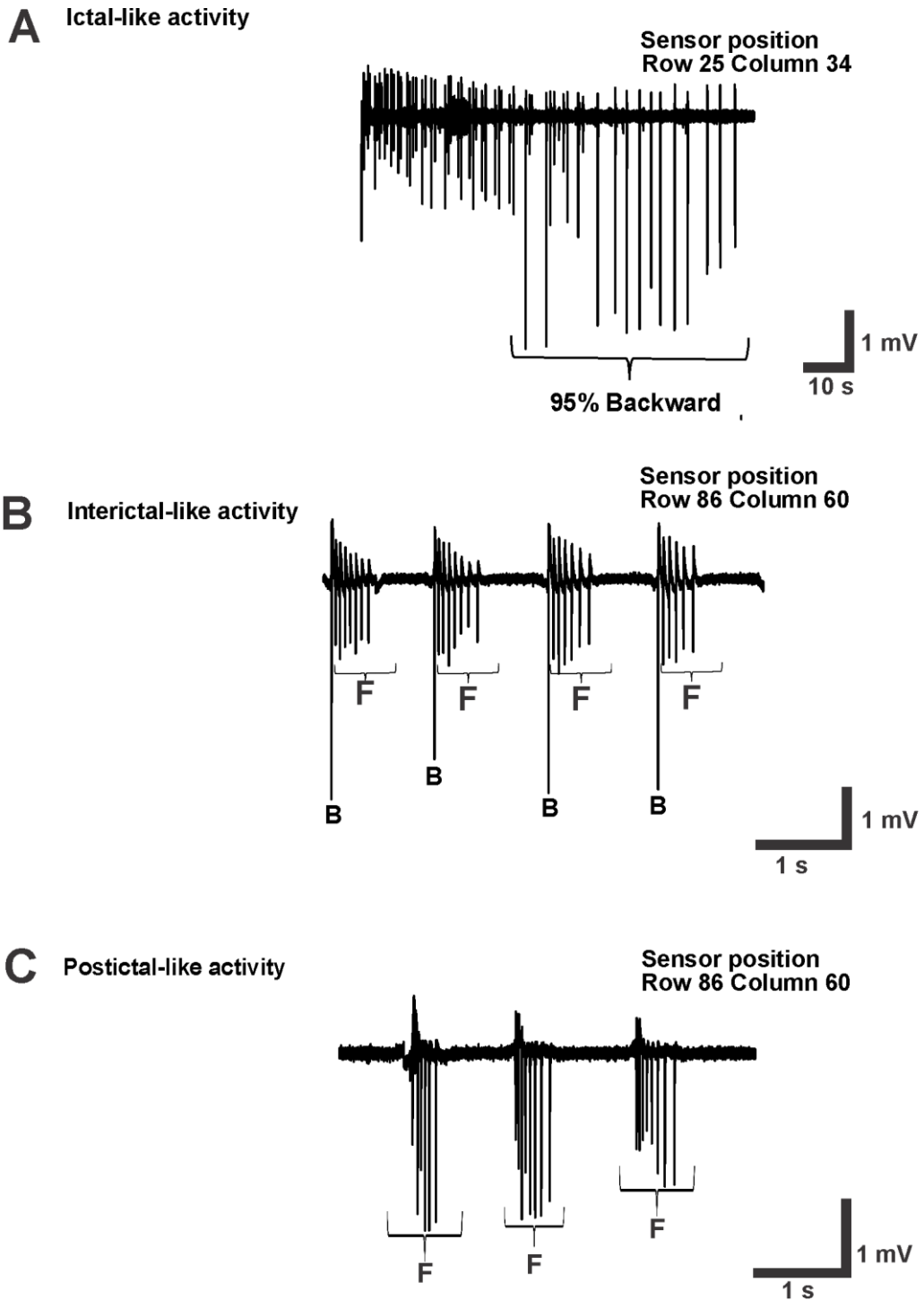
Figure 3.8A-C: Propagation patterns of p-spikes during different phases of high K$^+$ zero Mg^{2+} induced epileptiform-like activity. A: Temporal trace of an ictal-like activity, 95% of the LFPs were backward propagating. B: Temporal trace of an interictal-like activity with forward (F) and backward (B) propagating LFPs. C: Temporal trace of a postictal-like activity with forward propagating LFPs.
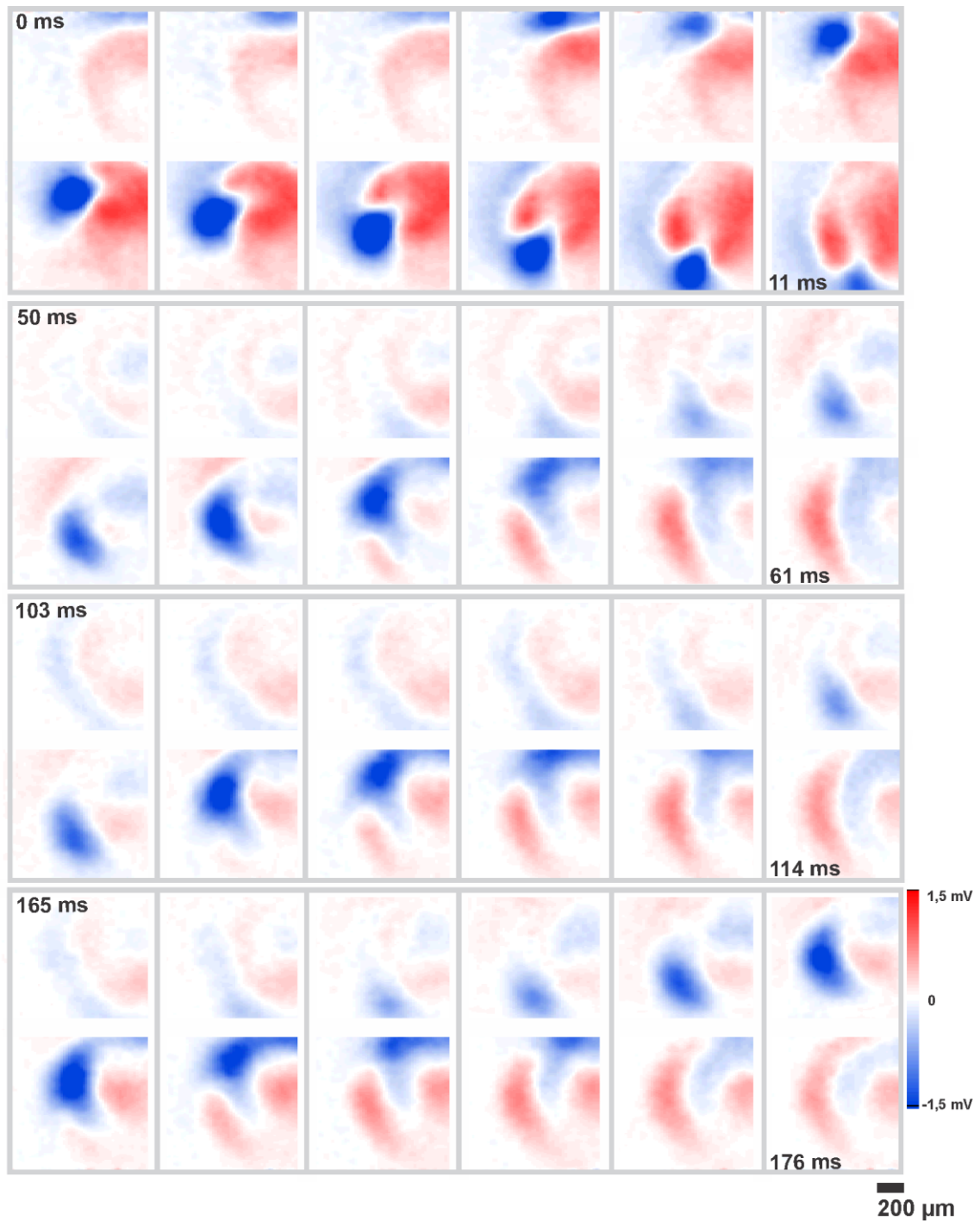
Figure 3.8D: Spatial electrical images of propagating local field potentials from the temporal trace shown in Figure 3.8B. Red colour marks positive extracellular voltage values with respect to ground potential; blue colour marks negative extracellular voltage values with respect to ground potential. Spatial electrical images of the first four LFPs with an inter-frame interval of 1 ms are shown. The first LFP (0 – 11 ms) was backward propagating and the following LFPs (50 – 61 ms, 103 – 114 ms, 165 – 176 ms) were forward propagating. The numbers in upper and lower left corner represent the time sequence with respect to the first LFP.
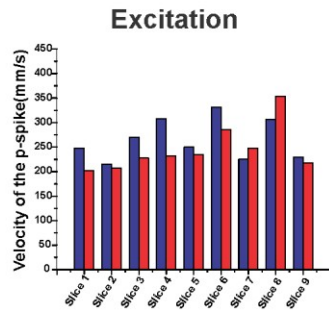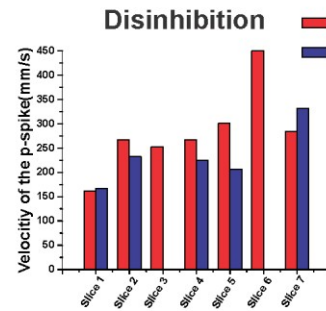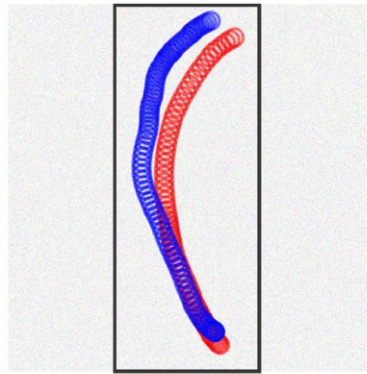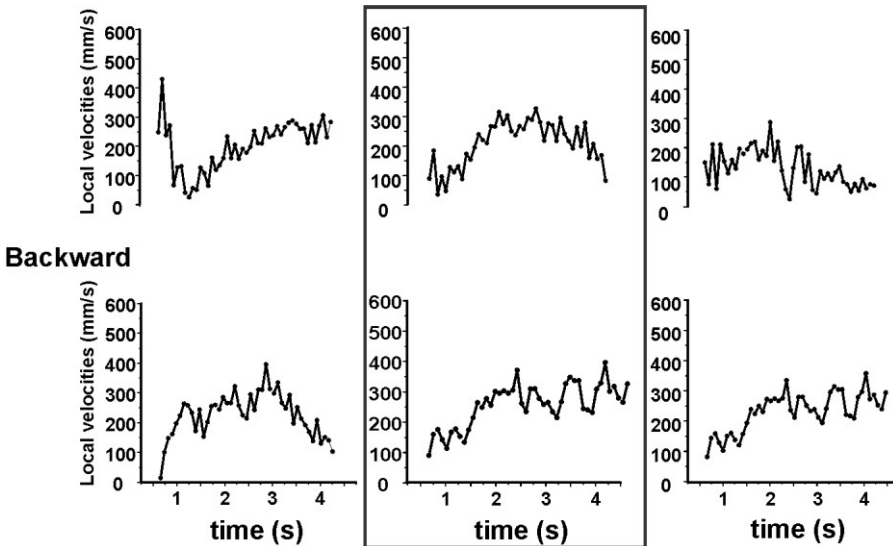
Figure 3.9: Propagation velocities and propagation path during induced epileptiform-like activity. Graphical representation of mean velocities - A: in high K^+ zero Mg^{2+} induced ELA. B: in BMI-induced ELA. C: Propagation path for forward (red) and backward (blue) propagating field potential. D: Velocity vs time plots for forward and backward propagating LFPs. The boxed middle column corresponds to the forward and backward propagating LFPs shown in Figure 3.9C.

3.1.6 Effect of AMPA/kainate receptor blocker DNQX on propagating local field potentials during high K$^+$ zero Mg^{2+} induced epileptiform-like activity

To investigate the role of excitatory synapses in LFP propagation in the OHCs during ELA, ionotropic glutamate receptors were blocked using DNQX (100 µM). Membrane interfaced OHCs were perfused with Mg^{2+} free high K$^+$ containing ACSF solution for ELA induction (Figure 3.10A). The ELA discharges were recorded during perfusion of the treatment buffer (Figure 3.10C). During ELA discharges, the LFPs propagated along the trisynaptic circuitry (Figure 3.10 E). During initial perfusion of the blocker, ELA discharges decreased and over time the field potentials did not show any p-spike during blocker application, instead showed only LFPs with amplitudes smaller than ±1 mV (Figure 3.10D). There was no clear LFP propagation (Figure 3.10F) and most of the field potentials appeared as patches in the CA3 pyramidal layer. This indicates that the cells are less excitable and exhibit less synaptic currents. We infer that, DNQX reduces LFP amplitude by lowering the contribution of synaptic currents.

Summary

Ionotropic receptor blocker DNQX disintegrated the large amplitude LFPs into smaller amplitude LFPs.
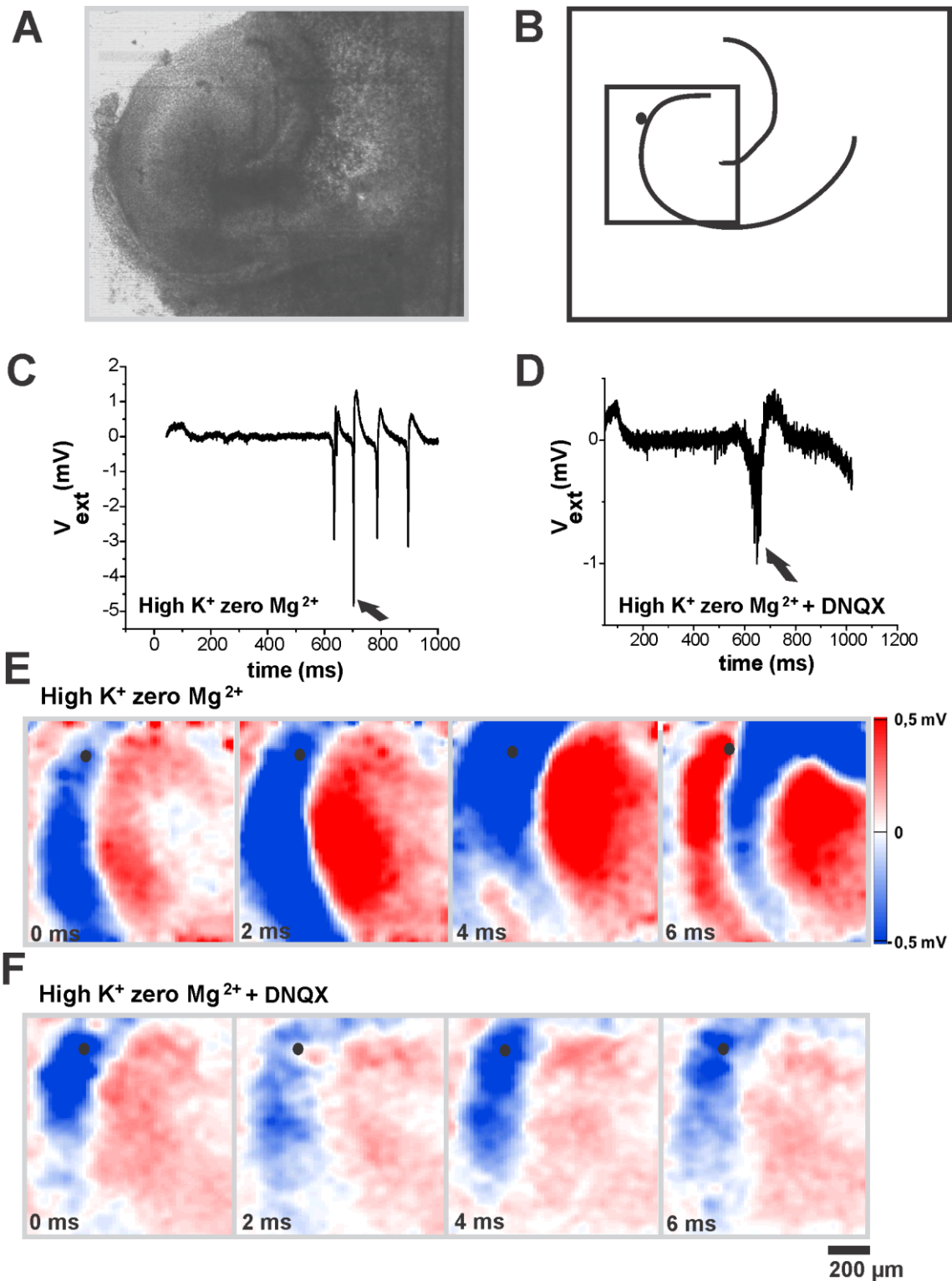
Figure 3.10: Effect of AMPA/kainate blocker DNQX on high K$^+$ zero Mg^{2+} induced epileptiform-like activity. A: OHC at DIV 8 interfaced to the recording array of the Neurochip. B: Schematic drawing of the region of the hippocampal slice imaged on the Neurochip. C: Temporal trace of LFPs during induced ELA. D: Temporal trace of an LFP during DNQX application. E: Spatial electrical images of propagating LFP during induced ELA. F: Spatial electrical images of disintegrated LFP during DNQX application. All the traces were taken from the marked sensor position (row 26, column 38).

3.1.7 Effect of gap junction blocker meclofenamic acid on propagating local field potentials during high K^+ zero Mg^{2+} induced epileptiform-like activity

To investigate if electrical synapses are involved in propagating LFPs (Rozental *et al.*, 2001) during induced ELA, extracellular recordings were performed on cultured hippocampal slices (n=3) interfaced to the recording array of the Neurochip (Figure 3.11A). Once the slice was stabilized for 15 to 20 minutes upon control ACSF perfusion, ELA was induced by perfusing with treatment buffer. Following ELA induction, the slice was perfused with treatment buffer containing meclofenamic acid (MFA, 100 µM, Sigma) for 20 minutes. Temporal traces of extracellular voltage recordings taken from the sensor position marked with a dark circle (Figure 3.11B) show a sequence of field potentials recorded before the addition of MFA (Figure 3 11C) and another sequence after the addition of MFA (Figure 3.11D). During perfusion of the treatment buffer (Figure 3.11.C), the detected LFPs propagated. Propagation of an LFP was evaluated with respect to centre of activation for each point of propagation (as shown in Figure 3.11G). Each blue circle represents the centre of activation of one LFP. Corresponding spatial electrical image of the propagating field potential (marked with an arrow in Figure 3.11C) is shown in Figure 3.11E. After the application of the blocker for 20 minutes, recordings of 4 to 5 seconds were made at arbitrary time points. Evaluation of the propagation velocity based on the centre of activation of each propagating point showed that the points clustered in a particular area (Figure 3 11H) of the slice indicating that there was no propagation of the field potential. Corresponding spatial electrical images of extracellular voltage trace of non-propagating field potential (marked with an arrow in 3.11D) are shown with an inter-frame interval of 2 ms in Figure 3.11F.

Summary

Application of the gap junction blocker MFA inhibited the propagation of the LFPs during induced ELA indicating that electrical synapses are involved in the propagation of these LFPs.
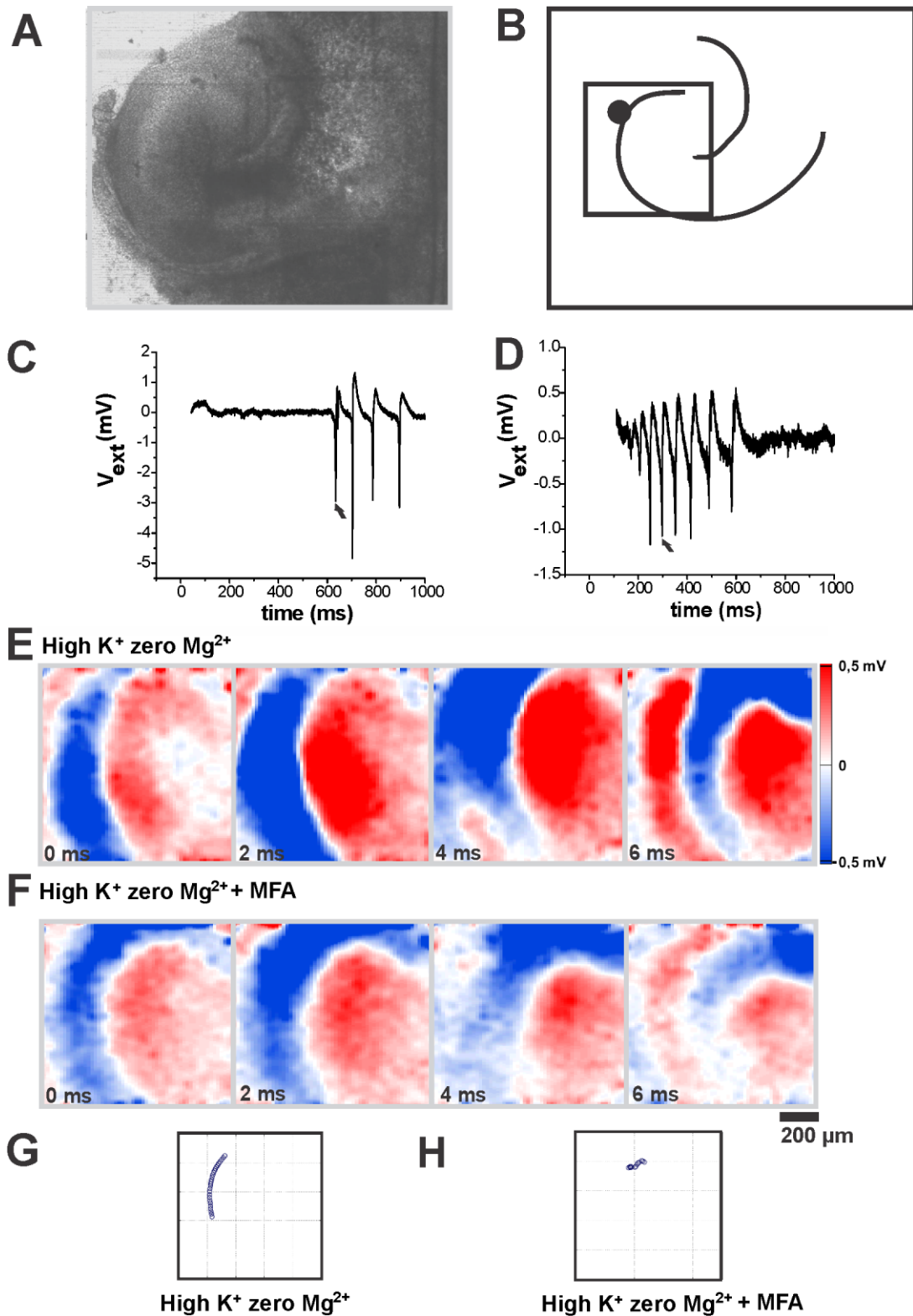
Figure 3.11: Effect of gap junction blocker meclofenamic acid on high K$^+$ zero Mg^{2+} induced epileptiform-like activity. A: OHC at DIV 8 interfaced to the recording array of the Neurochip. B: Schematic drawing of the region of the hippocampal slice imaged on the Neurochip. C: Temporal trace of LFPs during induced ELA. D Temporal trace of LFPs during MFA application. E: Spatial electrical images of a propagating LFP during induced ELA. F: Spatial electrical images of non-propagating LFP during MFA application. G and H: Representation of propagating and non-propagating LFP based on the centre of

activation of each point of propagation. All the traces were taken from the marked sensor position (row 26, column 38).

3.1.8 Characterization of high K$^+$ zero Mg^{2+} induced epileptiform-like activity in organotypic hippocampal slice cultures using low-density microelectrode arrays

The aim to repeat the recordings described above with low-density MEAs was to study the effect of anticonvulsants on longer timescales (minutes), which was not feasible with the Neurochips used in section 3.1.6.

For MEA experiments, extracellular recordings were made from OHCs between DIV 6 and DIV 14. The cultured slice from the membrane insert was cut along with the membrane insert and over laid on the recording array of a MEA (Figure 3.12A), such that, the slice is in direct contact with the recording electrodes. A close contact was established between the slice and the recording array by gently removing the excess buffer with a filter paper. The contact was made even more firmly by placing a light platinum grid (weighing 492 mg) over the insert. The slice was perfused throughout the experiment, with oxygenated (95% O$_2$ and 5% CO$_2$) ACSF solution at a flow rate of 1.5 ml/minute with a bath temperature between 36°C and 37°C.

3.1.8a Recording of high K$^+$ zero Mg^{2+} induced epileptiform-like activity in organotypic hippocampal slice cultures on microelectrode arrays

To characterize the ELA over extended time periods, OHCs were measured for 12 minutes continuously. All the slices were initially perfused with control ACSF solution for 15 to 20 minutes to establish normal physiological conditions. Control measurements were made to examine if the slices were spontaneously active. ELA developed after 5 to 10 minutes of perfusion of the treatment buffer. Induced ELA (Figure 3.12D) consisted of preictal (1.36±0.5 Hz), ictal (3.7±0.1 Hz) and postictal phase (1.13±0 Hz) as shown in the CA3 region (Figure 3.12C). A quantitative analysis is shown in Figure 3.12B. The mean LFP frequency evaluated using Savitzky-Golay algorithm (Gonzalez-Sulser *et al.*,

2011) during ictal phase was found to be 0.18Hz±0.04 (Mean±SEM, standard error of mean, n=4). The difference in LFP frequency is attributed to the difference in cutoff frequency. In the following sections, the LFP frequencies evaluated using Savitzky-Golay algorithm during the ELA discharges were compared with corresponding pharmacological treatments.

Summary

ELA was successfully induced and recorded from OHCs interfaced to microelectrode arrays.
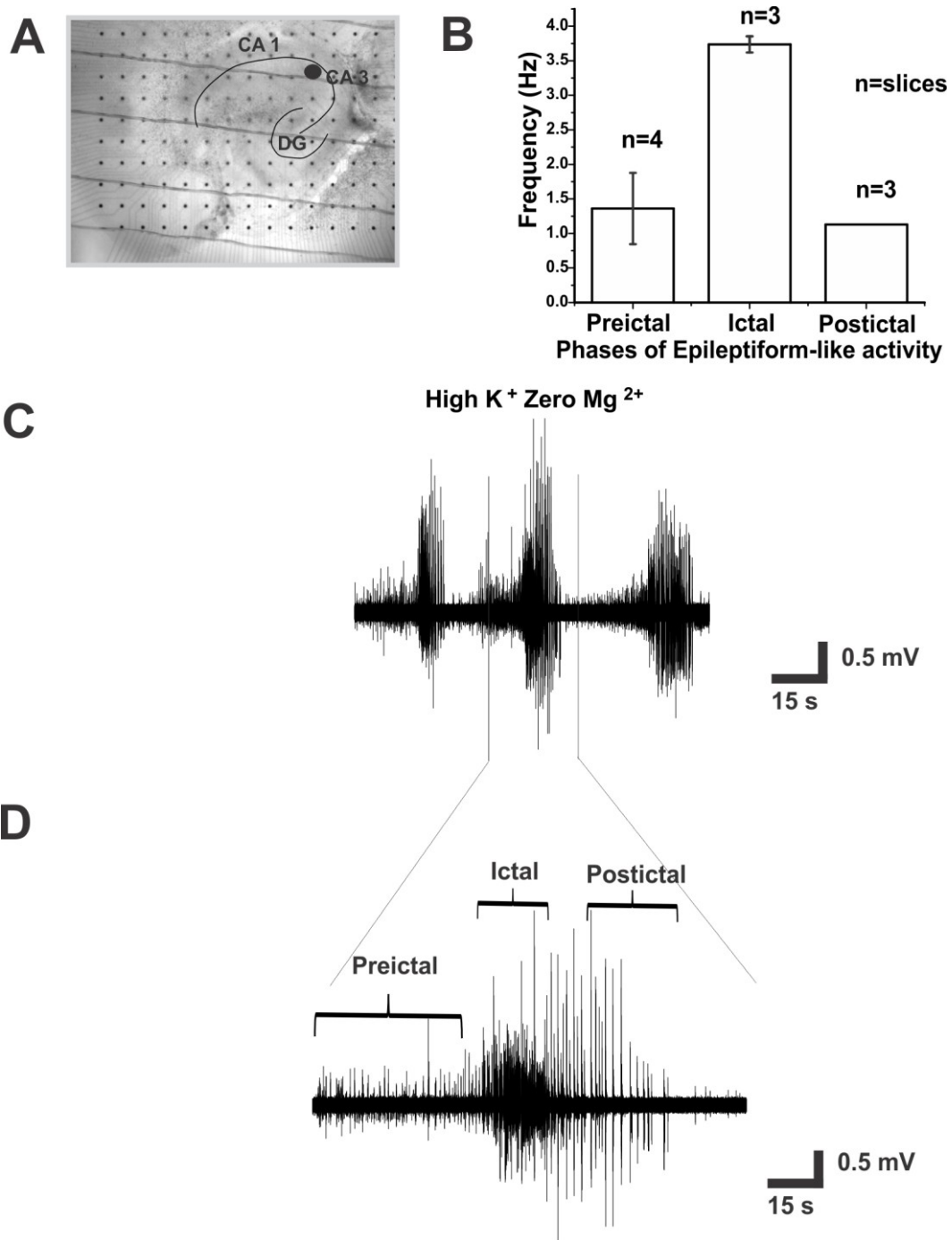
Figure 3.12: High K⁺ zero Mg²⁺ induced epileptiform-like activity recorded in organotypic hippocampal slices on low-density microelectrode arrays. A: OHC at DIV 7 interfaced to the recording array of the MEA. B: Quantitative comparison of frequencies during the preictal, ictal and postictal phase of an induced ELA. C: Temporal trace of an ELA under high K⁺ zero Mg²⁺ induced epileptiform-like activity taken from an electrode L8 (marked with a dark circle) in the CA3 region (Figure 3.12A). D: Zoomed temporal trace of an ELA showing preictal, ictal and postictal phase.

3.1.8b Effect of AMPA/kainate blocker DNQX on local field potentials during high K$^+$ zero Mg^{2+}induced epileptiform-like activity

To evaluate the role of AMPA and kainate specific glutamatergic signalling during induced ELA on extended time periods, OHCs (Figure 3.13A) were perfused with treatment buffer. ELA was observed within 5 to 10 minutes of treatment buffer perfusion. Following ELA induction, all the slices (n=4) were perfused with DNQX containing treatment buffer, which abolished the field potentials. After washout of DNQX, the slices exhibited ELA upon perfusion of treatment buffer (Figure 3.13B). This observation of drastic decrease in activity, together with the observation of disintegrated LFPs in Neurochip recording indicates that glutamatergic signalling plays a crucial role during ELA.

Summary

In accordance to the results obtained in the Neurochip recording, ionotropic glutamate receptor abolishes LFPs during induced ELA over time.

A
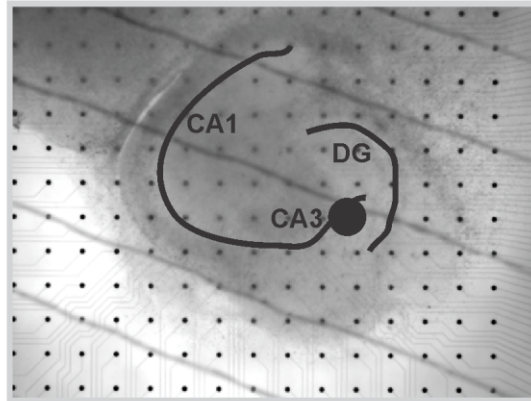
B
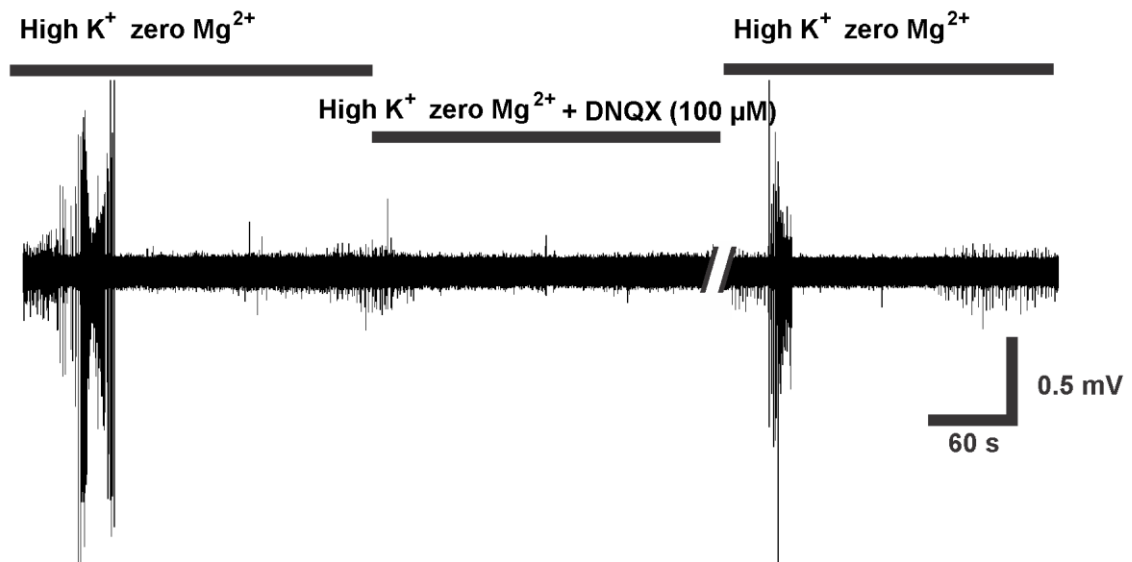
Figure 3.13: Effect of AMPA/kainate blocker on high K$^+$ zero Mg^{2+} induced epileptiform-like activity in organotypic hippocampal slices evaluated using low-density microelectrode arrays. A: OHC at DIV 12 interfaced to the recording array of the MEA B: Temporal trace from an electrode L8 (marked with a dark circle) in the CA3 region (Figure 3.13A.) under high K$^+$ zero Mg^{2+}, high K$^+$ zero Mg^{2+} with DNQX and high K$^+$ zero Mg^{2+} after washout.

3.1.8c Effect of gap junction blocker meclofenamic acid on local field potentials during high K^+ zero Mg^{2+} induced epileptiform-like activity

To confirm the role of gap junctions on induced ELA and to study long-term effects, OHCs cultivated on membrane insert were placed on the recording array of the MEA (Figure 3.14A). ELA was induced in all the slices (n=3) prior to application of MFA by perfusing high K^+ zero Mg^{2+} containing ACSF solution. ELA was observed in all the subregions of the hippocampus. Following ELA induction, all the slices were perfused with MFA (100 µM) containing high K^+ zero Mg^{2+} ACSF solution for 20 to 30 minutes. The effect of MFA was recorded after 20 minutes of incubation for duration of 20 minutes. An average LFP frequency was calculated from all the slices for different time points. A decrease in the frequency of the field potentials from 0.18 Hz±0.04 (mean±SEM) to 0.04 Hz was observed (Figure 3.14B). Here, an asterisk at 0 minute refers to the average frequency within 4 minutes of ELA activity recorded. Temporal trace from one of these slices during induced ELA followed by blocker application is shown (Figure 3.14C). Here, the asterisk indicates the ELA. Evaluation of the LFP propagation was not possible due to the large spacing (200 µm) between the recording electrodes. In Figure 3.14B and C, the red bar represents the first 0 to 4 minutes of recording, the green bar - 4 to 8 minutes, the yellow bar - 8 to 12 minutes, and the blue bar - 12 to 16 minutes.

Summary

The evaluation of the effect of gap junction blocker using low-density MEA's revealed that MFA reduced the frequency of LFPs considerably.
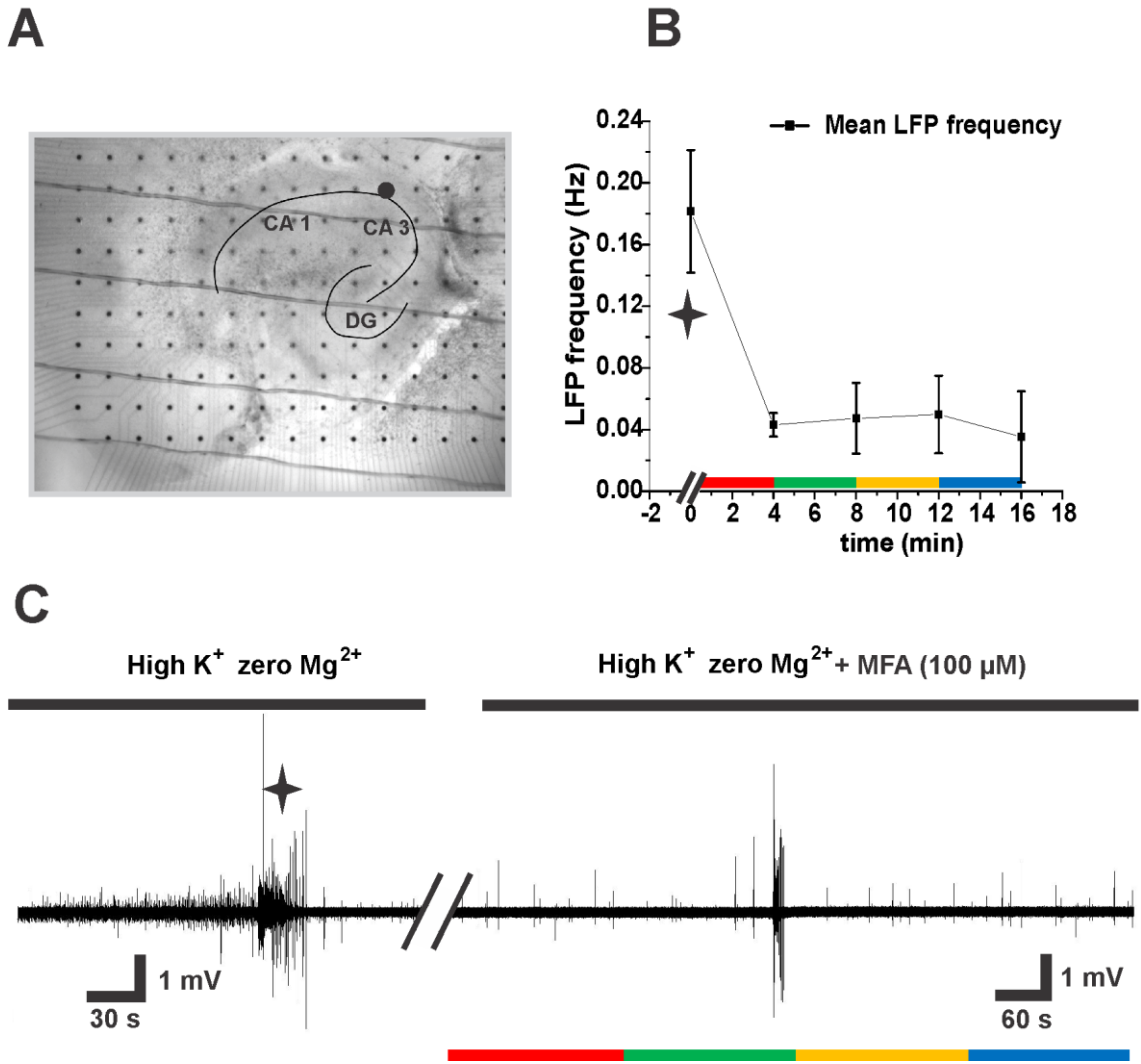
Figure 3.14: Effect of gap junction blocker meclofenamic acid on high K⁺ zero Mg²⁺ induced epileptiform-like activity in organotypic hippocampal slices evaluated using low-density microelectrode arrays. A: OHC at DIV 7 interfaced to the recording array of the MEA. B: Mean LFP frequency during ELA (marked with an asterisk) and during perfusion with MFA. C: Temporal trace under high K⁺ zero Mg²⁺ and high K⁺ zero Mg²⁺ with MFA from an electrode marked with a dark circle in the CA3 region. Colour bars in Figure C represent red – first 4 minutes of recording after 20 minutes of MFA perfusion, green – 4 to 8 minutes of recording, yellow - 8 to 12 minutes of recording, blue - 12 to 16 minutes of recording.

3.1.8d Effect of gap junction blocker carbenoxolone on local field potentials during high K$^+$ zero Mg^{2+} induced epileptiform-like activity

In addition to experiments with MFA, carbenoxolone (CBX) was used to confirm the role of gap junctions during induced ELA. OHCs cultivated on membrane insert were placed on the recording array of the microelectrode array (Figure 3.15A). ELA was induced in all the slices (n=3) prior to application of CBX by perfusing high K$^+$ zero Mg^{2+} containing ACSF. ELA was observed in all the subregions of the hippocampus. A temporal trace of an ELA from an electrode marked with a dark circle (Figure13.5 A) in the CA3 region is shown in Figure 3.15C. Following ELA induction, all the slices were perfused with CBX (100 µM) containing high K$^+$ zero Mg^{2+} ACSF solution for 120 minutes. Upon CBX perfusion, recordings were taken every 30 minutes at 0 min, 30 min, 60 min, 90 min and towards the end of the recording period at 110 min (Figure 3.15C). It was observed that the frequency of the field potentials decreased from 0.31±0.04 Hz (mean±SEM) to 0.017±0.013 Hz (mean±SEM) with time (Figure 3.15B).

Summary

With the application of CBX, it was observed that the frequency of LFPs decreased. The few LFPs detected in the presence of CBX occurred as bursts.
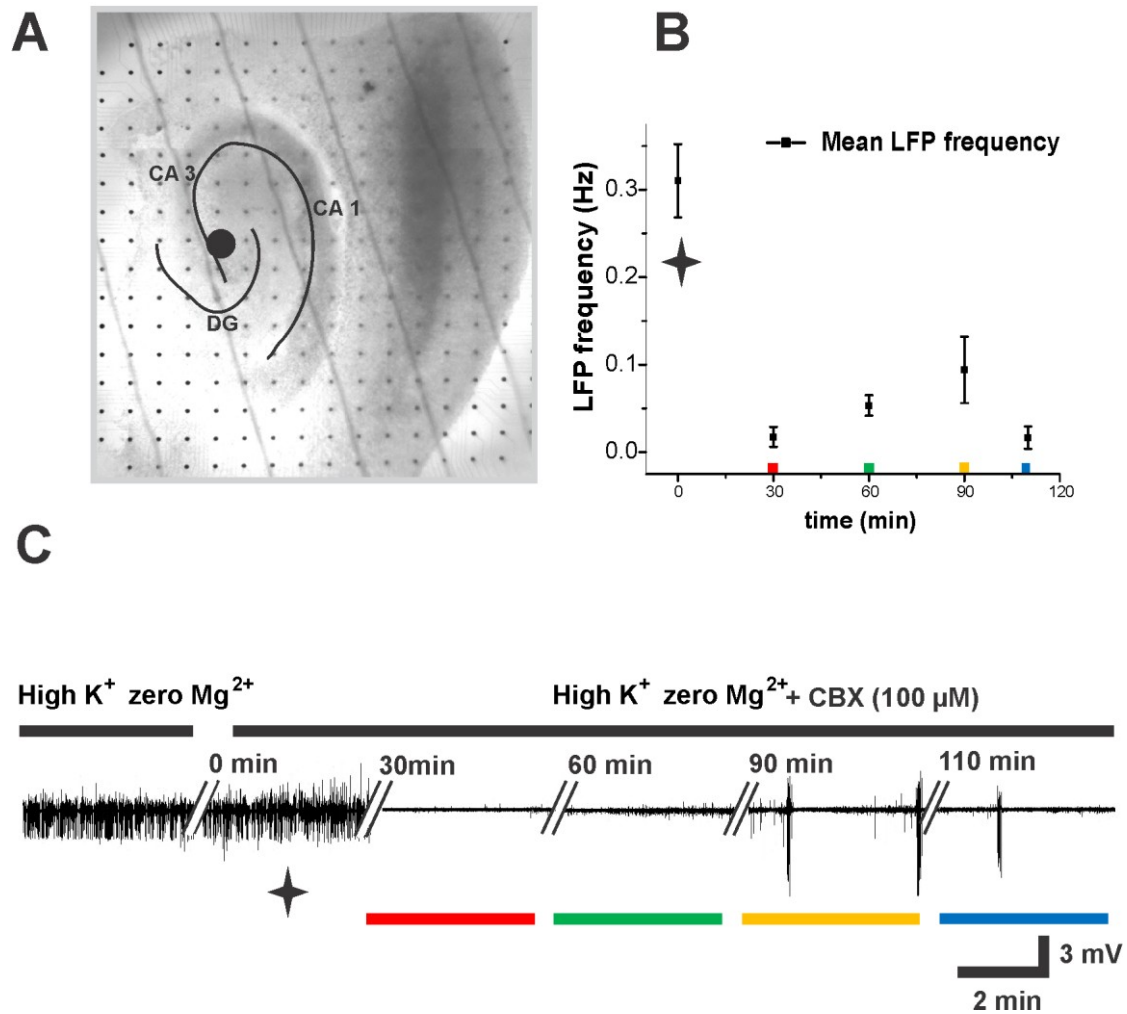
Figure 3.15: Effect of gap junction blocker carbenoxolone on high K$^+$ zero Mg^{2+} induced epileptiform-like activity in organotypic hippocampal slices evaluated using low-density microelectrode arrays. A: OHC at DIV 8 interfaced to the recording array of the MEA. B: Mean LFP frequency during ELA, marked with an asterisk and during perfusion with CBX. C: Temporal trace of an ELA during high K$^+$ zero Mg^{2+} and high K$^+$ zero Mg^{2+} with CBX perfusion from an electrode E8 marked with a dark circle in the CA3 region. A recording of 4 minutes duration at a time point of 0 min, 30 min, 60 min, 90 min and 110 minutes, after high K$^+$ zero Mg^{2+} with CBX perfusion are shown.

3.2 Characterization of electrical activity in acute hippocampal slices

Acute slices have the advantage of a well preserved cytoarchitecture and synaptic circuits. Apart from the afferent inputs, other features are preserved similar to the one prevalent in intact hippocampus. Additional advantages of acute slices over slice cultures are that they involve less preparatory work and maintenance, and the pattern of synaptic connections within the slice is not much altered during the preparation. In contrast, hippocampal slice culture preparation requires a lot more effort and care during preparation and maintenance. Any injury to the tissue during preparation may lead to synaptic reorganization and axonal remodelling, after harvesting of the tissue. Therefore, it appears mandatory to investigate electrophysiological signatures during an ELA in acute slice preparations to compare the characteristic patterns observed in organotypic slice preparations.

3.2.1 Electrical imaging of spontaneous local field potentials

For evaluation of spontaneous activity, acute hippocampal slices were perfused with control ACSF solution for 10 to 15 minutes. The slices did not exhibit any spontaneous field potentials. Due to the small chip area, the cortical region was trimmed. For organotypic hippocampal slice preparations trimming was not necessary as the slices prepared from younger animals were small.

3.2.2 Electrical imaging of local field potentials during high K^+ zero Mg^{2+} induced epileptiform-like activity

To electrically image the aberrant activity, ELA was induced in acute hippocampal slices prepared from Sprague Dawley rats between the age group P13 to P30. Acutely prepared cortico-hippocampal slices were trimmed to obtain hippocampal regions and the slice was placed on the recording array of the Neurochip (Figure 3.16A) pre-coated with poly-L-lysine (1 mg/ml for 1 hour). A schematic drawing of the region of the hippocampal slice electrically imaged

is shown (Figure 3.16B). The slice was initially perfused with control ACSF solution for 15 to 20 minutes, to establish a normal physiological environment. ELA was induced by perfusing treatment buffer. A temporal trace of a forward propagating field potential during an ELA is shown (Figure 3.16C). High-frequency oscillations (100-200 Hz) were detected during such an LFP (Figure 3.16D). Along with forward propagating field potentials, backward propagating field potentials were also observed (Figure 3.16E), as well as high-frequency oscillations similar to that observed in forward propagating field potentials (Figure 3.16F). Electrical images of a forward and backward propagating field potential is shown with an inter-frame interval of 5 ms (Figure 3.16G). The recorded p-spike resembled the p-spike observed in OHCs. However, it did not show similar propagation characteristics with respect to amplitude and velocity. The p-spikes had amplitudes between 0.5 mV and 0.8 mV; in contrast to that observed in OHC (>1 mV), and the detected propagation velocity was lower than that observed in the organotypic hippocampal slices. This could be either due to low signal-to-noise ratio caused by lack of firm attachment of the tissue to the recording array or due to matured synaptic connectivity.

Summary

In acute slice preparations, spontaneous LFPs or SUA were not detected under control conditions. However, during high K^+ zero Mg^{2+} induced ELA, both forward propagating and backward propagating field potentials were observed.
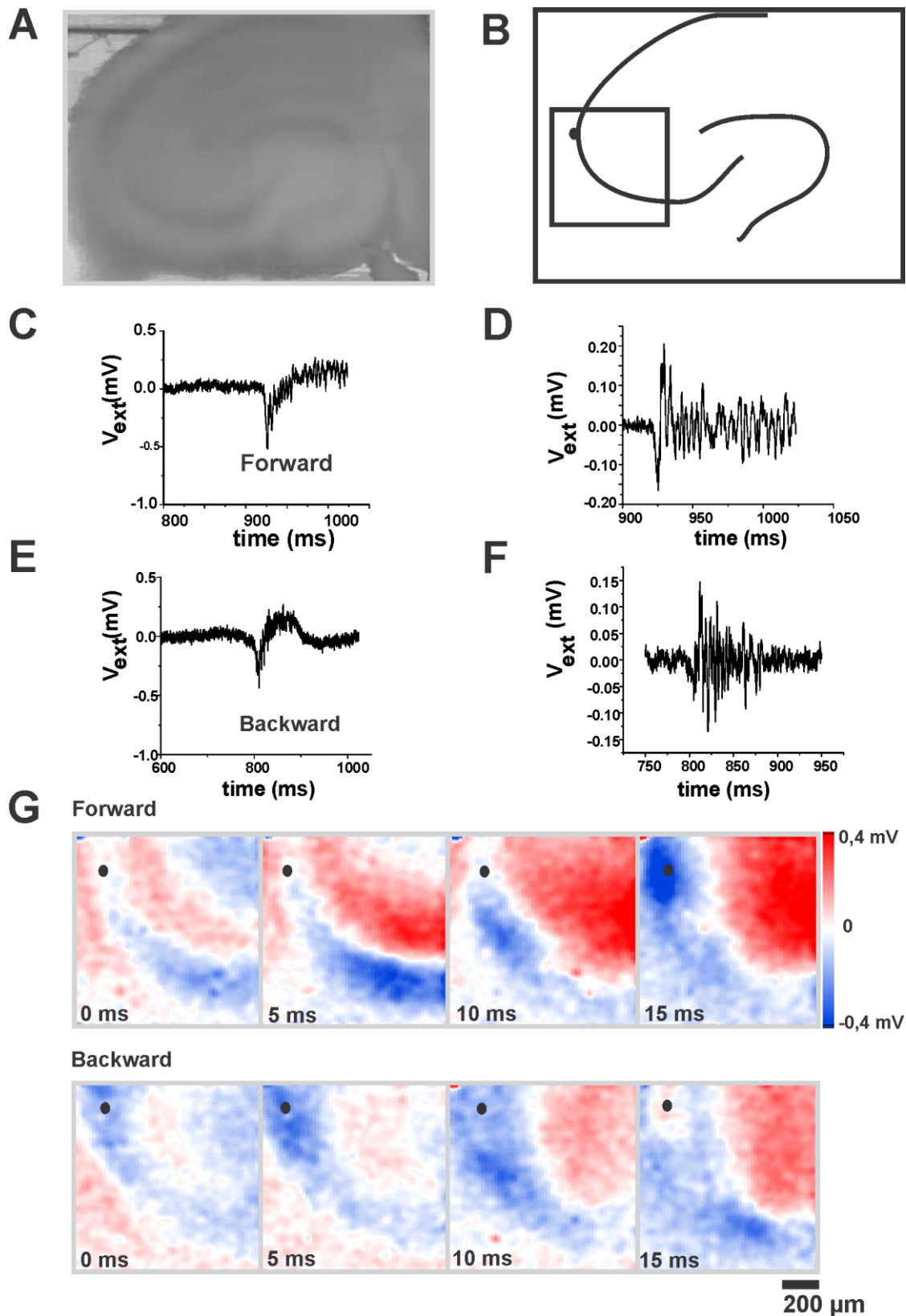
Figure 3.16: Electrical imaging of local field potentials during high K$^+$ zero Mg^{2+} induced epileptiform-like activity in acute hippocampal slices. A: Acute hippocampal slice placed on the recording array of the Neurochip. B: Schematic drawing of the region of the hippocampal slice imaged on the Neurochip. C: Temporal trace of an LFP (Forward propagating) D: Zoomed temporal trace of an

epileptiform burst in Figure 3.16C. E: Temporal trace of an LFP (Backward propagating) F: Zoomed temporal trace of an epileptiform burst in Figure 3.16E. G: Spatial electrical images of a forward (top row) and backward (bottom row) propagating field potential. All the traces were taken from the marked sensor position (row 26, column 22).

3.2.3 Electrical imaging of local field potentials during bicuculline methiodide induced epileptiform-like activity

To electrophysiologically characterize, verify the aberrant activity in a well preserved synaptic network during reduced inhibition and to confirm the back propagation in mature slices, ELA was induced by perfusing GABA$_A$ receptor antagonist bicuculline methiodide (BMI, 30 µM) containing ACSF solution in acutely prepared hippocampal slices (Figure 3.17A). ELA began after 5 to 10 min of perfusion of BMI containing ACSF. It is to be noted here, that lower concentrations of BMI did not effectively induce ELA. ELA was recorded in the DG – CA3 area (Figure 3.17B). Field potentials observed during induced ELA were analysed for propagation patterns. Both forward (Figure 3.17E) and backward propagating p-spike (Figure 3.14F) were observed. Forward propagating p-spikes had amplitudes between 0.4 and 0.6 mV (Figure 3.17C) and p-spikes with backward propagation had amplitudes between 0.8 and 1.2 mV (Figure 3.14D). The p-spike wave form patterns observed were similar to the one observed in OHCs. Spatial electrical images of the forward and backward propagating field potentials are represented in the form of colour-coded images of extracellular voltage traces with an inter-frame interval of 2 ms (Figure 3.17G), with upper row showing forward propagation and bottom row showing backward propagation. The number of successful recordings (good signal-to-noise ratio) was less here.

Summary

The experiments with acute slices constitute a qualitative approach towards confirmation of LFP propagation direction in mature slices. In acute slice preparations, both forward and backward propagating LFPs were observed during reduced inhibition. Due to the lower signal-to-noise ratio as compared to OHCs, estimation of propagation velocity, propagation path, and p-spike width was not feasible.
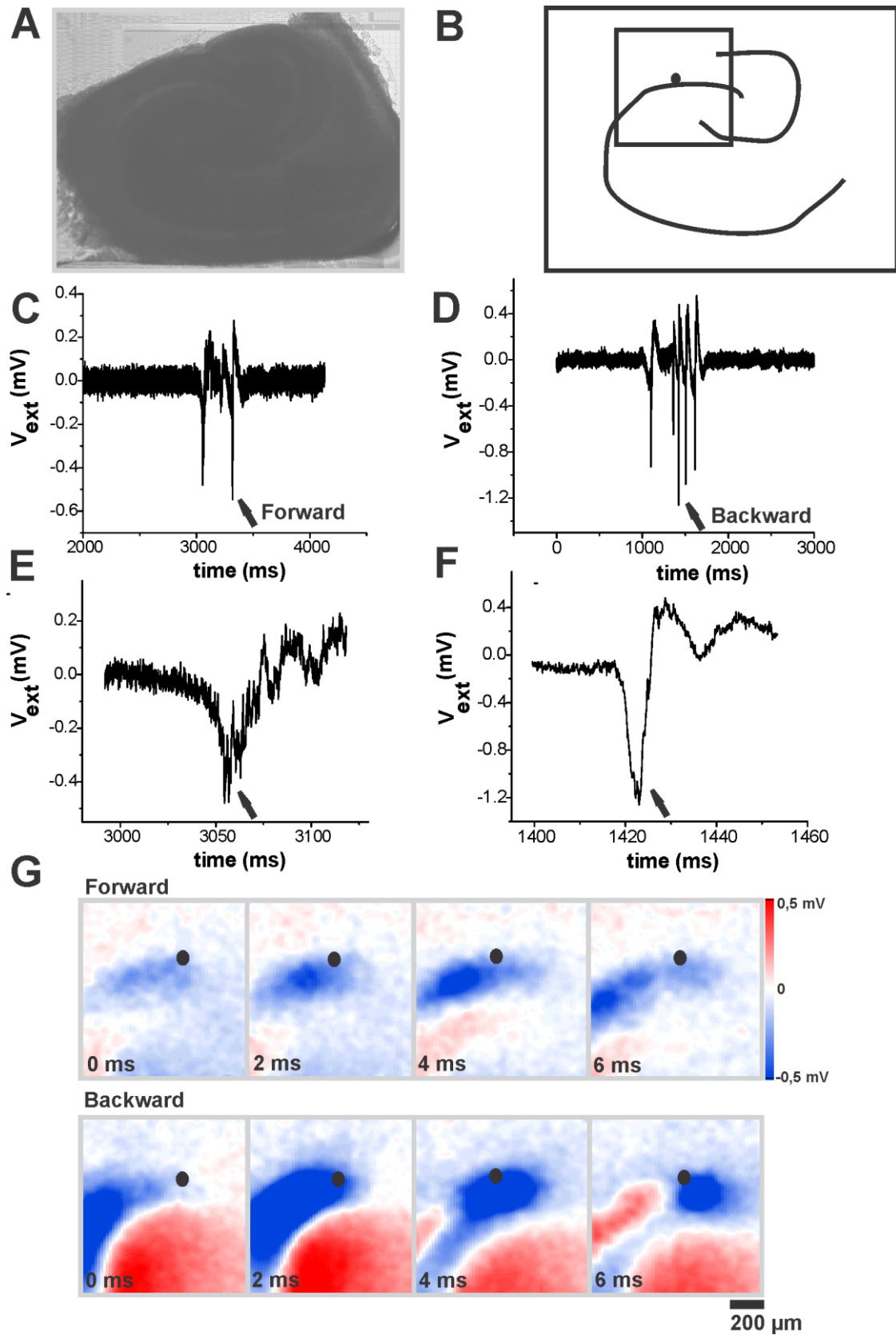
Figure 3.17: Electrical imaging of local field potentials during bicuclline methiodide induced epileptiform-like activity in acute hippocampal slices. A: Acutely prepared hippocampal slice placed on the recording array of the Neurochip. B: Schematic drawing of the region of the hippocampal slice imaged

on the Neurochip. C and D: Temporal trace of LFPs during an ELA with forward propagation and backward propagation respectively. E: Zoomed temporal trace of a forward propagating LFP, marked with an arrow in Figure 3.17C. F: Zoomed temporal trace of a backward propagating LFP, marked with an arrow in Figure 3.17D. G: Spatial electrical images of a forward propagating field potential (upper row) and backward propagating field potential (bottom row). All the traces are taken from the marked sensor position (row 51, column 70).

3.2.4 Characterization of epileptiform-like activity in acute hippocampal slices using low-density microelectrode arrays

3.2.4a Recording of high K^+ zero Mg^{2+} induced epileptiform-like activity in acute hippocampal slices on microelectrode arrays

To validate the characterization of ELA observed in recordings from OHCs on MEAs, acute slice measurements were carried out. Acute slices were placed on the recording array and a firm attachment of the slice was achieved by placing a platinum grid over it (Figure 3.18A). All the slices (n=3) were perfused with oxygenated ACSF solution (95%O_2 and 5% CO_2) for 20 minutes, with the bath temperature maintained between 36°C and 37°C to establish normal physiological condition. During perfusion of normal ACSF solution, there was no spontaneous activity observed in acute slices. Following perfusion of normal ACSF solution, treatment buffer was perfused. ELA with a frequency of 0.2 Hz was detected (Figure 3.18B, first 16 minutes) after 5 to 10 minutes of treatment buffer perfusion.

3.2.4b Effect of AMPA/kainate blocker DNQX on local field potentials during high K^+ zero Mg^{2+} induced epileptiform-like activity

To evaluate the role of glutamatergic signalling in well-established synaptic network, acute slice preparations were recorded on the MEAs (Figure 3.18A). All the slices (n=2) were perfused with control ACSF solution oxygenated with 95% O_2 and 5% CO_2. A perfusion rate of 1.5 ml/minute was maintained throughout the measurement and the bath temperature was maintained between 36°C and 37°C. During control buffer perfusion spontaneous activity was not observed. Following control ACSF solution perfusion, ELA was induced within 5 to 10 minutes of perfusion of the treatment buffer. After establishment

of the ELA, DNQX (100 µM) containing treatment buffer was perfused. Application of DNQX abolished LFPs within 4 minutes (Figure 3.18B).

Summary

Application of DNQX on acute hippocampal slice preparation abolished all the LFPs during high K^+ zero Mg^{2+} induced ELA.

A

B
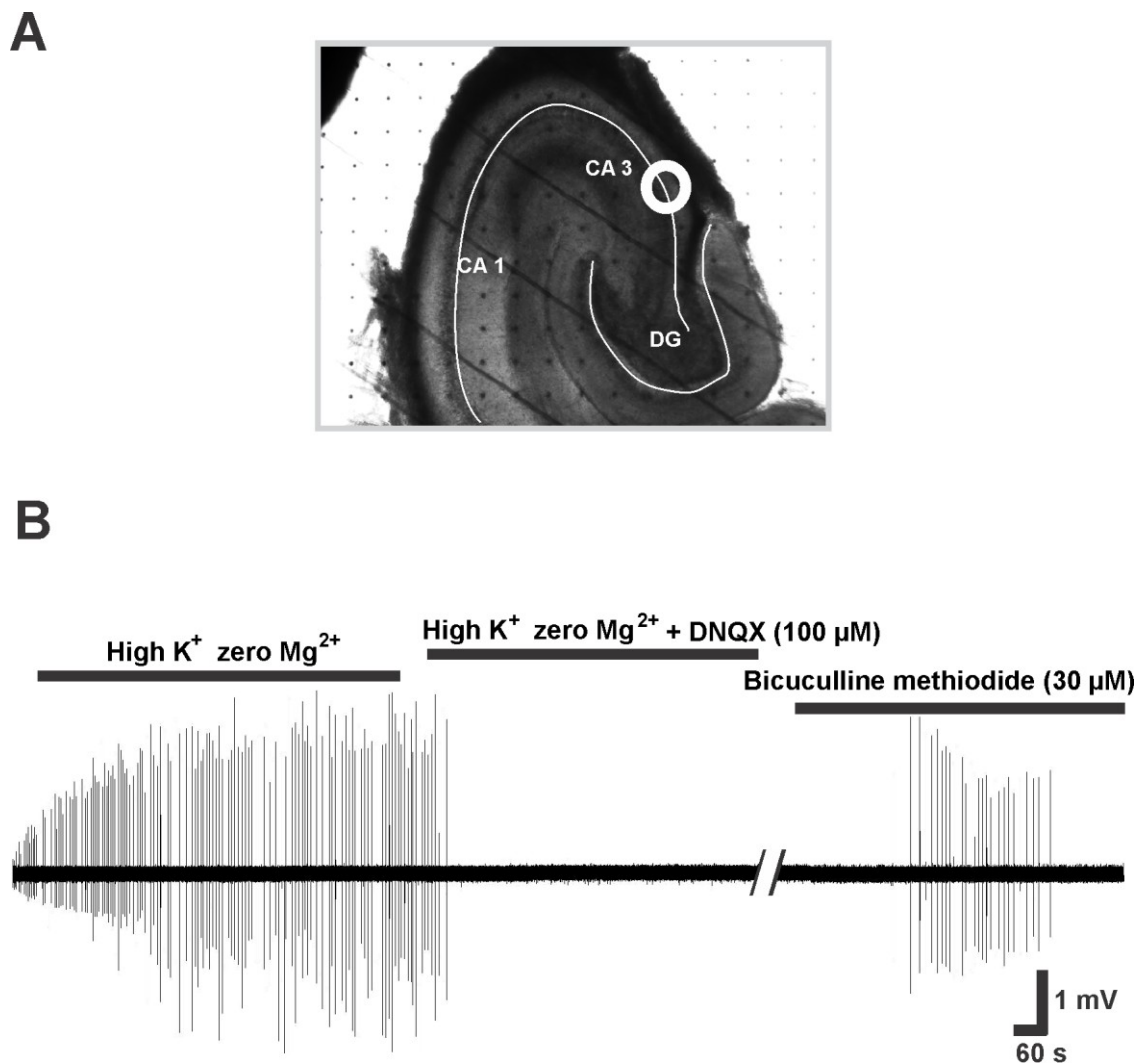
Figure 3.18: Effect of AMPA/kainate blocker DNQX on high K^+ zero Mg^{2+} induced epileptiform-like activity in acute hippocampal slices evaluated using low-density microelectrode arrays. A: Acute hippocampal slice interfaced to the recording array of the MEA B: Temporal trace of an ELA during high K^+ zero Mg^{2+} and high K^+ zero Mg^{2+} with DNQX perfusion from an electrode L5 marked with a white circle in Figure 3.18A in the CA3 region.

3.2.4c Effect of gap junction blocker meclofenamic acid on local field potentials during high K^+ zero Mg^{2+} induced epileptiform-like activity

To confirm the effect of gap junction blocker on induced ELA, which is prevalent in OHCs, ELA was induced in acute hippocampal slices placed on the MEA (Figure 3.19A) by perfusing the treatment buffer. ELA was observed after 5 to 10 minutes of perfusion of the treatment buffer (Figure 3.19C). MFA (100 µM) containing treatment buffer was perfused for 20 to 40 minutes. Following MFA incubation, extracellular recordings were made. MFA reduced the rhythmic field potentials to 0.03±0.02 Hz (mean±SEM) after 20 minutes of blocker application (Figure 3.19B). This result complements the recording of OHC in section 3.1.8c.

Summary

Application of gap junction blocker MFA on acute hippocampal slices decreased the frequency of LFPs; remaining activity was observed as short bursts of LFPs.
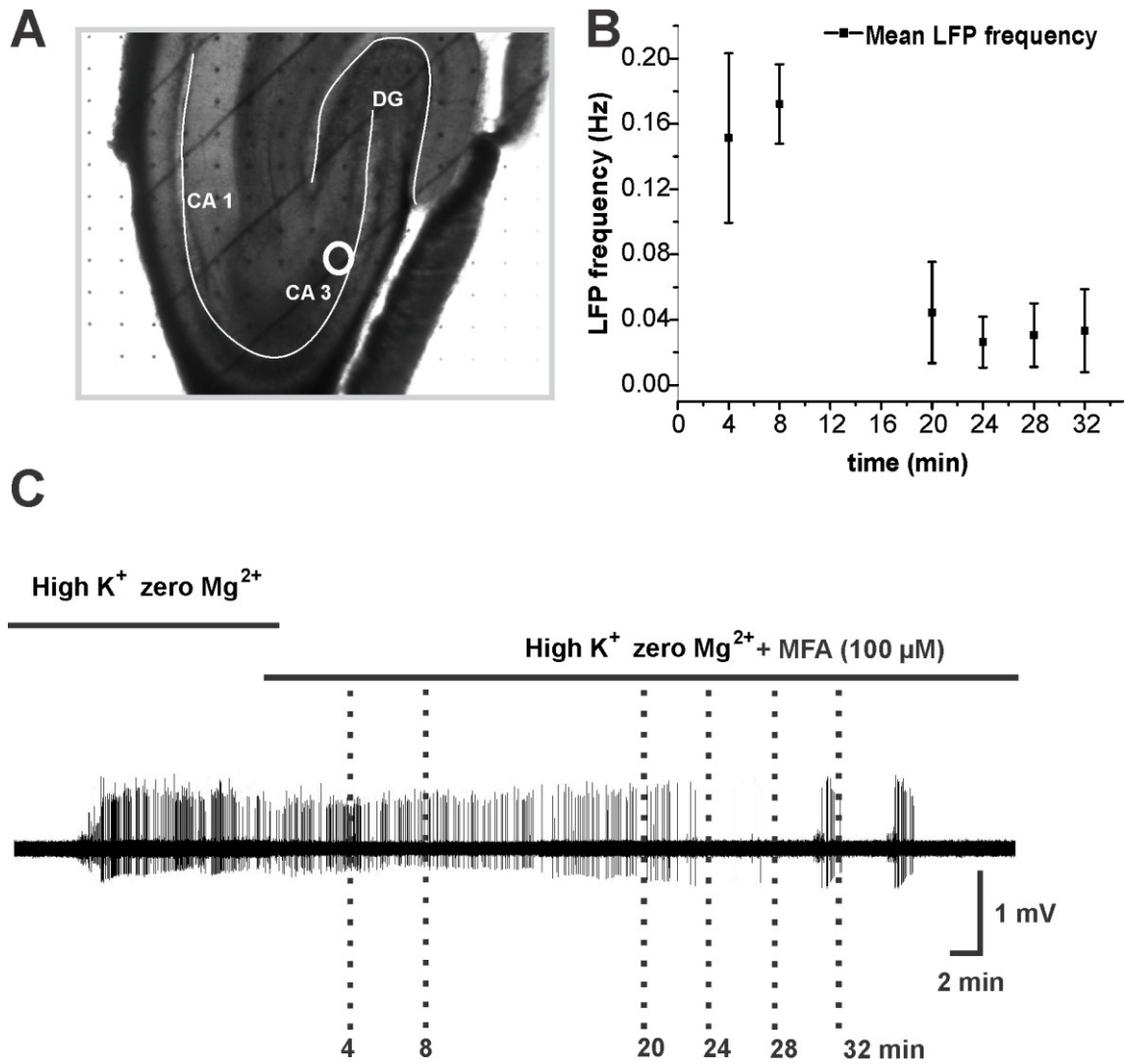
Figure 3.19: Effect of gap junction blocker MFA on high K$^+$ zero Mg^{2+} induced epileptiform-like activity in acute hippocampal slices evaluated using low-density microelectrode arrays. A: Acute hippocampal slice interfaced to the recording array of the MEA. B: Mean LFP frequency during high K$^+$ zero Mg^{2+} with MFA perfusion (first 8 minutes and after 20 minutes of perfusion). C: Temporal trace of ELA during high K$^+$ zero Mg^{2+} and high K$^+$ zero Mg^{2+} with MFA perfusion taken from an electrode I14 marked with a white circle in the CA3 region in Figure 3.19A.

3.3 Characterization of neuronal spiking during high K$^+$ zero Mg^{2+}/bicuculline methiodide induced epileptiform-like activity using Neurochips

To gain insights into the relation of neuronal spiking and LFPs, neuronal spiking activity was identified on Neurochips as described by Lambacher (Lambacher *et al.*, 2011). In this thesis, neuronal spiking was studied in high K$^+$ zero Mg^{2+}/bicuculline methiodide induced ELA to correlate spiking activity to LFPs. Neuronal spiking was detected in high-pass filtered extracellular recordings. It was identified by visual inspection of their waveforms and spatial localization. Neuronal spike waveforms are typically restricted to about 10 – 20 electrodes, unlike LFPs which cover several hundred of electrodes. Extracellular waveforms of the single unit and spike-triggered average analysis, aid in characterizing single units. Neuronal spiking activity was a unique feature observed only in our extracellular recordings from OHCs. Thinning of cell layers from 400 µm thickness to ~200 µm during long-term cultivation under *in vitro* condition enables electrophysiological recordings from individual neurons. Neuronal spiking was observed during induced ELA (n=18 slices). In total, 36 single units were identified and extracted for analysis from these recordings. In the following sections, analysis of these single unit activities will be discussed separately for different conditions. Understanding the individual neuronal activity or a group of neurons under pathological circumstances may provide information of cell groups that may trigger an aberrant activity or may reveal the cell groups that could be affected by the aberrant activity.

3.3.1 Neuronal spiking preceding a local field potential

Neuronal spiking preceding an LFP (n=4 cells) was observed during high K$^+$ zero Mg^{2+} induced ELA (n=3 slices). Neuronal spiking with a spike train preceding an LFP with an LFP frequency of ~1 Hz in one of these slices is shown (cell 1, Figure 3.20F, left panel). Additional neuronal units with different correlation pattern (cell 2 and cell 3) were also observed (Figure 3.20F, right panel). In the other two slices, each LFP was preceded by singular,

spontaneous spikes rather than spike train bursts. For extraction of neuronal spiking, extracellular recordings were high-pass filtered and identified based on the extracellular waveform and by visualization of spatial localization. Spiking which occurred at time t1 was followed by an LFP at time t2. Spiking was observed along the CA3 region of the hippocampus (Figure 3.20A). Neuronal activity was at the sensor position marked with a dark circle in the schematic drawing of the recorded slice (Figure 3.20B). The high-pass filtered trace shows neuronal spiking preceding the first two LFPs (Figure 3.20C). As the spiking and field potentials occurred at two different time points (t1 and t2 respectively), a minimal time difference of 10 ms was observed between neuronal spiking and LFP occurrence .The pattern of spikes preceding the field potential was clearly separable (Figure 3.20D). The electrical image of the LFP at time t2 which corresponds to time later than spiking is shown (Figure 3.20E). The electrical image of neuronal spiking (without averaging) at time t1 clearly shows the extracellular voltage recorded on few electrodes (Figure 3.20F). Interestingly, in none of the electrical images the trace of an axon was revealed. This is in contrast to recordings from retinal ganglion cells (Zeck *et al.*, 2011).
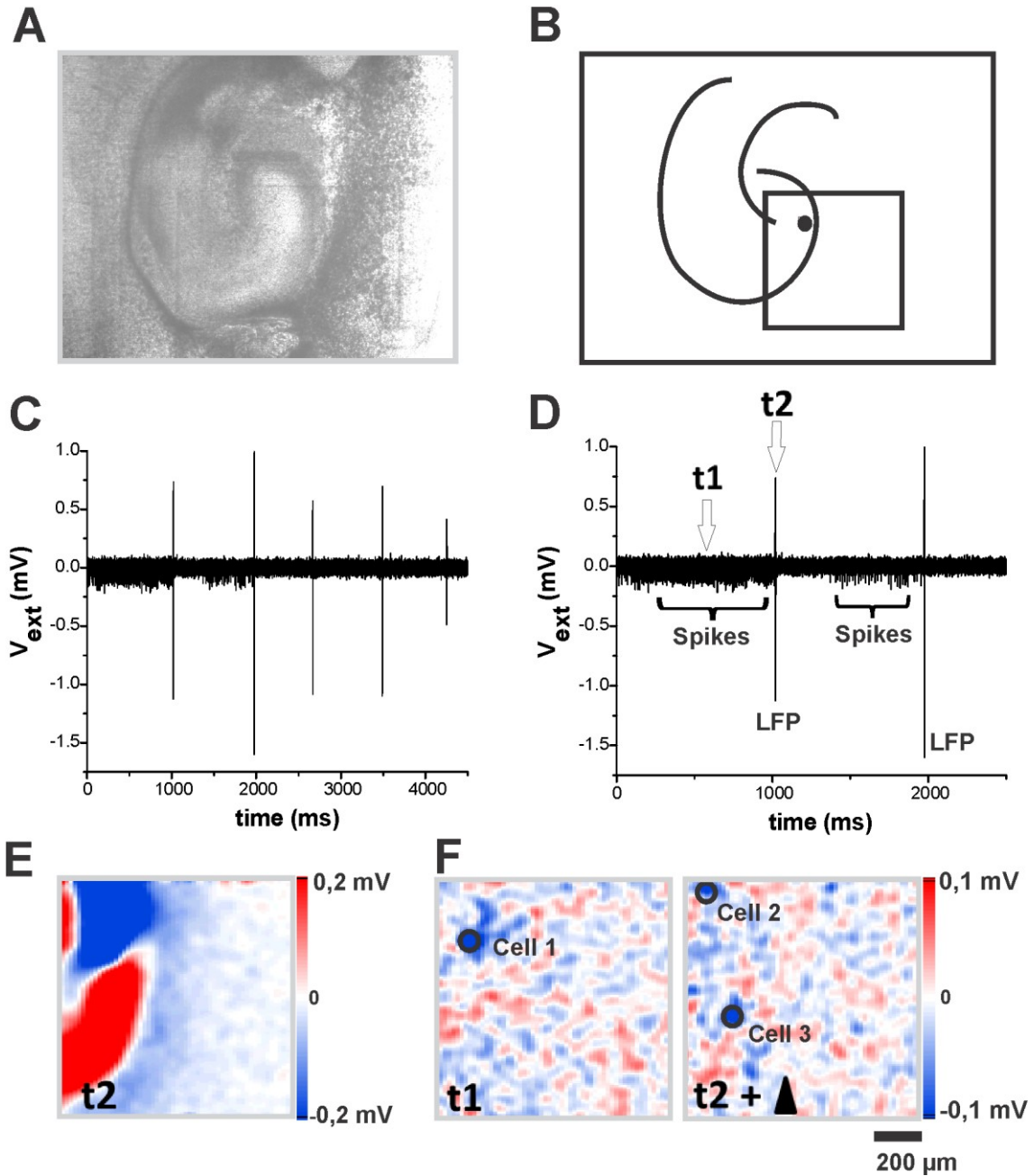
Figure 3.20: Neuronal spiking preceding a local field potential. A: OHC at DIV 7 interfaced on the recording array of the Neurochip. B: Schematic drawing of the hippocampal slice imaged on the Neurochip with the sensor position marked with a dark circle. C: High-pass filtered temporal trace of LFPs and neuronal spiking from the marked sensor. D: Zoomed temporal trace from Figure 3.20C showing LFPs and neuronal spikes. E: Spatial electrical image of an LFP occurring later to spiking at time t2. F: Left panel: Electrical image of cell 1 which spikes prior to an LFP at time t1; Right panel: Electrical image of cell 2 and cell 3 which spikes after time t2 with different correlation pattern

74

3.3.2 Neuronal spiking following a local field potential

Neuronal spiking following an LFP was observed during interictal discharges along the CA3 region (Figure 3.21A) in 8 slices: In the following, one example is presented. The sensor position is marked with a dark circle in the schematic drawing of the slice (Figure 3.21B). Spiking following an LFP was detected in 9 cells. A high-pass filtered trace of a neuronal spike train, later to an LFP with an LFP frequency less than 0.1 Hz is shown (Figure 3.21C). The minimal time difference of 10 ms was observed between the LFP and spike occurrence. The zoomed temporal trace shows the LFP preceding the spiking (Figure 3.21D). The electrical image of the LFP at t1 shows the extracellular voltages recorded over the recording array along the CA3 region in the pyramidal cell layer (Figure 3.21E). Electrical image of neuronal spiking marked with a black circle (cell 1) following an LFP is shown (Figure 3.21F, left panel). Additional neuronal spiking activity was detected at a different sensor (cell 2) with a similar spike-LFP correlation (Figure 3.21F, right panel).
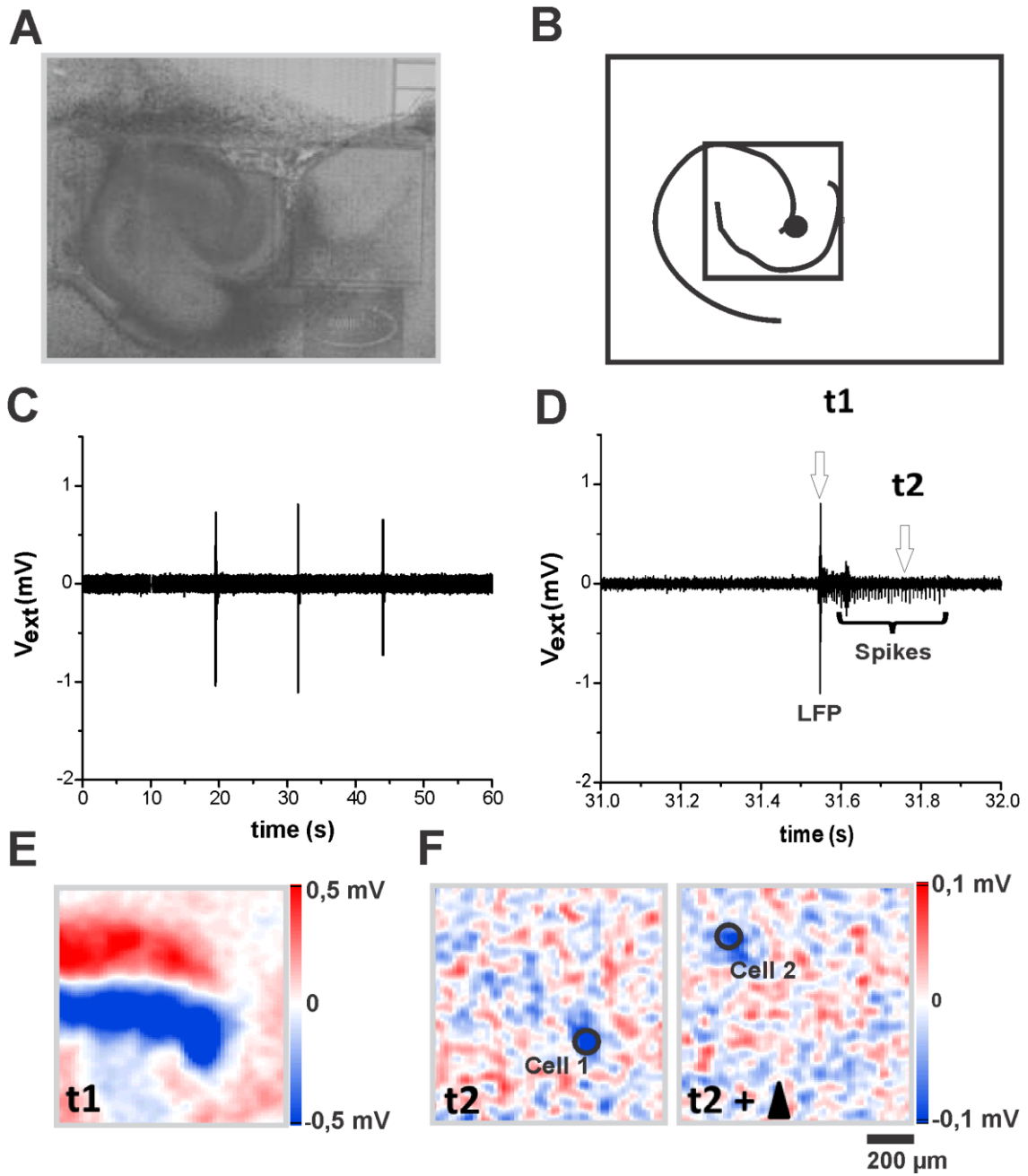
Figure 3.21: Neuronal spiking following a local field potential. A: OHC at DIV 10 interfaced to the recording array of the Neurochip. B: Schematic drawing of the hippocampal slice imaged on the Neurochip with the sensor position marked with a dark circle. C: High-pass filtered temporal trace of LFPs and neuronal spikes from the marked sensor D: Zoomed temporal trace from Figure 3.21C showing an LFP and neuronal spikes. E: Electrical image of an LFP occurring prior to spiking at time t1. F: Left panel: Electrical image of cell 1 which spikes after an LFP at time t2; Right panel: Electrical image of cell 2 with similar spike-LFP correlation which spikes after time t2. All the traces were taken from the marked sensor position (row 34, column 25).

3.3.3 Neuronal spiking preceding and following a local field potential

Neuronal spiking before and after an LFP was observed during interictal discharges (n= 2 slices). Neuronal units (n=3 cells) with spikes preceding and following an LFP were observed in a cell, along the CA3 region in one of the slice and in two cells along the CA1 region in another slice (Figure 3.22A). The sensor position marked with a dark circle and the schematic drawing of this slice with the CA1 region is shown (Figure 3.22B). A high-pass filtered temporal trace of 4 seconds duration shows epileptiform discharges with LFP frequency 5–10 Hz and spikes (Figure 3.22C). A zoomed temporal trace of a part of the trace shows SUA preceding and following an LFP with the time sequence of the spike (t1), LFP (t2), and spike (t3) (Figure 3.22D). A minimal time difference of 10 ms was observed between the spike and LFP occurrence. Neuronal spikes preceding and following an LFP is clearly visible in the zoomed temporal trace with the spikes and LFP labelled. An electrical image of the LFP at time t2 over the recording array is shown (Figure 3.22E). An electrical image of cell 1 which spikes before and after an LFP is shown (Figure 3.22F, left panel). Damaged sensors appearing as a single unit are marked with a triangle here. An additional single unit recorded on a different sensor (cell 2) with spikes preceding and following the LFP at time t3 was also observed (in Figure 3.22F, right panel).
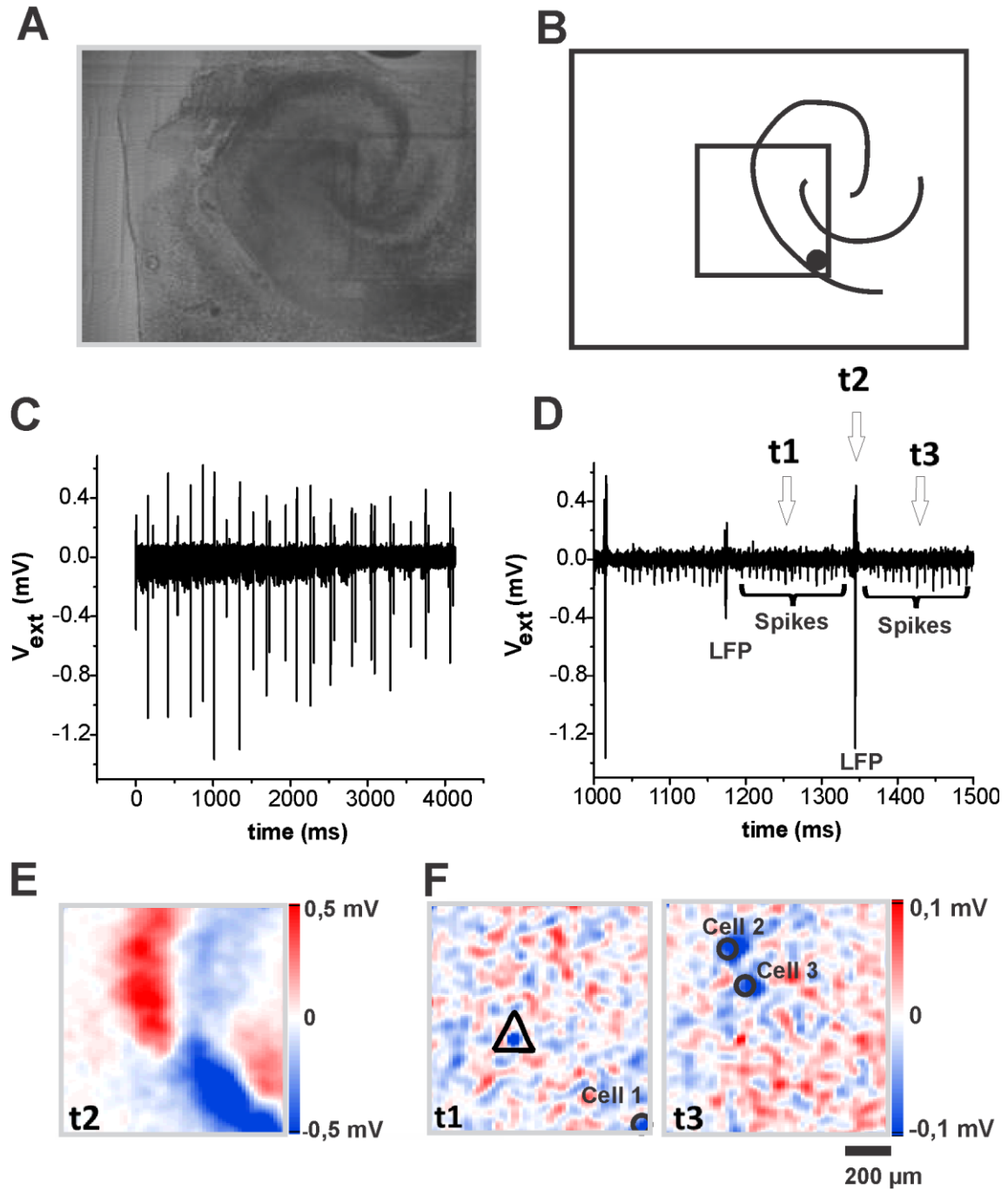
Figure 3.22: Neuronal spiking preceding and following a local field potential. A: OHC at DIV 7 interfaced to the recording array of the Neurochip. B: Schematic drawing of the hippocampal slice with the sensor position marked with a dark circle. C: High-pass filtered temporal trace showing LFPs and neuronal spiking. D: Zoomed temporal trace from Figure 3.22C showing LFPs and neuronal spikes. E: Spatial electrical image of an LFP at time t2. F: Left panel: Electrical image of cell 1 with spikes preceding at time t1 and following an LFP at time t3. Damaged sensors appearing as single units are marked with a triangle; Right panel: Cell 2 with fewer spikes before and after an LFP, Cell 3 with different spike-LFP correlation at time t3. All the traces were taken from the marked sensor position (row 119, column 118).

3.3.4 Classification of single units based on spike width

In principle, spike-triggered averages (STAs) may be used to separate neurons into pyramidal cells and interneurons (Csicsvari *et al.*, 1999). Based on the waveforms obtained from the STAs we attempted to identify pyramidal cells and interneurons by calculating the full-width at half-amplitude minimum (FWHM) of the extracellular waveform caused by the action potential. Spike waveforms of a single unit from nine adjacent transistors obtained from STAs were overlaid (Figure 3.23A) and normalized to the minimum peak amplitude by introducing a small jitter (Figure 3.23B). The FWHM of the action potential (spike) was calculated from the resulting waveform obtained by the average of all the normalized peak amplitude. Exemplary electrical images of the STA of a single unit with a FWHM of 0.27 ms are shown with an inter-frame interval of 0.1 ms (Figure 3.23C) from the sensor position marked by a black circle. STAs were calculated from 22 cells (7 slices). Based on the spike width, the cells were grouped into two groups: In group I, spikes with FWHM > 0.2 ms were averaged and mean spike duration of 0.29±0.01 ms was calculated. In group II, spikes with FWHM < 0.2 ms were averaged and mean spike duration of 0.15±0.02 ms was calculated (Figure 3.23D). Due to the limited sample size (n=22) no formal clustering was performed.

Summary

The evaluation of the spiking behaviour revealed neuronal spiking preceding an LFP, neuronal spiking following an LFP and neuronal spiking preceding and following an LFP. Spike-triggered average analysis and estimation of spike duration based on full-width at half-amplitude minimum analysis showed two kinds of waveforms. Recording with faster sampling rate and more cells are needed to draw a conclusion.
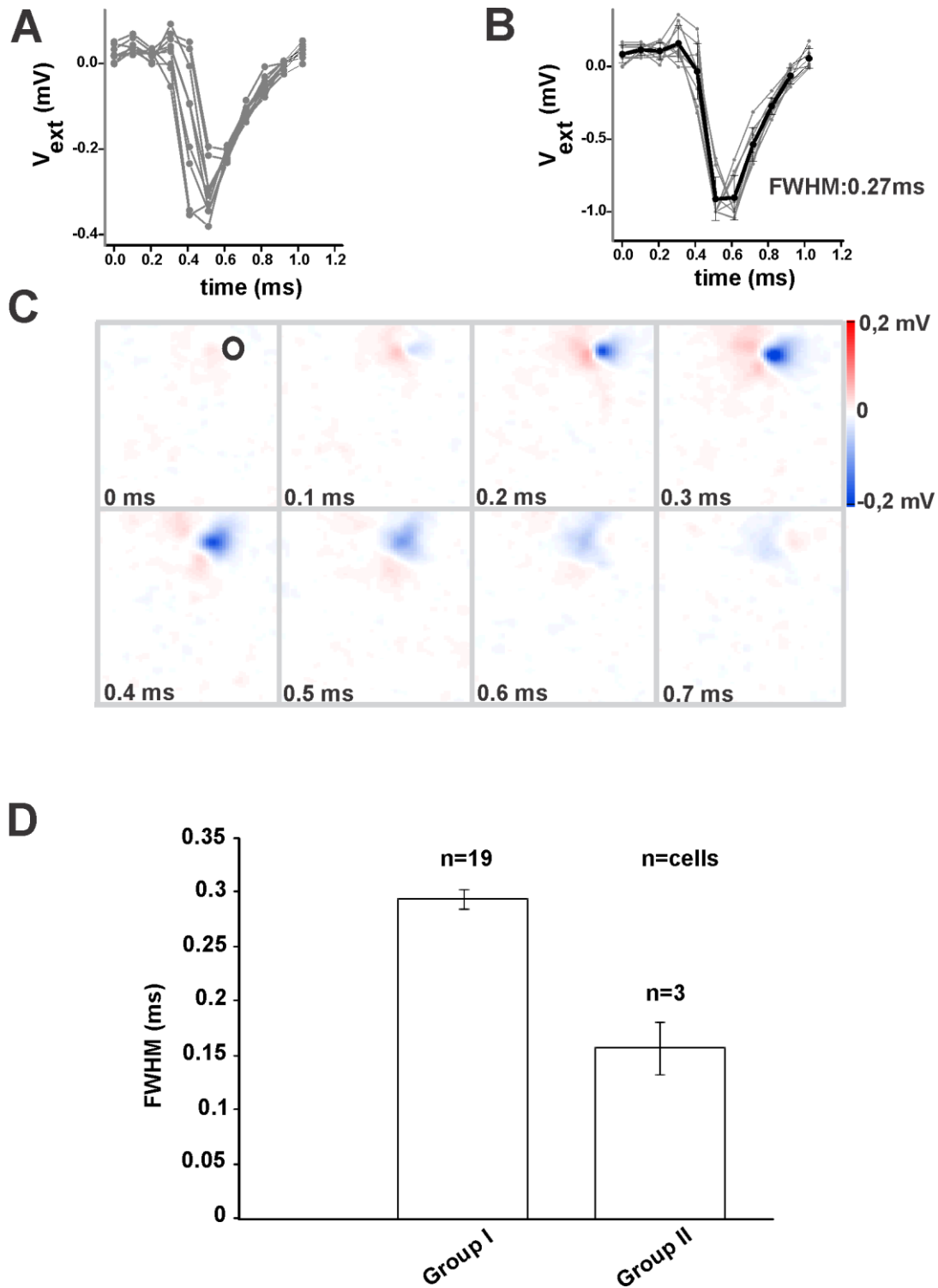
Figure 3.23: Spike triggered averages of single unit activity. A: Voltage waveforms recorded on 9 adjacent transistors at the same time are overlaid. B: Normalized spike amplitudes shown in Figure 3.23A. A small time jitter was introduced to match the signal minima. C: Electrical images of one single unit with an inter-frame interval of 0.1 ms (at sensor position row 20, column 78) recorded on many adjacent sensors are shown. D: Histogram showing two cell groups - Group I – spike duration > 0.20 ms; Group II – spike duration < 0.20 ms.

3.4 Electrical imaging of aberrant network activity in degenerated *rd10* retina

The results presented in this chapter are part of the publication:

"Rhythmic Ganglion Cell activity in Bleached and Blind Adult Mouse Retinas".J.Menzler, L.Channappa, G.Zeck (2014) *PLoS One., 9*(8), e106047.

3.4.1 Spontaneous retinal ganglion cell activity in *rd10* retina

Spontaneous activity of retinal ganglion cells was recorded from *rd10* retina (P90 – 100, Figure 3.24B (n = 3 retinas)). This activity was compared to recordings from wild-type retinas (Figure. 3.24A) which were performed previously by J.Menzler. At the recording time, all photoreceptors in the *rd10* retinas were lost. A mean firing rate of 20±2 Hz was calculated from 62 RGCs (Figure 3.24C) identified in these retinas. The mean fundamental frequency, i.e. oscillatory frequency, evaluated from 32 rhythmic *rd10* RGCs was 6.5±0.2 Hz (Figure 3.24D). This value is somewhat smaller as the fundamental frequency reported for *rd1* RGCs (7 – 10 Hz, Menzler & Zeck, 2011).
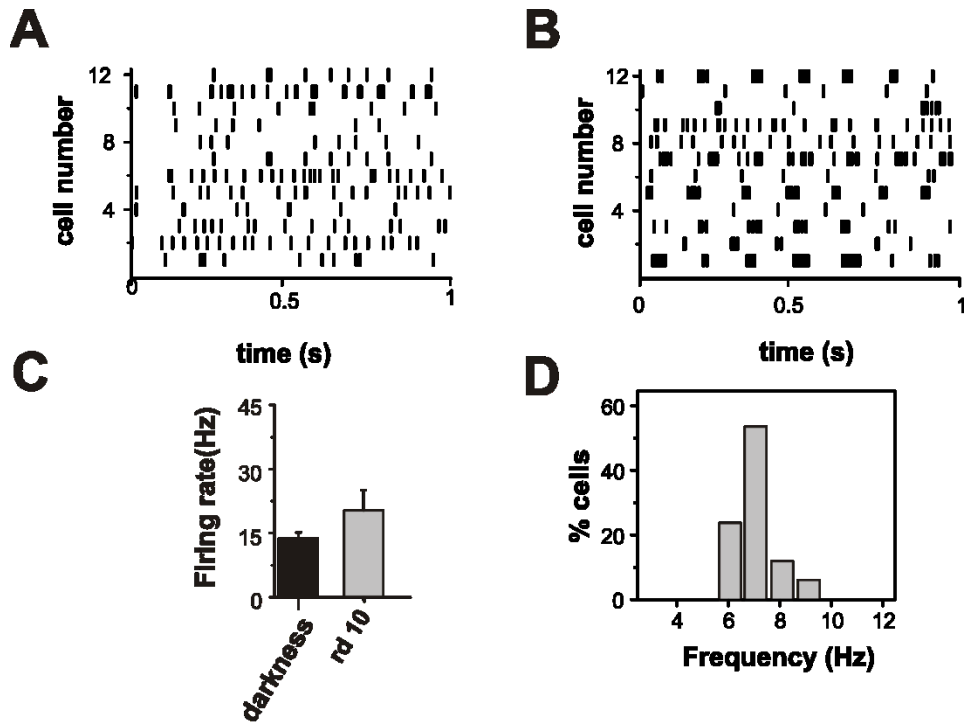
Figure 3.24: Spontaneous rhythmic ganglion cell activity in C57BL/6 and *rd10* retina. A: Raster plot of spontaneous RGC activity recorded in C57BL/6 retinas in darkness. B: Raster plot of spontaneous RGC activity recorded from *rd10* retinas. C: Average RGC maintained activity measured in wild type and *rd10* retinas. D: Histogram of the fundamental frequency of 32 rhythmic RGCs evaluated from three *rd10* retinas. Figure modified from Menzler *et al* (Menzler *et al*., 2014).

In addition to spontaneous RGC activity, spontaneous field potentials were also detected in *rd10* retina. The field potentials observed in *rd10* retinas were stationary. They occurred at random positions over the 1 mm^2 recording array. A temporal trace of field potentials at a sensor position marked with a dark circle is shown in Figure 3.25A. Corresponding electrical images at two different time points (t1 and t2) showing LFPs at similar positions (Figure 3.25B) illustrate that the field potentials did not propagate from one location to another.
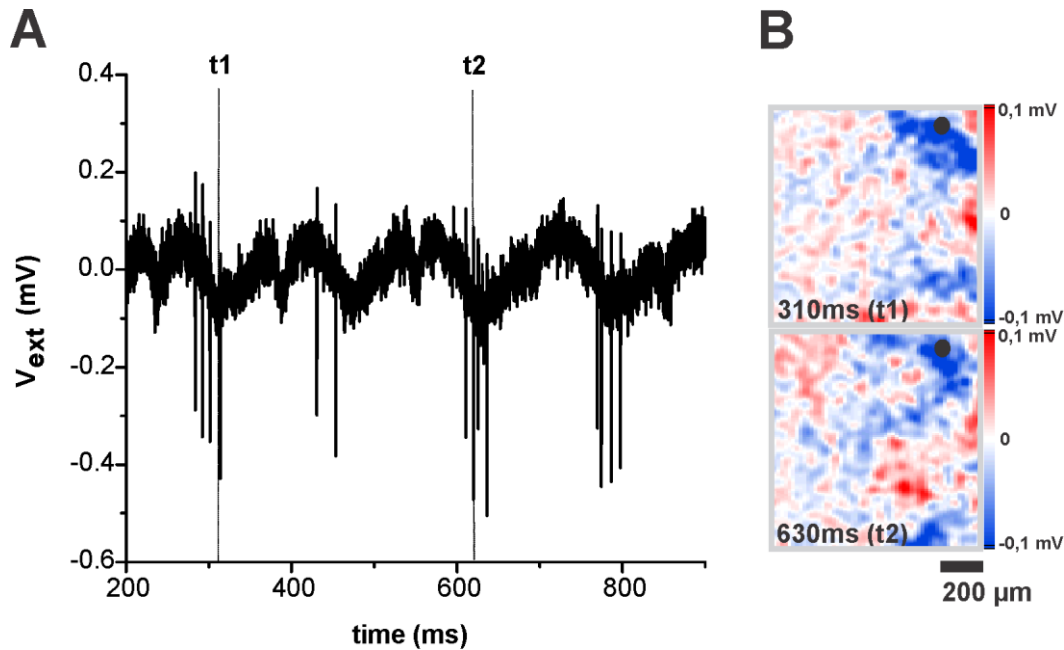
Figure 3.25: Spontaneous local field potentials in *rd10* retina. A: Temporal trace of rhythmic stationary field potentials at sensor position (row 15, column 102) marked with a dark circle in Figure 3.25B. B: Electrical images of the field potential at time t1 and t2. Figure modified from Menzler *et al* (Menzler *et al.*, 2014).

3.4.2 Effect of pharmacological treatment on aberrant activity in *rd10* retina

To evaluate the role of glutamate receptor signalling for the spontaneous rhythmic activity in *rd10* retina, the major ionotropic glutamate receptors of the RGCs were blocked using AMPA/kainate receptor blocker DNQX (20 µM). After application of the blocker, rhythmic RGC spiking disappeared (Figure 3.26A). Within continuous recording up to 5 seconds, no rhythmic activity could be detected. Thus, we exclude rhythmic spiking with frequencies higher 0.2 Hz.

Additionally, to assess the role of electrical coupling underlying the rhythmic activity in these degenerated *rd10* retinas, gap junction blocker MFA (100 µM) was used to block the electrical synapses. Following the blocker addition, the rhythmic activity was abolished (Figure 3.26B). This is consistent with the idea that the network of electrically coupled bipolar and amacrine cells (Trenholm *et al.*, 2012) is likely also responsible for the rhythmic activity observed in *rd10*.
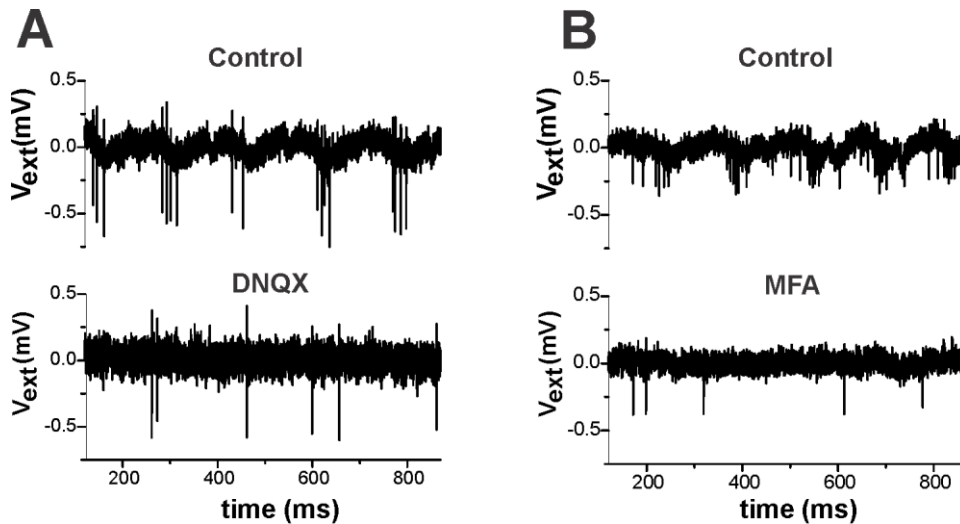
Figure 3.26: Effect of pharmacological blockade on aberrant network activity in *rd10* retina. Spontaneous aberrant rhythmic spiking activity abolished by A: ionotrophic glutamate receptor blocker DNQX (20 μM) B: gap junction blocker MFA (100 μM). Figure modified from Menzler *et al* (Menzler *et al.*, 2014).

To evaluate the role of inhibition, a mixture of the glycinergic receptor blocker strychnine (2 μM) and the GABA$_A$ receptor blocker gabazine (20 μM) was used. After addition of the mixture to the recording solution, strong stationary LFPs were detected over the array from different sensors (Figure 3.27A and B). Spatial electrical images of the stationary field potential marked with an arrow in Figure 3.27B are shown with an inter-frame interval of 20 ms (Figure 3.27C). As before, the observed LFPs did not propagate. Evaluation based on the centre of activation of each propagating point showed that the points clustered within a particular area without any propagation (Figure 3.27 D and E).

Summary

Extracellular recordings of *rd10* retina revealed spontaneous stationary field potentials. Upon application of DNQX or MFA, rhythmic LFPs were abolished. Under reduced inhibition by application of strychnine and gabazine, the amplitude of the stationary LFPs increased.
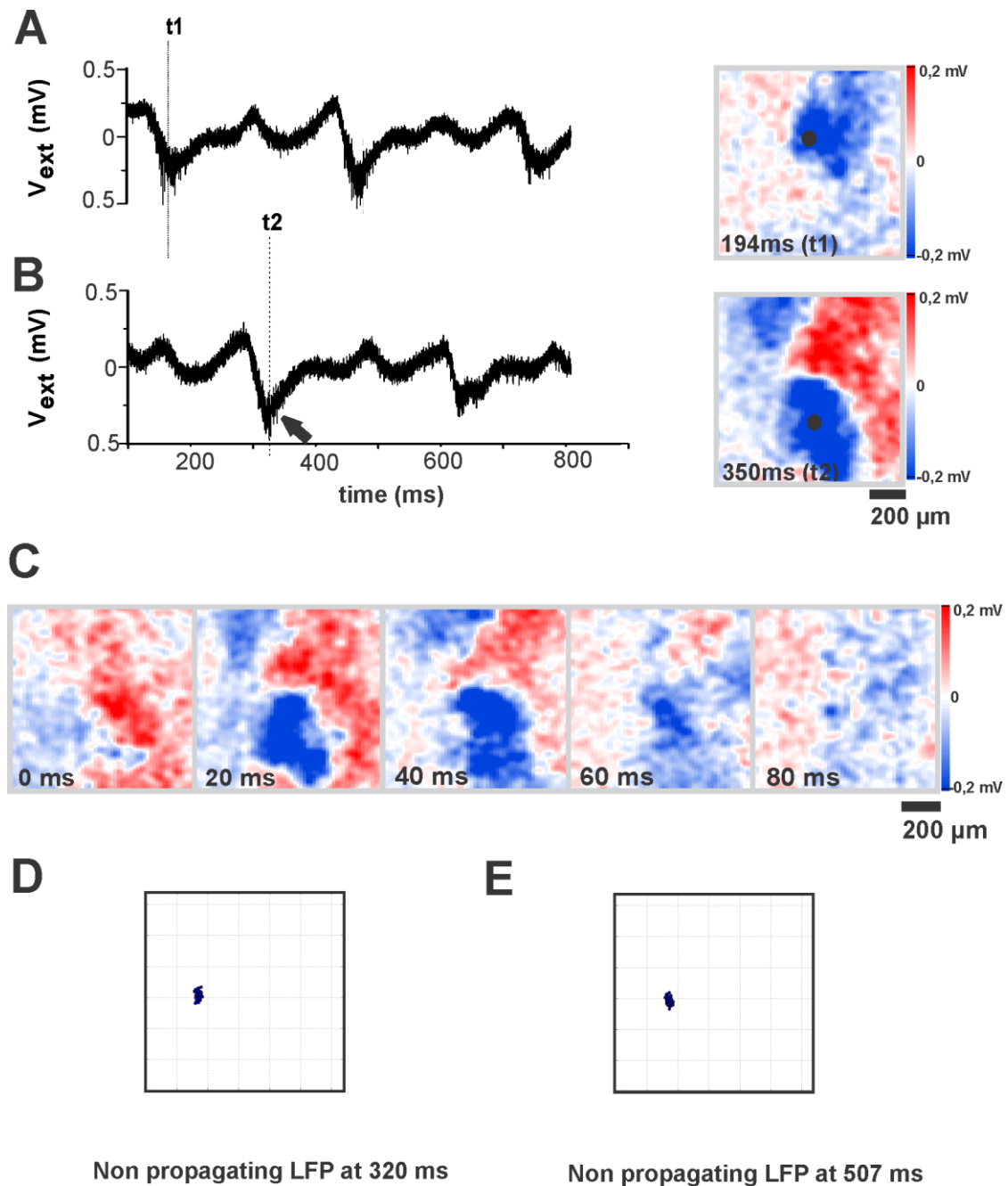
Figure 3.27: Effect of strychnine and gabazine on *rd10* retina. A: Temporal trace of LFPs from the marked sensor position (row 44, column 64) and corresponding spatial electrical image of the LFP at time t1 in the right panel, sensor position marked with a dark circle. B: Temporal trace of LFPs at a different sensor position (row 84, column 70) with corresponding spatial electrical image of the LFP at time t2 in the right panel, sensor position marked with a dark circle. C: Electrical images of a stationary field potential marked with an arrow in Figure 3.27B with an inter-frame interval of 20 ms. D Representation of non-propagating LFP based on centre of activation of each point of propagation at two different time points.

4 Discussion

The key findings of this thesis are the following

i)   During epileptiform–like activity (ELA), the population spike (p-spike) of an LFP propagates in hippocampal slices along the trisynaptic pathway, not only in forward (classical) direction but also in backward direction.

ii) These two propagation patterns electrically imaged using a high-density multielectrode arrays were found in excitation and disinhibition induced models of ELA in organotypic and in acute hippocampal slices. Backward propagation was detected predominantly in the ictal phase of ELA.

iii) Gap junction blocker, MFA inhibited LFP propagation and decreased LFP frequency over time in high K^+ zero Mg^{2+} induced ELA in hippocampal slices. AMPA/kainate receptor blocker DNQX abolished this ELA.

iv) In *ex vivo* photoreceptor degenerated retinas (*rd10*), rhythmic ganglion cell spiking and LFPs were detected. The LFPs were rhythmic, non-propagating and inhibited by either blocking electrical synapses (with MFA) or excitatory transmission via ionotropic glutamate receptors (with DNQX).

4.1 Technical Considerations

All recordings were performed with two types of MEAs: a high-density MEA, where the continuous recording time is restricted to ~5 seconds with a recording area of 1 mm^2 (Eversmann *et al.*, 2003; Hutzler *et al.*, 2006; Zeck *et al.*, 2011) and a low-density MEA with unrestricted recording time. This was chosen as the new CMOS-based high-density MEAs with unrestricted recording time and larger recording area (Bertotti *et al.*, 2014) were not available for the conducted experiments. Evidence has been provided in the results section that, despite different recording modes, the results are comparable. As high-density MEAs have smaller inter-electrode distance (<20 µm), they provide better spatial

resolution and are able to spatially characterize the field potentials more accurately than those obtained from low-density MEAs having larger inter-electrode distances: 42 μm (Ferrea *et al.*, 2012), 200 μm (Gonzalez-Sulser *et al.*, 2012), 400 μm/300 μm (Zhang *et al.*, 2014).

4.2 Aberrant activity in hippocampal slices

The hippocampus is one of the most extensively studied parts of the brain, investigated amongst others for its role in epileptic seizure propagation (Pisciotta *et al.*, 2010; Zhang *et al.*, 2014), seizure onset and transition from normal to epileptic state, i.e. from interictal to ictal activity (Dzhala & Staley, 2003; Cymerblit-Sabba & Schiller, 2010). With advancements in recording technology, network activity in the hippocampal slices has been studied recently, using high-density multitransistor arrays (Hutzler *et al.*, 2006; Ferrea *et al.*, 2012).

Spontaneous activity has been an inherent feature of developing neural networks in different parts of the nervous system, such as the hippocampus, the cochlea, the retina, the spinal cord and the cerebellum (Blankenship & Feller, 2010). In the current study, spontaneous activity was studied in i) OHCs - where the neural networks develop under *in vitro* condition ii) acute slices - where the neural networks develop under *in vivo* condition.

In our recordings, spontaneous LFPs in the OHCs appeared within the hippocampal region with apical sinks and basal sources. These LFPs were emerging and disappearing along the trisynaptic circuitry. Additionally, stationary field potentials appearing only on a part of the array were also observed. Emergence of spontaneous activity in OHCs could be due to early rewiring of the network during development. In acute hippocampal slices, spontaneous activity was not observed in our recordings. This could be due to the mature and stable network present in the adult tissues.

4.2.1 Local field potentials under induced epileptiform-like activity

In our study, ELA was induced by application of high K^+ zero Mg^{2+} containing ACSF solution as excitatory model for ELA induction. BMI containing ACSF solution was used as the disinhibitory model for ELA induction. Elevated K^+ in the extracellular medium produces spontaneous tonic-clonic discharges by increasing the neuronal excitability and causing neuronal and glial swelling (Traynelis & Dingledine, 1988). Mg^{2+}free ACSF favours interictal discharges by removing the Mg^{2+} blockade of NMDA receptors and enhancing the glutamatergic excitation (Mody *et al.*, 1987). Therefore, this chemical combination was appropriate to study complex network activity that leads to transition from interictal to ictal-like activity during ELA. BMI as a GABA$_A$ receptor antagonist, blocks fast GABAergic neurotransmission and thereby enhances the fast glutamatergic transmission, and favours interictal-like bursts. Based on the mechanism of epileptiform induction, many other models are also available to elicit similar ELA discharges. Examples include the 4-AP model, where the potassium channel blocker, 4-aminopyridine, depolarizes the membrane potential and increases the excitability of the neurons. In the picrotoxin-induced model, epileptiform-like activity is induced through GABA$_A$ receptor chloride channel blocker (Pitkänen *et al.*, 2005).

We have shown under chemically induced epileptiform-like activity that the field potentials propagated within the trisynaptic circuitry of the hippocampus from DG towards CA3 and most importantly, the backward propagation from CA3 towards DG during high K^+ zero Mg^{2+} induced ELA. Interestingly these propagating field potentials propagated at similar speeds during both forward and backward propagation. Since this observation was under increased excitation, we additionally confirmed the propagation pattern under reduced inhibition. Bicuculline methiodide, a GABA$_A$ receptor antagonist elicited ELA by reducing the inhibitory drive and produced field potentials which also propagated within the trisynaptic circuitry from DG towards CA3 and from CA3 towards DG. This result is in contrast to the field potentials which failed to

propagate from CA3 to DG under bicuculline methobromide (Gonzalez-Sulser *et al.*, 2011). On a whole, this unusual backward propagation of field potentials from CA3 towards DG is of significant importance in pathological conditions such as epilepsy.

Additionally, the finding of backward propagating field potentials were strengthened with our experiments performed in acute slices using both models of epilepsy induction. Propagating field potentials from CA3 towards hilus has also been reported, but in a 4-AP model of induced epilepsy using high-density multielectrode array (Ferrea *et al.*, 2012). Though the results reported by Gonzalez-Sulzer (Gonzalez-Sulser *et al.*, 2011) and Ferrea (Ferrea *et al.*, 2012) are comparable to ours, propagation path and velocity were not investigated in these earlier studies. Our approach is the first to support with evidence the bidirectional propagation within the trisynaptic circuitry between CA3 and DG with electrical imaging. The propagation path is similar for both forward and backward propagating field potential in high K^+ zero Mg^{2+} and bicuculline methiodide induced model of epilepsy.

Anatomical evidence of CA3 pyramidal cell projecting into the DG dates back to earlier research (Schwerdtfeger & Sarvey, 1982). Additionally, dye injection techniques also provided the evidence of back-projecting axons of pyramidal cells in "proximal" CA3 (near to DG) with collaterals in the hilus (Li *et al.*, 1994). These findings were strengthened with physiological evidence from stimulation studies suggesting that fimbria activation of CA3 pyramidal cells with single electrodes led to hilar neuron activation apparently by hilar collaterals present in the CA3 region (Scharfman, 1993).

We also estimated the velocities of forward and backward propagating LFP p-spikes based on the centre of activation of the extracellular field potential. In our study, the observed velocity ranged between 0.2 m/s - 0.3 m/s for both forward and backward propagation. There was no significant difference between the two propagation velocities. These velocities are in agreement with the reported axonal conduction velocity of 0.3 m/s (Kibler and Durand, 2011) suggesting, that the propagation occurs along the mossy fibres connecting the DG and CA3.

A wide range of LFP propagation velocities ranging between 0.08 m/s to 0.14 m/s has been reported in the literature depending on the tissue preparation used and model of epileptiform-like activity induction: 0.1 to 0.15 m/s in intact whole hippocampus under low Mg^{2+} ACSF (Quilichini *et al.*, 2002); 0.07 to 0.1 m/s in transverse hippocampal slices under high K^+ ACSF (Liu *et al.*, 2013); 0.1±0.04 to 0.12±0.03 m/s along transverse and longitudinal direction respectively in unfolded hippocampus under 4-AP induced epileptiform-like activity (Zhang *et al.*, 2014). Propagating field potentials (~0.1 m/s) have also been observed in normal physiological activity under *in vitro* conditions (Lubenov & Siapas, 2009).

In summary, our findings of forward and backward propagating field potentials observed during induced ELA through electrical imaging at high spatial resolution and further characterization of the field potential properties (propagation velocity; propagation path) is the key finding achieved using advanced recording techniques with the high-density MEAs.

A unique pattern of propagating LFPs during different phases of the ELA was observed only in our recordings: (i) backward propagating (CA3 to DG) p-spikes were detected during ictal-like activity (ii) Forward and backward alternating p-spikes were observed during interictal-like activity and (iii) only forward propagating p-spikes were detected towards the end of the epileptic discharge. We are not aware of any other study reporting such patterns except for maybe one showing distinctive propagating spatial patterns during ictal onset in the neocortex of a feline model under induced epilepsy. In this study, spatial patterns obtained using micro-electrocorticography (μECoG) were designated as planar wave and spiral waves. Propagation of planar waves were observed in two directions and spiral waves were rotating in clockwise and in a counter-clockwise direction (Viventi *et al.*, 2011). Irrespective of the terminologies used to describe the propagation patterns, a basic concept that unique spatial patterns are exhibited during ictal onset remains the same. Thus,

a treatment to prevent such aberrant spatial patterns which lead to ictal onset would be of concern.

4.2.2 Effect of gap-junction blockers on propagating local field potentials

Gap junctions connect the adjacent cells via cytosol and provide electrical and metabolic coupling. They play an important role in brain development and are involved in many brain diseases (Dere & Zlomuzica, 2012), neurological disorders such as epilepsy (Jin & Zhong, 2011) or stroke (Frantseva, 2002). Also, gap junction openers are involved in prolonging the epileptiform discharges (Kohling *et al.*, 2001). To investigate the role of gap junctions on propagating LFPs and electrical discharges during induced ELA in hippocampal slices, we studied the effects of gap junction blockers using: MFA with high and low-density MEAs and, CBX with low-density MEAs.

In our recordings, upon MFA application during induced ELA, the field potentials propagation was inhibited and their frequency decreased under both MFA and CBX. Evaluation based on the centre of activation of extracellular field potential did not show any propagation upon MFA treatment, in contrast to what was observed in induced ELA (Figure. 3.11). This clearly indicated that the size of the LFPs could be decreased and prevented from entraining larger areas into epileptiform activity with the application of gap junction blockers.

Additionally, our experiments with low-density MEAs showed a decrease in LFP frequency upon addition of gap junction blockers during induced ELA. Various studies have also reported the antiepileptic effect of gap junction blockers like CBX and MFA. These and other anticonvulsants have a profound effect in suppressing the seizures (Nilsen *et al.*, 2006), reducing the seizure duration (Jahromi *et al.*, 2002; Gajda *et al.*, 2003), epileptiform discharge frequency, amplitude (Medina-Ceja *et al.*, 2008) and propagation of seizures (Zhang *et al.*, 2014) in different regions of the brain. **Therefore, our results show that gap junction blockers have an antiepileptic effect in (i) reducing the LFPs**

frequency and, therefore, the seizure duration together with (ii) reducing the LFP amplitude, spatial extent and, therefore, the seizure strength.

4.2.3 Effect of ionotropic glutamate receptor blockers on local field potentials

In addition to electrical coupling and field effects, synaptic transmission is also involved in the epileptiform activity. Excessive glutamatergic neurotransmission is an underlying cause of certain types of epilepsy, such as temporal lobe epilepsy. In the recent times, AMPA receptors are targeted for anticonvulsant drug development (Citraro *et al.*, 2014) due to their involvement in temporal lobe epilepsy (Mathern *et al.*, 1997). The potential efficacy of antiepileptic effect of numerous AMPA antagonists, e.g. talampanel and perampanel, has been reported in the literature (Russo *et al.*, 2012). Therefore, here we investigated the effect of AMPA/kainate receptor antagonist on propagating LFPs and epileptiform discharges during high K^+ zero Mg^{2+} induced ELA.

We observed that upon application of DNQX, propagating field potentials disintegrated into LFPs of smaller size and amplitude and were completely abolished later within four minutes following onset of application as evaluated using low-density microelectrode arrays. Washout of DNQX led to large LFPs. As it is well known that the released glutamate plays a major role in initiating and spreading seizures (Meldrum, 1994; Chapman, 2000), excitation mediated transmission is necessary for the propagation of epileptiform activity.

4.2.4 Neuronal spiking under induced epileptiform-like activity

Neurons involved during the transition to seizure activity could be either excitatory or inhibitory neurons. Single unit activities are isolated and categorized into excitatory and inhibitory neurons based on spike waveform and frequency efficiently (Csicsvari *et al.*, 1999). Increased firing rates of excitatory neurons (Fujita *et al.*, 2014) and also of inhibitory neurons (Toyoda *et al.*, 2015) in the dentate gyrus, the subiculum, and the CA1 region has been observed

during the preictal phase in an *in vivo* model of induced epilepsy. Investigating the spiking behaviour of different neuronal units during onset and course of the ictal-like activity, to examine what populations of neurons increase their activity or inactivate during onset and course of the ictal-like activity could help in understanding the possible mechanisms that may play a role in transition between interictal and ictal states. Additionally, several stimulation studies in the recent times have given hopes in reducing seizure by targeting specific cell populations, for example, through interneuron mediated entrainment with low frequency optical stimulation (Ladas *et al.*, 2015). Therefore, investigation at the level of single units also plays an important role in designing seizure reduction protocols.

In our study, single spikes during control conditions and during induced ELA were observed. Neuronal spiking was observed in the pyramidal cell layer of the CA3 region. With the interest to correlate neuronal spiking to the generation of field potentials, neuronal spiking preceding the LFP, following the LFP and neuronal spiking preceding as well as following the LFP was detected. Spiking was observed irrespective of the propagation direction of the field potential's p-spike.

Using the spike-triggered average analysis, spatial electrical images of single neuron activity were constructed. Based on the waveform obtained from the STAs and, spike width, we attempted to classify cells by comparing the full-width at half-amplitude minimum of individual STAs as shown in Figure 3.23. However, the small number of recorded single units did not allow a formal clustering and clear separation. More number of single units are needed to draw a conclusion. Overcoming the limitations of single unit recordings by decreasing the noise of the CMOS MEAs may reveal if excitatory and inhibitory units can be distinguished based on their extracellular signature alone. Selective fluorescent labelling of inhibitory cell types in transgenic animals might serve as an appropriate control.

4.3 Aberrant activity in retina

4.3.1 Local field potentials in dystrophic mouse retinae

Spontaneously occurring LFPs are a characteristic feature of *rd1* and *rd10* blind retinas (Ye & Goo, 2007; Goo *et al.*, 2011; Menzler & Zeck, 2011; Menzler *et al.*, 2014). Due to a relatively large spacing of 200 µm between electrodes, the precise spatial characterization was limited (Ye & Goo, 2007; Goo *et al.*, 2011). In our study, high-density array clearly imaged the stationary LFPs in unperturbed *rd10* retinae similar to the propagating LFPs reported in *rd1* retina (Menzler & Zeck, 2011). Application of TTX at low concentration (0.2 µM) abolished the RGC spiking alone leaving behind the field potentials active in the *rd1* retina. We can only speculate that large, synchronous membrane currents occur in dystrophic retinas and lead to the generation of the detected LFPs (Reimann *et al.*, 2013).

The detected field potentials were propagating in the *rd1* blind retina (Menzler & Zeck, 2011); however, no propagation could be detected in *rd10* retina (Menzler *et al.*, 2014). Furthermore, in *rd10* retina, LFPs remained also stationary under disinhibited conditions in contrast to *rd1* retina (Menzler & Zeck, 2011).

We found that addition of ionotropic glutamate receptor blocker (DNQX) and gap junction blocker (MFA) abolished all the LFPs in *rd10* retina. This effect was similar to that observed in the *rd1* retina (Menzler, 2011; Menzler & Zeck, 2011). Our data, therefore, suggest that similar mechanisms lead to aberrant activity and LFPs in *rd1* and *rd10* retinas. One of the main differences, however, was the stationary LFPs in *rd10* compared to the propagating LFPs in *rd1*. Further pharmacological experiments are required to establish under what condition propagating LFPs in *rd1* can be transformed into stationary ones. **Our experiments in hippocampal slices (section 3.1.7) indicate that gap-junction blockers transform strongly propagating LFPs into stationary ones. A careful "titration" of the gap junction blocker might be required, given that initial experiments (Menzler & Zeck, 2011) did not show stationary LFPs upon MFA treatment.**

4.3.2 Spiking in dystrophic retinas

The augmented maintained and rhythmic spiking activity in dystrophic mouse models – *rd1* and *rd10* has been established in many studies (Stasheff, 2008; Borowska *et al.*, 2011; Menzler & Zeck, 2011; Stasheff *et al.*, 2011). In this thesis, we evaluated the spontaneous rhythmic activity, spatial characteristics of the field potentials and effect of pharmacological blockade on synaptic transmission and electrical coupling in *rd10* retina using high-density multielectrode arrays. The mean firing rate calculated from RGCs in *rd10* was lower compared to that of *rd1* RGCs (Menzler *et al.*, 2014) in agreement with Stasheff *et al.*, (Stasheff *et al.*, 2011). Rhythmic spiking in *rd10* retina correlates with LFPs. Spiking in *rd10* retina occurs even during the LFP, in contrast to that observed in the hippocampal slices. Furthermore, about 50% of the RGCs were rhythmic in *rd10* retina. Comparatively, this percentage of rhythmic ganglion cells was lower to that observed in the *rd1* retina (~70%). We hypothesize that the remaining circuitry could be intact in *rd10* retina and it is easier to stimulate the silent cells than the spontaneously active ones, which confound the induced activity. This indicates a possibility that the remaining 50% of the RGCs in *rd10* could be targeted for further evaluation to investigate for their potentiality, based upon which vision restoration or preservation treatments could be addressed.

4.4 Comparison of local field potentials in hippocampal slices and degenerated retinas at different developmental stages

Aberrant network activity arising in cortical areas of the brain due to abnormal neuronal synchronization is a characteristic feature of many neurological disorders such as epilepsy, Parkinson's disease and Alzheimer's disease (Uhlhaas & Singer, 2006). Such an aberrant activity has also been reminiscent of network activity arising in degenerated retinas (Euler & Schubert, 2015; Trenholm & Awatramani, 2015).

Certain neuronal networks differing in architecture share similar spontaneous electrical activity (Mazzoni *et al.*, 2007). And, certain intra-neuronal networks which are diversely organized at different levels, as in the case of retina, also share similarities and certain differences (Euler & Schubert, 2015). In order to understand better, the aberrant activity, general principles underlying aberrant activity common to different neuronal tissues are highly attractive. Towards such a goal, we studied two tissues: hippocampal slices and the retina – both of which display LFPs under certain experimental conditions.

OHCs have certain similarities with the degenerated *rd1* retina. Spontaneous propagating field potentials are common in both the tissues. However, the propagation in the hippocampus occurs along the trisynaptic path in comparison to the propagation that occurs randomly in the *rd1* retina (Menzler, 2011; Menzler & Zeck, 2011).

Aberrant activity in acute hippocampal slices prepared from the mature tissue is compared to *rd10* retina (Table 4.2), where aberrant activity (rhythmic LFPs) originates after maturation of the circuitry. Spontaneous field potentials were not observed in acute hippocampal slices, but they were observed as small stationary field potentials in *rd10* retinae. Application of BMI/gabazine ($GABA_A$ receptor antagonist) induced LFPs in acute hippocampal slices and increased the LFP amplitude in *rd10* retina. AMPA/kainate blocker DNQX inhibited LFPs in both systems. In the case of gap junction blocker application, the frequency of the field potentials decreased in hippocampal slices while in *rd10* retinae, the field potentials were completely inhibited. Furthermore, in acute hippocampal slices, LFPs leading to ictal-like activity developed. Although this was not detected in *rd10* retina, a recent study (Biswas *et al.*, 2014) reports that in *rd10* retinas rhythmic LFPs stop and restart during the recording time of several minutes. It remains an open question, if the emergence of rhythmic retinal LFPs could be compared to the emergence of ictal LFPs in hippocampal slices. One important difference was in acute hippocampal slices, LFPs propagated and there were no spikes detected, whereas in *rd10* retinae, LFPs were stationary and 50% of the retinal ganglion cells were spiking rhythmically.

	Organotypic hippocampal slice cultures	rd1 retina	Acute Hippocampal slices	rd10 retina
Spontaneous LFPs ➜ Stationary ➜ Propagating	✓ ✓ Along the trisynaptic pathway	- ✓ Random	- -	✓ -
LFPs during disinhibition ➜Stationary ➜ Propagating	✓ ✓ Along the trisynaptic pathway – forward and backward	- ✓ Random	- ✓ Along the trisynaptic pathway – forward and backward	✓ -
AMPA/kainate blocker	Inhibits LFPs	Inhibits LFPs	Inhibits LFPs	Inhibits LFPs
Gap Junction blocker	Inhibits LFP propagation and decreases LFP frequency with smaller LFPs persisting	Inhibits LFPs	Decreases LFP frequency	Inhibits LFPs
Neuronal spiking	Phase locking not evaluated	Phase locked to LFPs	Not recorded	Phase locked to LFPs

Table 4.1: Comparison of characteristics of local field potentials in organotypic hippocampal slices to *rd1* retina and characteristics of local field potentials in acute hippocampal slices to *rd10* retina under different experimental conditions.

In summary, the morphological differences in the two tissues (hippocampus and retina) exclude a one-to-one comparison. Some of the similarities listed in Table 4.1 are noteworthy. Excitatory and inhibitory synaptic blockers had a similar effect on both the tissues, where the

excitatory synaptic blockers abolished the LFPs and inhibitory synaptic blockers exacerbated the field potentials. This may indicate general principles underlying aberrant activity at the level of synaptic connectivity and it also may provide clues for determining the origin of network activity under pathological conditions. Blockage of gap junctions inhibited the field potentials completely in the retina, whereas at the same concentration a five-fold reduction in frequency and complete halt in propagation stop was detected in the hippocampal slices. This difference in the effect of the gap junction blocker may suggest that the gap junctional coupling strength varies in both networks and have differences in influence over aberrant network activity. Future research should be directed towards a more detailed understanding of similarities and differences, which may ultimately lead to strategies to reduce these non-physiological extracellular potentials.

5 Summary

Neuronal cell populations form neuronal networks and generate spontaneous field potentials. Interconnected inhibitory and excitatory cell populations balance the activity in neural networks. Under neuropathological conditions, such neural networks are altered and an imbalance between excitatory and inhibitory drive lead to synchronous activity reflected in local field potentials. Such synchronous activity is one of the hallmarks of neuropathological disorder such as epilepsy and it accompanied the disease of Retinitis Pigmentosa as well. In this thesis, aberrant activity in two neural tissues, i.e. hippocampal slices and blind mouse retina (*rd10*) was investigated using a high-density microelectrode array "Neurochip" which has 16,384 sensor transistors in 1 mm^2 recording area.

In the first part of the thesis, transverse sections of the hippocampal slices with 400 µm thickness were prepared for organotypic and acute hippocampal slices. In both tissues/preparations aberrant activity was studied by inducing epileptiform-like activity with high K^+ zero Mg^{2+} or bicuculline methiodide. Local field potentials and neuronal spiking were characterized under different physiological conditions. Local field potentials were stationary, as well as propagating (along trisynaptic pathway) during spontaneous activity. During induced epileptiform-like activity, forward propagating field potentials i.e., from the dentate gyrus towards the CA3 region of the hippocampus were observed. Propagation of the signals occurred along the trisynaptic pathway. Most interestingly, in addition to forward propagating field potentials, backward propagating field potentials from the CA3 region towards the dentate gyrus were observed in both organotypic hippocampal slice cultures and acute hippocampal slices. The backward propagating field potentials occurred along the same path as forward propagating field potentials. Unique alternating propagation patterns of forward and backward propagating field potentials occurred during different phases of induced epileptiform-like activity. The propagation of field potentials was inhibited by gap junction blockers and by ionotropic glutamate receptor blocker. Characterization of single units revealed

single units spiking before an LFP, after an LFP and single units spiking before and after an LFP.

Investigation of aberrant network activity in *rd10* retina revealed spontaneous stationary field potentials which upon disinhibition exhibited larger amplitudes. Rhythmic spontaneous spiking activity was observed in a subpopulation of retinal ganglion cells. Local field potentials in *rd10* retinas were inhibited by the same pharmacological blockers used to inhibit hippocampal slice activity.

Comparison of such patho-electrophysiological activity between different tissues i.e., hippocampus and *rd10* retina during (degenerative) circuit alterations suggests that the situation in organotypic hippocampal slices may be comparable to photoreceptor-degenerated retinal model (*rd1*), where degeneration occurs early and still during development. The mature network present in acute hippocampal slices from adult animals, however, shows some similarities (but also differences) to *rd10* retina, where degeneration occurs well after development is completed.

6 Outlook

Extracellular recordings were performed using a high-density multi-transistor array "Neurochip". This comprises 16,384 sensors packed in 1 mm^2 area with an adjacent stimulation area of 1 mm^2 comprising 400 stimulation sites. Local field potentials exhibiting varying propagation properties were observed under stimulated neuropathological conditions. That is in the hippocampus under induced epilepsy and in the retina of a Retinitis Pigmentosa mouse model (*rd10*). The sensor array used in this thesis had a rather small recording area of 1 mm^2. As a result, simultaneous recording from all hippocampal regions was not feasible. With the development of a new Neurochip (Bertotti *et al.*, 2014) with a sensor area of 4 mm^2, comprising 4,225 sensors (Figure 6.1A and Figure 6.1D), multiple regions within the same tissue can be electrically imaged simultaneously. Furthermore, the addition of an array of 1,024 stimulation sites interleaved into the recording area (Figure.6.1.B) enables simultaneous recording and stimulation from the same hippocampal region.

On the newer version of CMOS microelectrode arrays, epileptiform-like activity was induced in organotypic hippocampal slice cultures (Figure 6.2A). A schematic drawing of the region of organotypic hippocampal slice imaged is shown (Figure 6.2B). Using these newer versions of CMOS microelectrode arrays (Figure 6.2C), extracellular field potentials similar to that obtained on earlier Neurochips were recorded during induced epileptiform-like activity. A colour coded electrical image of a field potential from the temporal trace in Figure 6.2C is shown in Figure 6.2D. The recorded and analyzed synchronous activity reflected in propagating local field potentials along the trisynaptic hippocampal formation, constitutes a hallmark of seizure-like events. Disrupting these seizure-like events by interfering the aberrant network activity with electrical stimulation (Fisher & Velasco, 2014) may provide a potential approach to reducing or even avoiding such aberrant activity. And, most importantly, timely detection of backward propagating LFPs and counteracting it may also represent one strategy to detect seizure onsets.
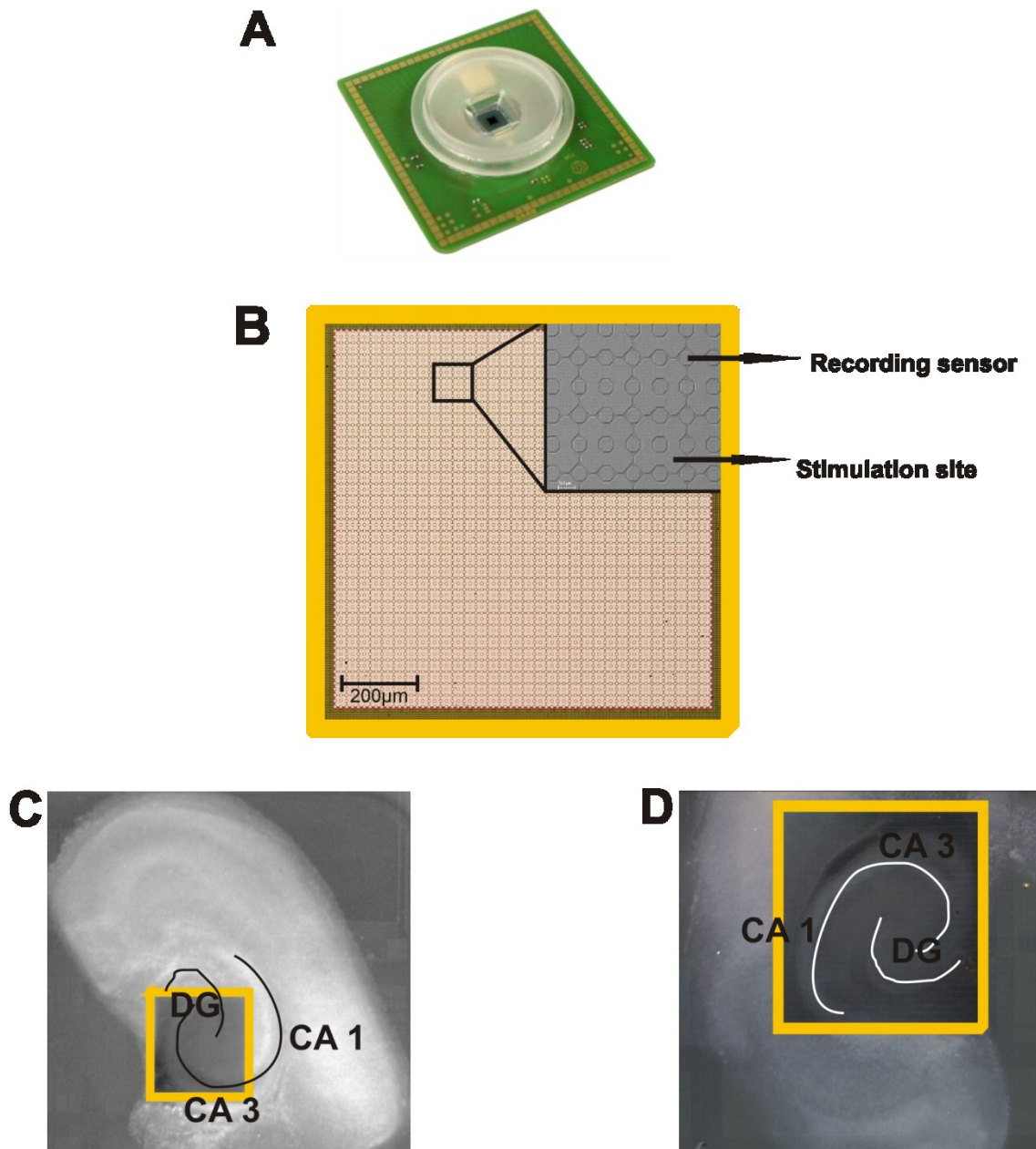
Figure 6.1: CMOS based microelectrode arrays. A: Photographic image of an assembled chip B: Surface of the recording and stimulation array C: OHC at DIV 10 with the CA3 region interfaced to 1 mm^2 recording and stimulation array D: OHC at DIV 11 with DG, CA3 and CA1 region interfaced to 4 mm^2 recording and stimulation array.

In the case of Retinitis Pigmentosa model, the small stationary local field potentials detected in *rd10* model and the large percentage of non-rhythmic ganglion cells (50%) indicate a neuronal system which is more stable as compared to the above described epileptiform activity of hippocampal slices.
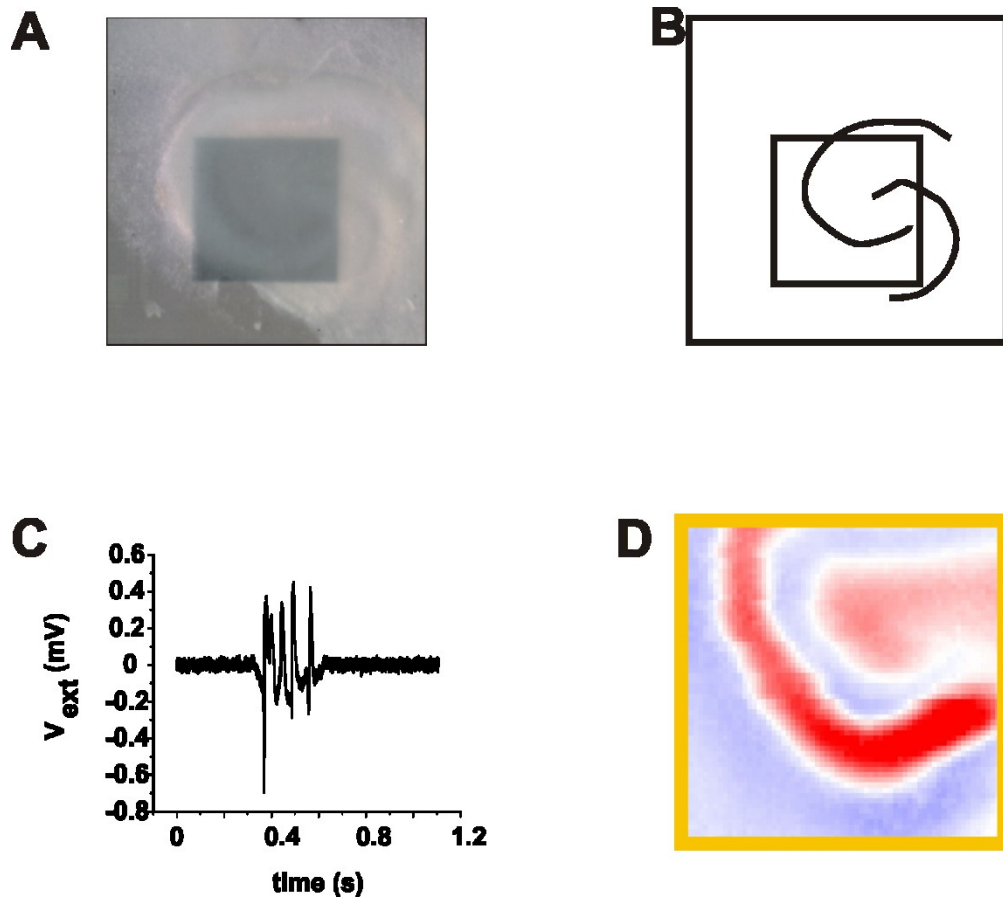
Figure 6.2: Extracellular recordings achieved with new CMOS microelectrode arrays. A: OHC at DIV 10 with the CA3 region interfaced to a new CMOS MEA. B: Schematic drawing of the CA3 region interfaced to the recording and stimulation array. C: Temporal trace of field potentials during BMI-induced ELA. D: Electrical image of a field potential shown in C. The spatio-temporal features of the LFPs detected on these arrays are similar to the features shown in the result section.

The retinal ganglion cell layer of *rd10* retinas appears more robust in electrophysiological terms as compared to the ganglion cell layer of *rd1* retinas, which displays strong LFP activity. This mouse model may, therefore, appear more attractive for studying the effect of vision restoration strategies.

7 Bibliography

Albus, K., Heinemann, U. & Kovacs, R. (2013) Network activity in hippocampal slice cultures revealed by long-term in vitro recordings. *Journal of neuroscience methods*, **217**, 1-8.

Alvarado-Rojas, C., Lehongre, K., Bagdasaryan, J., Bragin, A., Staba, R., Engel, J., Jr., Navarro, V. & Le Van Quyen, M. (2013) Single-unit activities during epileptic discharges in the human hippocampal formation. *Frontiers in computational neuroscience*, **7**, 140.

Amaral, D.G. (1978) A Golgi study of cell types in the hilar region of the hippocampus in the rat. *The Journal of comparative neurology*, **182**, 851-914.

Amaral, D.G., Ishizuka, N. & Claiborne, B. (1990) Neurons, numbers and the hippocampal network. *Progress in brain research*, **83**, 1-11.

Andersen, P., Bliss, T. & Skrede, K.K. (1971) Lamellar organization of hippocampal excitatory pathways. *Experimental brain research*, **13**, 222-238.

Andersen, P., Morris, R., Amaral, D., Bliss, T. & O'Keefe, J. (2006) *The hippocampus book*. Oxford University Press.

Anderson, W.W., Lewis, D.V., Swartzwelder, H.S. & Wilson, W.A. (1986) Magnesium-free medium activates seizure-like events in the rat hippocampal slice. *Brain research*, **398**, 215-219.

Angeles, D. (1981) Proposal for Revised Clinical and Electrenchephalographic Classifiction of Epilepstic seizures.

Avoli, M. (1990) Epileptiform discharges and a synchronous GABAergic potential induced by 4-aminopyridine in the rat immature hippocampus. *Neuroscience letters*, **117**, 93-98.

Avoli, M. & Barbarosie, M. (1999) Interictal-ictal interactions and limbic seizure generation. *Revue neurologique*, **155**, 468-471.

Avoli, M., Louvel, J., Kurcewicz, I., Pumain, R. & Barbarosie, M. (1996) Extracellular free potassium and calcium during synchronous activity induced by 4-aminopyridine in the juvenile rat hippocampus. *The Journal of physiology*, **493**, 707-717.

Ayoub, G.S. & Copenhagen, D.R. (1991) Application of a fluorometric method to measure glutamate release from single retinal photoreceptors. *Journal of neuroscience methods*, **37**, 7-14.

Benini, R., D'Antuono, M., Pralong, E. & Avoli, M. (2003) Involvement of amygdala networks in epileptiform synchronization in vitro. *Neuroscience*, **120**, 75-84.

Berens, P., Logothetis, N.K. & Tolias, A.S. (2010) Local field potentials, BOLD and spiking activity–relationships and physiological mechanisms. *Visual Population Codes–Towards a Common Multivariate Framework for Cell Recording and Functional Imaging*, 599-624.

Bertotti, Gabriel, et al. "A capacitively-coupled CMOS-MEA with 4225 recording sites and 1024 stimulation sites." *Proc. of the 9th Int. Meeting on Substrate-Integrated Microelectrodes, Reutlingen, Germany*. 2014.

Biswas, S., Haselier, C., Mataruga, A., Thumann, G., Walter, P. & Müller, F. (2014) Pharmacological Analysis of Intrinsic Neuronal Oscillations in rd10 Retina.

Blackstad, T.W., Brink, K., Hem, J. & Jeune, B. (1970) Distribution of hippocampal mossy fibers in the rat. An experimental study with silver impregnation methods. *The Journal of comparative neurology*, **138**, 433-449.

Blankenship, A.G. & Feller, M.B. (2010) Mechanisms underlying spontaneous patterned activity in developing neural circuits. *Nature reviews. Neuroscience*, **11**, 18-29.

Bloomfield, S.A. & Volgyi, B. (2004) Function and plasticity of homologous coupling between AII amacrine cells. *Vision research*, **44**, 3297-3306.

Borowska, J., Trenholm, S. & Awatramani, G.B. (2011) An intrinsic neural oscillator in the degenerating mouse retina. *The Journal of neuroscience*, **31**, 5000-5012.

Brandstätter, J., Hartveit, E., Sassoe-Pognetto, M. & Wässle, H. (1994) Expression of NMDA and high-affinity kainate receptor subunit mRNAs in the adult rat retina. *European Journal of Neuroscience*, **6**, 1100-1112.

Burneo, J.G., Black, L., Knowlton, R.C., Faught, E., Morawetz, R. & Kuzniecky, R.I. (2005) Racial disparities in the use of surgical treatment for intractable temporal lobe epilepsy. *Neurology*, **64**, 50-54.

Capogna, M. (2011) Neurogliaform cells and other interneurons of stratum lacunosum-moleculare gate entorhinal-hippocampal dialogue. *The Journal of physiology*, **589**, 1875-1883.

Chapman, A.G. (2000) Glutamate and epilepsy. *The Journal of nutrition*, **130**, 1043S-1045S.

Cho, S., Wood, A. & Bowlby, M.R. (2007) Brain slices as models for neurodegenerative disease and screening platforms to identify novel therapeutics. *Current neuropharmacology*, **5**, 19.

Citraro, R., Aiello, R., Franco, V., De Sarro, G. & Russo, E. (2014) Targeting α-amino-3-hydroxyl-5-methyl-4-isoxazole-propionate receptors in epilepsy. *Expert opinion on therapeutic targets*, **18**, 319-334.

Claiborne, B.J., Amaral, D.G. & Cowan, W.M. (1986) A light and electron microscopic analysis of the mossy fibers of the rat dentate gyrus. *The Journal of comparative neurology*, **246**, 435-458.

Connelly, C.A., Chen, L.C. & Colquhoun, S.D. (2000) Metabolic activity of cultured rat brainstem, hippocampal and spinal cord slices. *Journal of neuroscience methods*, **99**, 1-7.

Csicsvari, J., Hirase, H., Czurko, A., Mamiya, A. & Buzsaki, G. (1999) Oscillatory coupling of hippocampal pyramidal cells and interneurons in the behaving Rat. *The Journal of neuroscience*, **19**, 274-287.

Cymerblit-Sabba, A. & Schiller, Y. (2010) Network dynamics during development of pharmacologically induced epileptic seizures in rats in vivo. *The Journal of neuroscience*, **30**, 1619-1630.

De Lanerolle, N.C., Kim, J.H., Williamson, A., Spencer, S.S., Zaveri, H.P., Eid, T. & Spencer, D.D. (2003) A retrospective analysis of hippocampal pathology in human temporal lobe epilepsy: evidence for distinctive patient subcategories. *Epilepsia*, **44**, 677-687.

Deng, W., Aimone, J.B. & Gage, F.H. (2010) New neurons and new memories: how does adult hippocampal neurogenesis affect learning and memory? *Nature reviews. Neuroscience*, **11**, 339-350.

Dere, E. & Zlomuzica, A. (2012) The role of gap junctions in the brain in health and disease. *Neuroscience and biobehavioral reviews*, **36**, 206-217.

Dyer, M.A. & Cepko, C.L. (2001) Regulating proliferation during retinal development. *Nature Reviews Neuroscience*, **2**, 333-342.

Dzhala, V.I. & Staley, K.J. (2003) Transition from interictal to ictal activity in limbic networks in vitro. *The Journal of neuroscience*, **23**, 7873-7880.

Engel, J., Jr. (2001) A proposed diagnostic scheme for people with epileptic seizures and with epilepsy: report of the ILAE Task Force on Classification and Terminology. *Epilepsia*, **42**, 796-803.

Engel, J., Jr., Bragin, A., Staba, R. & Mody, I. (2009) High-frequency oscillations: what is normal and what is not? *Epilepsia*, **50**, 598-604.

Engel, J., Pedley, T.A. & Aicardi, J. (2008) *Epilepsy: a comprehensive textbook*. Lippincott Williams & Wilkins.

Euler, T., Schneider, H. & Wässle, H. (1996) Glutamate responses of bipolar cells in a slice preparation of the rat retina. *The Journal of neuroscience*, **16**, 2934-2944.

Euler, T. & Schubert, T. (2015) Multiple Independent Oscillatory Networks in the Degenerating Retina. *Frontiers in cellular neuroscience*, **9**, 444.

Eversmann, B., Jenkner, M., Hofmann, F., Paulus, C., Brederlow, R., Holzapfl, B., Fromherz, P., Merz, M., Brenner, M. & Schreiter, M. (2003) A 128× 128 CMOS biosensor array for extracellular recording of neural activity. *Solid-State Circuits, IEEE Journal of*, **38**, 2306-2317.

Famiglietti Jr, E. & Kolb, H. (1975) A bistratified amacrine cell and synaptic circuitry in the inner plexiform layer of the retina. *Brain research*, **84**, 293-300.

Feigenspan, A., Teubner, B., Willecke, K. & Weiler, R. (2001) Expression of neuronal connexin36 in AII amacrine cells of the mammalian retina. *The Journal of Neuroscience*, **21**, 230-239.

Ferrea, E., Maccione, A., Medrihan, L., Nieus, T., Ghezzi, D., Baldelli, P., Benfenati, F. & Berdondini, L. (2012) Large-scale, high-resolution electrophysiological imaging of field potentials in brain slices with microelectronic multielectrode arrays. *Frontiers in neural circuits*, **6**, 80.

Filatov, G., Krishnan, G.P., Rulkov, N.F. & Bazhenov, M. (2011) Dynamics of epileptiform activity in mouse hippocampal slices. *Journal of biological physics*, **37**, 347-360.

Fisher, R.S., van Emde Boas, W., Blume, W., Elger, C., Genton, P., Lee, P. & Engel, J., Jr. (2005) Epileptic seizures and epilepsy: definitions proposed by the International League Against Epilepsy (ILAE) and the International Bureau for Epilepsy (IBE). *Epilepsia*, **46**, 470-472.

Fisher, R.S. & Velasco, A.L. (2014) Electrical brain stimulation for epilepsy. *Nature Reviews Neurology*, **10**, 261-270.

Freund, T.F. & Buzsaki, G. (1996) Interneurons of the hippocampus. *Hippocampus*, **6**, 347-470.

Fujita, S., Toyoda, I., Thamattoor, A.K. & Buckmaster, P.S. (2014) Preictal Activity of Subicular, CA1, and Dentate Gyrus Principal Neurons in the Dorsal Hippocampus before Spontaneous Seizures in a Rat Model of Temporal Lobe Epilepsy. *The Journal of Neuroscience*, **34**, 16671-16687.

Gähwiler, B. (1981) Organotypic monolayer cultures of nervous tissue. *Journal of neuroscience methods*, **4**, 329-342.

Gähwiler, B. (1984) Development of the hippocampus in vitro: Cell types, synapses and receptors. *Neuroscience*, **11**, 751-760.

Gajda, Z., Gyengési, E., Hermesz, E., Ali, K.S. & Szente, M. (2003) Involvement of gap junctions in the manifestation and control of the duration of seizures in rats in vivo. *Epilepsia*, **44**, 1596-1600.

Ghosh, K.K., Bujan, S., Haverkamp, S., Feigenspan, A. & Wassle, H. (2004) Types of bipolar cells in the mouse retina. *The Journal of comparative neurology*, **469**, 70-82.

Gonzalez-Sulser, A., Wang, J., Motamedi, G.K., Avoli, M., Vicini, S. & Dzakpasu, R. (2011) The 4-aminopyridine in vitro epilepsy model analyzed with a perforated multi-electrode array. *Neuropharmacology*, **60**, 1142-1153.

Gonzalez-Sulser, A., Wang, J., Queenan, B.N., Avoli, M., Vicini, S. & Dzakpasu, R. (2012) Hippocampal neuron firing and local field potentials in the in vitro 4-aminopyridine epilepsy model. *Journal of neurophysiology*, **108**, 2568-2580.

Goo, Y.S., Ahn, K.N., Song, Y.J., Ahn, S.H., Han, S.K., Ryu, S.B. & Kim, K.H. (2011) Spontaneous Oscillatory Rhythm in Retinal Activities of Two Retinal Degeneration (rd1 and rd10) Mice. *The Korean journal of physiology & pharmacology : official journal of the Korean Physiological Society and the Korean Society of Pharmacology*, **15**, 415-422.

Gosche, K.M., Mortimer, J.A., Smith, C.D., Markesbery, W.R. & Snowdon, D.A. (2002) Hippocampal volume as an index of Alzheimer neuropathology: Findings from the Nun Study. *Neurology*, **58**, 1476-1482.

Green, J. (1964) The hippocampus. *Physiol. Rev*, **44**, 561-592.

Greschner, M., Field, G.D., Li, P.H., Schiff, M.L., Gauthier, J.L., Ahn, D., Sher, A., Litke, A.M. & Chichilnisky, E.J. (2014) A polyaxonal amacrine cell population in the primate retina. *The Journal of neuroscience*, **34**, 3597-3606.

Hablitz, J.J. & Heinemann, U. (1987) Extracellular K^+ and Ca^{2+} changes during epileptiform discharges in the immature rat neocortex. *Developmental Brain Research*, **36**, 299-303.

Hamlyn, L.H. (1962) The fine structure of the mossy fibre endings in the hippocampus of the rabbit. *Journal of anatomy*, **96**, 112-120.

Haq, W., Arango-Gonzalez, B., Zrenner, E., Euler, T. & Schubert, T. (2014) Synaptic remodeling generates synchronous oscillations in the degenerated outer mouse retina. *Frontiers in neural circuits*, **8**, 108.

Hartveit, E. (1997) Functional organization of cone bipolar cells in the rat retina. *Journal of neurophysiology*, **77**, 1716-1730.

Hauser, W. (1995) Recent developments in the epidemiology of epilepsy. *Acta neurologica Scandinavica*, **92**, 17-21.

Haverkamp, S., Grünert, U. & Wässle, H. (2001) Localization of kainate receptors at the cone pedicles of the primate retina. *Journal of Comparative Neurology*, **436**, 471-486.

Hirtz, D., Thurman, D.J., Gwinn-Hardy, K., Mohamed, M., Chaudhuri, A.R. & Zalutsky, R. (2007) How common are the "common" neurologic disorders? *Neurology*, **68**, 326-337.

Hutzler, M., Lambacher, A., Eversmann, B., Jenkner, M., Thewes, R. & Fromherz, P. (2006) High-resolution multitransistor array recording of electrical

field potentials in cultured brain slices. *Journal of neurophysiology*, **96**, 1638-1645.

Ishizuka, N., Weber, J. & Amaral, D.G. (1990) Organization of intrahippocampal projections originating from CA3 pyramidal cells in the rat. *The Journal of comparative neurology*, **295**, 580-623.

Jahromi, S.S., Wentlandt, K., Piran, S. & Carlen, P.L. (2002) Anticonvulsant actions of gap junctional blockers in an in vitro seizure model. *Journal of neurophysiology*, **88**, 1893-1902.

Jarrard, L.E. (1993) On the role of the hippocampus in learning and memory in the rat. *Behavioral and neural biology*, **60**, 9-26.

Jin, M.-M. & Zhong, C. (2011) Role of gap junctions in epilepsy. *Neuroscience Bulletin*, **27**, 389-406.

Jiruska, P., Csicsvari, J., Powell, A.D., Fox, J.E., Chang, W.C., Vreugdenhil, M., Li, X., Palus, M., Bujan, A.F., Dearden, R.W. & Jefferys, J.G. (2010) High-frequency network activity, global increase in neuronal activity, and synchrony expansion precede epileptic seizures in vitro. *The Journal of neuroscience*, **30**, 5690-5701.

Johnston, D., Wu, S.M.-S. & Gray, R. (1995) *Foundations of cellular neurophysiology*. MIT press Cambridge, MA.

Jones, B.W. & Marc, R.E. (2005) Retinal remodeling during retinal degeneration. *Experimental eye research*, **81**, 123-137.

Jung, R. (1949) Hirnelektrische Untersuchungen über den Elektrokrampf: Die Erregungsabläufe in corticalen und subcorticalen Hirnregionen bei Katze und Hund. *Archiv für Psychiatrie und Nervenkrankheiten*, **183**, 206-244.

Kibler, A.B. & Durand, D.M. (2011) Orthogonal wave propagation of epileptiform activity in the planar mouse hippocampus in vitro. *Epilepsia*, **52**, 1590-1600.

Kohara, K., Pignatelli, M., Rivest, A.J., Jung, H.Y., Kitamura, T., Suh, J., Frank, D., Kajikawa, K., Mise, N., Obata, Y., Wickersham, I.R. & Tonegawa, S. (2014) Cell type-specific genetic and optogenetic tools reveal hippocampal CA2 circuits. *Nature neuroscience*, **17**, 269-279.

Kolb, H. & Nelson, R. (1993) Off-alpha and OFF-beta ganglion cells in cat retina: II. Neural circuitry as revealed by electron microscopy of HRP stains. *Journal of Comparative Neurology*, **329**, 85-110.

Kolb, H. & Nelson, R. (1995) The organization of photoreceptor to bipolar synapses in the outer plexiform layer *Neurobiology and clinical aspects of the outer retina*. Springer, pp. 273-296.

Kotsopoulos, I.A., Van Merode, T., Kessels, F.G., De Krom, M.C. & Knottnerus, J.A. (2002) Systematic Review and Meta-analysis of Incidence Studies of Epilepsy and Unprovoked Seizures. *Epilepsia*, **43**, 1402-1409.

Kullmann, D.M. (2002) Genetics of epilepsy. *Journal of neurology, neurosurgery, and psychiatry*, **73 Suppl 2**, II32-35.

Ladas, T.P., Chiang, C.-C., Gonzalez-Reyes, L.E., Nowak, T. & Durand, D.M. (2015) Seizure reduction through interneuron-mediated entrainment using low frequency optical stimulation. *Experimental neurology*, **269**, 120-132.

Lambacher, A., Jenkner, M., Merz, M., Eversmann, B., Kaul, R.A., Hofmann, F., Thewes, R. & Fromherz, P. (2004) Electrical imaging of neuronal activity by multi-transistor-array (MTA) recording at 7.8µm resolution. *Applied Physics A*, **79**.

Lambacher, A., Vitzthum, V., Zeitler, R., Eickenscheidt, M., Eversmann, B., Thewes, R. & Fromherz, P. (2011) Identifying firing mammalian neurons in networks with high-resolution multi-transistor array (MTA). *Applied Physics A*, **102**, 1-11.

Lein, P.J., Barnhart, C.D. & Pessah, I.N. (2011) Acute hippocampal slice preparation and hippocampal slice cultures. *Methods in molecular biology*, **758**, 115-134.

Li, X.G., Somogyi, P., Ylinen, A. & Buzsaki, G. (1994) The hippocampal CA3 network: an in vivo intracellular labeling study. *The Journal of comparative neurology*, **339**, 181-208.

Liu, J.S., Li, J.B., Gong, X.W., Gong, H.Q., Zhang, P.M., Liang, P.J. & Lu, Q.C. (2013) Spatiotemporal dynamics of high-K+-induced epileptiform discharges in hippocampal slice and the effects of valproate. *Neurosci Bull*, **29**, 28-36.

Lopes da Silva, F., Blanes, W., Kalitzin, S.N., Parra, J., Suffczynski, P. & Velis, D.N. (2003) Epilepsies as dynamical diseases of brain systems: basic models of the transition between normal and epileptic activity. *Epilepsia*, **44 Suppl 12**, 72-83.

Lorente de Nó, R. (1934) Studies on the structure of the cerebral cortex. II. Continuation of the study of the ammonic system. *Journal für Psychologie und Neurologie*.

Lubenov, E.V. & Siapas, A.G. (2009) Hippocampal theta oscillations are travelling waves. *Nature*, **459**, 534-539.

Margolis, D.J., Gartland, A.J., Singer, J.H. & Detwiler, P.B. (2014) Network oscillations drive correlated spiking of ON and OFF ganglion cells in the rd1 mouse model of retinal degeneration. *PloS one*, **9**, e86253.

Masland, R.H. (2001) The fundamental plan of the retina. *Nature neuroscience*, **4**, 877-886.

Mathern, G.W., Pretorius, J.K., Kornblum, H.I., Mendoza, D., Lozada, A., Leite, J.P., Chimelli, L.M., Fried, I., Sakamoto, A.C. & Assirati, J.A. (1997) Human hippocampal AMPA and NMDA mRNA levels in temporal lobe epilepsy patients. *Brain : a journal of neurology*, **120**, 1937-1959.

Mazzoni, A., Broccard, F.D., Garcia-Perez, E., Bonifazi, P., Ruaro, M.E. & Torre, V. (2007) On the dynamics of the spontaneous activity in neuronal networks. *PloS one*, **2**, e439.

Medina-Ceja, L., Cordero-Romero, A. & Morales-Villagran, A. (2008) Antiepileptic effect of carbenoxolone on seizures induced by 4-aminopyridine: a study in the rat hippocampus and entorhinal cortex. *Brain research*, **1187**, 74-81.

Meldrum, B.S. (1994) The role of glutamate in epilepsy and other CNS disorders. *Neurology*.

Menzler, J. (2011) Discharge patterns of retinal ganglion cells in rodent models of degenerative retinal diseases (Doctoral dissertation, lmu, 2012).

Menzler, J., Channappa, L. & Zeck, G. (2014) Rhythmic ganglion cell activity in bleached and blind adult mouse retinas. *PloS one*, **9**, e106047.

Menzler, J. & Zeck, G. (2011) Network oscillations in rod-degenerated mouse retinas. *The Journal of neuroscience*, **31**, 2280-2291.

Milton, J. & Jung, P. (2003) *Epilepsy as a dynamic disease*. Springer.

Mody, I., Lambert, J.D. & Heinemann, U. (1987) Low extracellular magnesium induces epileptiform activity and spreading depression in rat hippocampal slices. *Journal of neurophysiology*, **57**, 869-888.

Murray, E.A. & Mishkin, M. (1984) Severe tactual as well as visual memory deficits follow combined removal of the amygdala and hippocampus in monkeys. *The Journal of neuroscience*, **4**, 2565-2580.

Nelson, R., Kolb, H. & Freed, M.A. (1993) OFF-alpha and OFF-beta ganglion cells in cat retina. I: Intracellular electrophysiology and HRP stains. *Journal of Comparative Neurology*, **329**, 68-84.

Ngugi, A.K., Bottomley, C., Kleinschmidt, I., Sander, J.W. & Newton, C.R. (2010) Estimation of the burden of active and life-time epilepsy: a meta-analytic approach. *Epilepsia*, **51**, 883-890.

Nilsen, K.E., Kelso, A.R. & Cock, H.R. (2006) Antiepileptic effect of gap-junction blockers in a rat model of refractory focal cortical epilepsy. *Epilepsia*, **47**, 1169-1175.

Nomura, A., Shigemoto, R., Nakamura, Y., Okamoto, N., Mizuno, N. & Nakanishi, S. (1994) Developmentally regulated postsynaptic localization of a metabotropic glutamate receptor in rat rod bipolar cells. *Cell*, **77**, 361-369.

O'Keefe, J. & Recce, M.L. (1993) Phase relationship between hippocampal place units and the EEG theta rhythm. *Hippocampus*, **3**, 317-330.

Pisciotta, M., Morgavi, G. & Jahnsen, H. (2010) Characterization of the in vitro propagation of epileptiform electrophysiological activity in organotypic

hippocampal slice cultures coupled to 3D microelectrode arrays. *Brain research*, **1358**, 46-53.

Pitkänen, A., Schwartzkroin, P.A. & Moshé, S.L. (2005) *Models of seizures and epilepsy.* Academic Press.

Preux, P.-M. & Druet-Cabanac, M. (2005) Epidemiology and aetiology of epilepsy in sub-Saharan Africa. *The Lancet Neurology*, **4**, 21-31.

Quilichini, P.P., Diabira, D., Chiron, C., Ben-Ari, Y. & Gozlan, H. (2002) Persistent epileptiform activity induced by low Mg2+ in intact immature brain structures. *European Journal of Neuroscience*, **16**, 850-860.

Rasch, M., Logothetis, N.K. & Kreiman, G. (2009) From neurons to circuits: linear estimation of local field potentials. *The Journal of neuroscience*, **29**, 13785-13796.

Raviola, E. & Gilula, N.B. (1973) Gap junctions between photoreceptor cells in the vertebrate retina. *Proceedings of the National Academy of Sciences*, **70**, 1677-1681.

Reimann, M.W., Anastassiou, C.A., Perin, R., Hill, S.L., Markram, H. & Koch, C. (2013) A biophysically detailed model of neocortical local field potentials predicts the critical role of active membrane currents. *Neuron*, **79**, 375-390.

Rodieck, R.W. & Rodieck, R.W. (1998) *The first steps in seeing.* Sinauer Associates Sunderland, MA.

Rozental, R., Andrade-Rozental, A., Zheng, X., Urban, M., Spray, D. & Chiu, F. (2001) Gap junction-mediated bidirectional signaling between human fetal hippocampal neurons and astrocytes. *Developmental neuroscience*, **23**, 420-431.

Russo, E., Gitto, R., Citraro, R., Chimirri, A. & De Sarro, G. (2012) New AMPA antagonists in epilepsy. *Expert opinion on investigational drugs*, **21**, 1371-1389.

Sander, J.W. (2003) The epidemiology of epilepsy revisited. *Current opinion in neurology*, **16**, 165-170.

Schaffer, K. (1892) Beitrag zur histologie der ammonshornformation. *Archiv für Mikroskopische Anatomie*, **39**, 611-632.

Scharfman, H.E. (1993) Activation of dentate hilar neurons by stimulation of the fimbria in rat hippocampal slices. *Neuroscience letters*, **156**, 61-66.

Schwartzkroin, P.A. (1994) Role of the hippocampus in epilepsy. *Hippocampus*, **4**, 239-242.

Schwerdtfeger, W. & Sarvey, J. (1982) Connectivity of the hilar region of the hippocampal formation in the rat. *Journal fur Hirnforschung*, **24**, 201-207.

Skrede, K.K. & Westgaard, R.H. (1971) The transverse hippocampal slice: a well-defined cortical structure maintained in vitro. *Brain research*, **35**, 589-593.

Somjen, G. & Giacchino, J. (1985) Potassium and calcium concentrations in interstitial fluid of hippocampal formation during paroxysmal responses. *Journal of neurophysiology*, **53**, 1098-1108.

Stasheff, S.F. (2008) Emergence of sustained spontaneous hyperactivity and temporary preservation of OFF responses in ganglion cells of the retinal degeneration (rd1) mouse. *Journal of neurophysiology*, **99**, 1408-1421.

Stasheff, S.F., Shankar, M. & Andrews, M.P. (2011) Developmental time course distinguishes changes in spontaneous and light-evoked retinal ganglion cell activity in rd1 and rd10 mice. *Journal of neurophysiology*, **105**, 3002-3009.

Steward, O. & Scoville, S.A. (1976) Cells of origin of entorhinal cortical afferents to the hippocampus and fascia dentata of the rat. *The Journal of comparative neurology*, **169**, 347-370.

Stoppini, L., Buchs, P.-A. & Muller, D. (1991) A simple method for organotypic cultures of nervous tissue. *Journal of neuroscience methods*, **37**, 173-182.

Storm-Mathisen, J. (1977) Localization of transmitter candidates in the brain: the hippocampal formation as a model. *Progress in neurobiology*, **8**, 119-181.

Thompson, S.M. & Mason, S.E. (2005) Preparation of organotypic hippocampal slice cultures. *Cell Biology, Four-Volume Set: A Laboratory Handbook*, 407.

Tikidji-Hamburyan, A., Reinhard, K., Seitter, H., Hovhannisyan, A., Procyk, C.A., Allen, A.E., Schenk, M., Lucas, R.J. & Munch, T.A. (2015) Retinal output changes qualitatively with every change in ambient illuminance. *Nature neuroscience*, **18**, 66-74.

Toyoda, I., Fujita, S., Thamattoor, A.K. & Buckmaster, P.S. (2015) Unit Activity of Hippocampal Interneurons before Spontaneous Seizures in an Animal Model of Temporal Lobe Epilepsy. *The Journal of Neuroscience*, **35**, 6600-6618.

Traynelis, S.F. & Dingledine, R. (1988) Potassium-induced spontaneous electrographic seizures in the rat hippocampal slice. Am Physiological Soc.

Trenholm, S. & Awatramani, G.B. (2015) Origins of spontaneous activity in the degenerating retina. *Frontiers in cellular neuroscience*, **9**.

Trenholm, S., Borowska, J., Zhang, J., Hoggarth, A., Johnson, K., Barnes, S., Lewis, T.J. & Awatramani, G.B. (2012) Intrinsic oscillatory activity arising within the electrically coupled AII amacrine-ON cone bipolar cell network is driven by voltage-gated Na+ channels. *The Journal of physiology*, **590**, 2501-2517.

Truccolo, W., Donoghue, J.A., Hochberg, L.R., Eskandar, E.N., Madsen, J.R., Anderson, W.S., Brown, E.N., Halgren, E. & Cash, S.S. (2011) Single-neuron dynamics in human focal epilepsy. *Nature neuroscience*, **14**, 635-641.

Uhlhaas, P.J. & Singer, W. (2006) Neural synchrony in brain disorders: relevance for cognitive dysfunctions and pathophysiology. *Neuron*, **52**, 155-168.

Vaney, D., Peichl, L. & Boycott, B. (1988) Neurofibrillar long-range amacrine cells in mammalian retinae. *Proceedings of the Royal society of London. Series B. Biological sciences*, **235**, 203-219.

Viventi, J., Kim, D.H., Vigeland, L., Frechette, E.S., Blanco, J.A., Kim, Y.S., Avrin, A.E., Tiruvadi, V.R., Hwang, S.W., Vanleer, A.C., Wulsin, D.F., Davis, K., Gelber, C.E., Palmer, L., Van der Spiegel, J., Wu, J., Xiao, J., Huang, Y., Contreras, D., Rogers, J.A. & Litt, B. (2011) Flexible, foldable, actively multiplexed, high-density electrode array for mapping brain activity in vivo. *Nature neuroscience*, **14**, 1599-1605.

Voss, L.J., Jacobson, G., Sleigh, J.W., Steyn-Ross, A. & Steyn-Ross, M. (2009) Excitatory effects of gap junction blockers on cerebral cortex seizure-like activity in rats and mice. *Epilepsia*, **50**, 1971-1978.

Wassle, H. & Boycott, B.B. (1991) Functional architecture of the mammalian retina. *Physiol. Rev*, **71**, 447-480.

Wassle, H., Puller, C., Muller, F. & Haverkamp, S. (2009) Cone contacts, mosaics, and territories of bipolar cells in the mouse retina. *The Journal of neuroscience*, **29**, 106-117.

Wittner, L. & Miles, R. (2007) Factors defining a pacemaker region for synchrony in the hippocampus. *The Journal of physiology*, **584**, 867-883.

Wong, R. & Hughes, A. (1987) The morphology, number, and distribution of a large population of confirmed displaced amacrine cells in the adult cat retina. *Journal of Comparative Neurology*, **255**, 159-177.

Ye, J.H. & Goo, Y.S. (2007) The slow wave component of retinal activity in rd/rd mice recorded with a multi-electrode array. *Physiological measurement*, **28**, 1079-1088.

Zeck, G., Lambacher, A. & Fromherz, P. (2011) Axonal transmission in the retina introduces a small dispersion of relative timing in the ganglion cell population response. *PloS one*, **6**, e20810.

Zhang, M., Ladas, T.P., Qiu, C., Shivacharan, R.S., Gonzalez-Reyes, L.E. & Durand, D.M. (2014) Propagation of epileptiform activity can be independent of synaptic transmission, gap junctions, or diffusion and is consistent with electrical field transmission. *The Journal of neuroscience*, **34**, 1409-1419.

Zimmer, J. & Gähwiler, B. (1984) Cellular and connective organization of slice cultures of the rat hippocampus and fascia dentata. *Journal of Comparative Neurology*, **228**, 432-446.

8 Declaration of own contribution

During my PhD thesis I performed the following experiments and data analysis.

- ➢ Standardized protocol and prepared organotypic hippocampal slice culture preparations.
- ➢ Standardized extracellular recording protocols and performed extracellular recordings from organotypic hippocampal slices, acute hippocampal slices using high-density microelectrode arrays and low-density microelectrode arrays.
- ➢ Extracellular recordings from *rd10* retina using high-density microelectrode arrays.
- ➢ Analysis of high-density microelectrode array recordings using the "Neurochip reader" software.
- ➢ Analysis of low-density microelectrode array recordings using MatLab scripts written by Thoralf Hermann.
- ➢ Analysis of propagation velocities and propagation path using Python scripts written by Florian Helmhold.

9 Curriculum Vitae

Personal Information

Name	Lakshmi Channappa
Date of Birth, place	31st August 1984, Tumkur, India.

Education

2011 to 2014	PhD student in the group of Dr. Guenther Zeck, Neurochip research group, Natural and Medical Sciences Institute at the University of Tübingen.
2005 to 2007	MSc (Biotechnology), The Oxford College of Science, Bangalore University, India
2002 to 2005	BSc (Biotechnology), Government Science College, Bangalore University, India.

Research position

2008 to 2011	Junior research fellow under Dr. Sudha Mishra, Department of Biophysics, National Institute for Mental Health and Neurosciences, Bangalore, India.

Publication

Menzler, J., Channappa, L., & Zeck, G. (2014). Rhythmic Ganglion Cell Activity in Bleached and Blind Adult Mouse Retinas. *PLoS one*, *9*(8), e106047.

Oral presentation

"Electrical imaging of local field potentials in Organotypic and acute hippocampal slices using CMOS MEA's" at MEA Meeting 2014, 9th Substrate-Integrated Microelectrode arrays, July 1-July 4, Reutlingen, Germany.

Poster presentations

- ❖ "Electrical Imaging of Local Field Potentials and Single Unit Activity in Organotypic Hippocampal Slices using a High-Density Multi-Transistor Array (Neurochip)" at 10th Gottingen Meeting of the German Neuroscience Society, Gottingen, 13-16 March 2013.
- ❖ "Characterization of electrical activity in hippocampal subfields using Neurochips" at Networks! The German Neurophysiology PhD Meeting, Tübingen, 13-14 September, 2013.

Workshops

Demonstrated organotypic hippocampal slice culture preparations and recordings from hippocampal slice cultures on multielectrode arrays to international participants (PhD students, Technical assistants and Scientists) in four workshops on "Neuronal Applications on Microelectrode arrays" conducted by Multi Channel systems in collaboration with Natural and Medical Sciences Institute, Reutlingen during 2012-2014.